Summer 2007

Polymer light emitting diodes based on polyfluorenes

Quishu Zhang
Louisiana Tech University

POLYMER LIGHT EMITTING DIODES

BASED ON POLYFLUORENES

by

Qiushu Zhang, MS

A Dissertation Presented in Partial Fulfillment
of the Requirements for the Degree
Doctor of Philosophy

COLLEGE OF ENGINEERING AND SCIENCE
LOUISIANA TECH UNIVERSITY

August, 2007

LOUISIANA TECH UNIVERSITY

THE GRADUATE SCHOOL

JUNE 19, 2007
Date

We hereby recommend that the dissertation prepared under our supervision by QIUSHU ZHANG entitled POLYMER LIGHT EMITTING DIODES BASED ON POLYFLUORENES be accepted in partial fulfillment of the requirements for the Degree of PHD IN ENGINEERING

Sandra Selmic
Supervisor of Dissertation Research

Head of Department
ELECTRICAL ENGINEERING
Department

Recommendation concurred in:

Advisory Committee

Approved:
Director of Graduate Studies

Approved:
Dean of the Graduate School

Dean of the College

GS Form 13
(5/03)

ABSTRACT

This dissertation is devoted to the study on Polymer Light-Emitting Diodes (PLEDs) based on polyfluorenes (PFs), a promising class of semiconductive polymers for Light-Emitting Diode (LED) applications. Recently Light Emitting Polymers (LEPs) have clearly made their entry into display technology by virtue of their potential application for large-area flat-panel displays with the advantages of low cost, wide viewing angle, fast switching time, high efficiency, low driving voltage, as well as their flexibility and adaptability. Compared to inorganic materials, the efficiency of PLEDs is, however, still low. And for the application of PFs in PLEDs, an undesired long-wavelength emission band is a main barrier, which occurs during device operation and results in both color instability and reduced efficiency. In this study, several types of PLED devices based on neat PFs or PF blends were designed, fabricated, and characterized: (1) PF2/6:PFB blended devices, (2) end-capped PF2/6 devices, (3) F8BT:PPB blended devices, and (4) end-capped PF2/6:F8BT blended devices. DMP-end-capped PF2/6, PFB and PPB are novel polymers. For PF2/6, only a few results have been reported although it is of great significance for study of effect of blending and end-capping on device performance and color stability.

In comparison with pure PFs, the enhanced properties were observed from blend devices although the improvement might result from different reasons. For example, DMP-end-capped PF2/6:F8BT blended devices demonstrated better performance than

either of the blend components with a maximum luminance of 1074 cd/m^2 at 213.6 mA/cm^2, a maximum external quantum efficiency of 0.16% and a maximum luminance efficiency of 0.514 cd/A at 205.2 mA/cm^2, which was assigned to efficient energy transfer of excitations.

Besides the increase in efficiencies as compared to PF2/6, long-wavelength emission is significantly suppressed for end-capped PF2/6, which dominates the EL spectrum of PF2/6. In the case of DMP-end-capping, EL spectrum peaked at 420, 445, and 485 nm, all maxima falling into violet-blue region. This might be due to the efficient hole trapping at the end-capper groups, the shift of the exciton recombination zone, or the enhancement in the polymer resistance to oxidation.

The pristine PF2/6 device was modeled by using space charge limited current theory for the hole-only case. The hole mobility is regarded as field-dependent. The calculated current density-voltage characteristics fit the experimental data very well at electric fields above 6.5×10^5 V/cm. The electrical characteristics of neat PF2/6 and neat F8BT-based devices were also simulated via exploiting a commercial TCAD software package.

APPROVAL FOR SCHOLARLY DISSEMINATION

The author grants to the Prescott Memorial Library of Louisiana Tech University the right to reproduce, by appropriate methods, upon request, any or all portions of this Dissertation. It is understood that "proper request" consists of the agreement, on the part of the requesting party, that said reproduction is for his personal use and that subsequent reproduction will not occur without written approval of the author of this Dissertation. Further, any portions of the Dissertation used in books, papers, and other works must be appropriately referenced to this Dissertation.

Finally, the author of this Dissertation reserves the right to publish freely, in the literature, at any time, any or all portions of this Dissertation.

Author Qinshu Zhang

Date 7/26/2007

GS Form 14
(5/03)

TABLE OF CONTENTS

LIST OF TABLES

LIST OF FIGURES

ACKNOWLEDGEMENTS

I would like to thank my advisor, Dr. Sandra Selmic, for her advice and help during the last four years. She gave me insightful theoretical advice, which proved highly important for understanding and explaining the experimental results.

I would like to thank all of my other advisory committee members, Mr. Ji Fang, Dr. Hisham Hegab, Dr. Rastko Selmic, and Dr. Kody Varahramyan (in the alphabetical order of last name), for their precious advice and useful discussion.

Dr. Kody Varahramyan provided me with careful and helpful advice in electrical theories and modeling. Mr. Abdul Khaliq rendered me useful assistance in TCAD simulation. I greatly appreciate these.

I would like to thank David Keith Chambers, Difei Qi, and Joseph Paul Cannon for their assistance and discussion in device fabrication and testing.

This work has been benefited by the resources in the Institute for Micromanufacturing (IfM). The laboratory support provided by the IfM staff is also appreciated. The staff includes Ji Fang, Karen Xu, Donald Tatum, John McDonald, Deborah Wood, and Scott Williams.

I would like to thank my parents, my sisters and their families who helped me a lot when I pursued my PhD studies in the U.S. And I would like to thank my own family. It was family warmth that helped me overcome difficulties in my research and study.

ABBREVIATION AND SYMBOLS

PF: Polyfluorene

LED: Light-Emitting Diode

PLED: Polymer Light-Emitting Diode

LEP: Light-Emitting Polymer

ITO: Indium Tin Oxide

PL: Photoluminescence

EL: Electroluminescence

PEDOT:PSS: Poly(3,4-oxyethyleneoxythiophene) doped with Poly(Styrene Sulfonate)

CIE: Commission Internationale de L'Eclairage

HTL: Hole Transporting Layer

ETL: Electron Transporting Layer

DBR: Distributed Bragg Reflector

LUMO: Lowest Unoccupied Molecular Orbital

HOMO: Highest Occupied Molecular Orbital

FWHM: Full Width at Half Maximum

SAM: Self-Assembled Monolayer

MEH-PPV: Poly[2-methoxy-5-(2'-ethylhexyloxy)-1,4-phenylenevinylene]

EQE: External Quantum Efficiency

PFO: Poly(9,9-dioctylfluorene)

PF2/6: Poly[9,9-di-(2'-ethylhexyl)fluorenyl-2,7-diyl]

PFB: Poly[(9,9- dioctylfluorenyl-2,7-diyl)-co-(N,N'-bis(4-butylphenyl-1,1'-biphenylene-4,4'-diamine))]

TPA: N,N-bis(4-methylphenyl)-N-phenylamine

DMP: Dimethylphenyl

F8BT: Poly[(9,9-dioctylfluorenyl-2,7-diyl)-co-(1,4-benzo-{2,1'-3}-thiadiazole)]

PPB: Poly(N,N'-bis(4-butylphenyl)-N,N'-bis(phenyl)benzidine)

CHAPTER 1

THEORIES OF POLYMER LIGHT-EMITTING DIODES

Electroluminescence (EL) from conjugated polymer was first discovered in 1990 [1]. Since then Polymer Light-Emitting Diodes (PLEDs) have been considered promising candidates for large-area display applications due to their mechanical flexibility and low cost. In this chapter, device structure, operation, and characterization of PLEDs are described. We also present Space Charge Limited Current (SCLC) theory that can provide satisfactory explanation for the electrical characteristics of PLEDs.

1.1 PLED Structure

The typical device structure of a PLED is shown in Fig. 1.1 (a), where the emissive layer is sandwiched between two metallic electrodes. Fig. 1.2 shows energetic position of the frontier levels of the materials used in ITO/MEH-PPV/Al device and its band diagram under forward bias. ITO that is deposited on glass substrate is usually chosen as anode since it has a relatively high work function (~4.8 eV), and is therefore suitable for serving as a hole-injecting electrode (Fig. 1.2). In addition, the transparency of ITO allows the light produced within the active layer to exit the device. The top electrode (cathode) is deposited onto the emissive layer via thermal evaporation of a

metal. A low-work-function metal like Al (~4.2 eV), Mg (~3.7 eV) or Ca (~2.9 eV) is selected as the cathode, which facilitates electron injection (Fig. 1.2). In order to improve device performance, the hole transport layer and electron transport layer are incorporated into the device structure to form the multilayer PLED (Fig. 1.1 (b)).

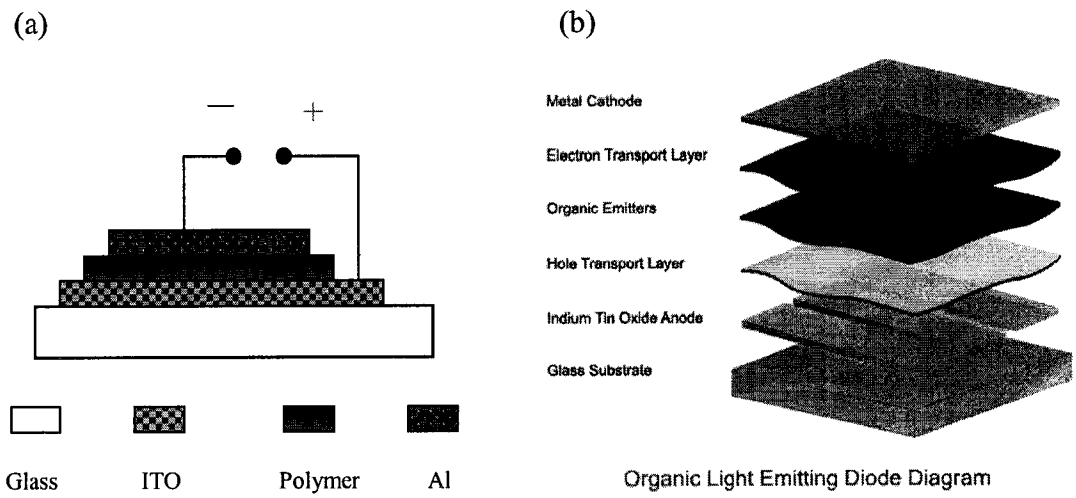

Fig. 1.1 Device structure of a PLED: (a) the basic structure, (b) the structure of a multilayer device.

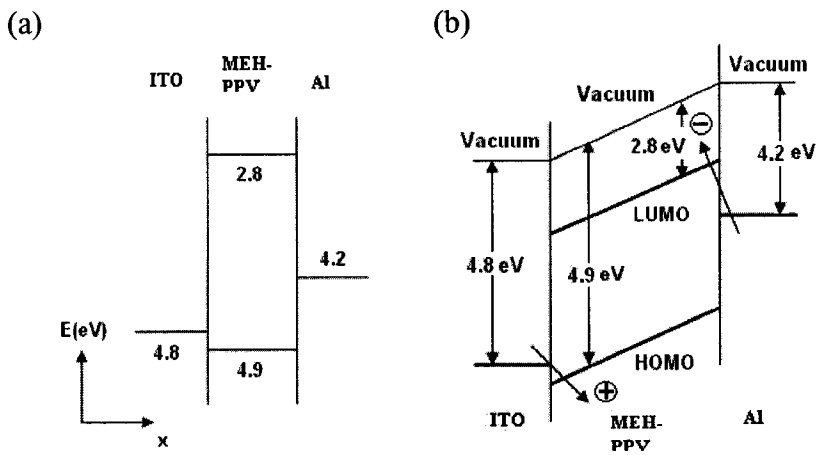

Fig. 1.2 (a) Energetic position, relative to the vacuum level, of the frontier levels of the materials used in the device with a configuration of ITO/MEH-PPV/Al, (b) band diagram for the same device under forward bias.

The emissive layer consists of a conjugated polymer that has a structural framework of alternating single and double carbon-carbon bonds. The single bond is a σ-bond, and the double bond is comprised of a σ-bond and a π-bond. The semiconducting properties of conjugated polymers originate from the π-bond along the polymer chain. The π-bond is easily broken since the electrons in this bond are loosely bound. Actually, these π electrons are the conduction electrons in conjugated polymers. The chemical structures of some conjugated polymers that are used as Light-Emitting Polymer (LEP) in PLED fabrication are shown in Fig. 1.3. The emissive layer can be formed by spin casting onto the ITO-coated glass from a polymer solution with a thickness typically no more than 100 nm. The film thickness produced in this way is highly uniform.

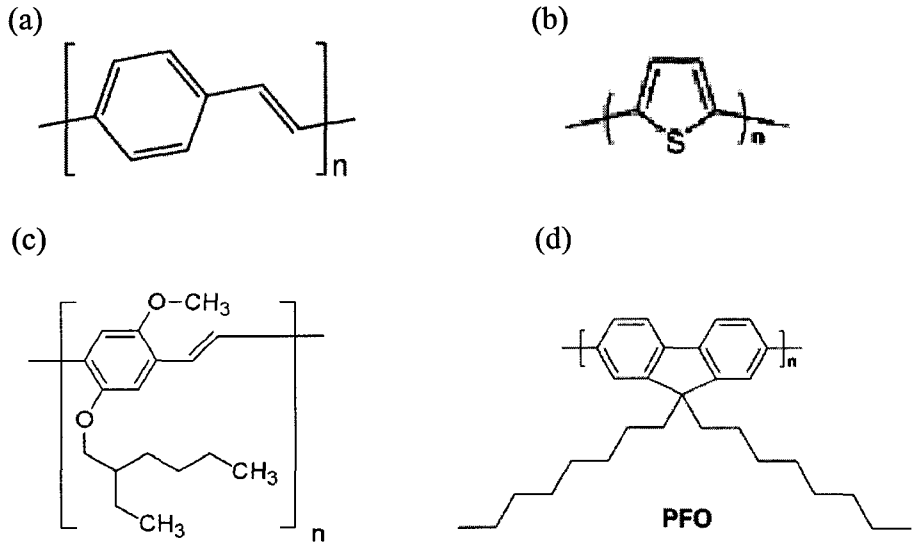

Fig. 1.3 Chemical structures of some conjugated polymers that are used in electroluminescent diodes: (a) Poly(p-Phenylene Vinylene) (PPV), (b) PolyThiophene (PT), (c) poly[2-Methoxy-5-(2-EthylHexyloxy)-1,4-PhenyleneVinylene] (MEH-PPV), (d) Poly(9,9-dioctylFluOrene) (PFO).

1.2 Device Operation

In the basic operation mode of a PLED, positive and negative charge carriers are injected from opposite electrodes when the device is sufficiently biased. Driven by the applied electric field, holes and electrons move through the polymer over a certain distance until they recombine each other within the polymer layer to form excitons (neutral bound excited states). Finally, luminous emission takes place as a result of radiative decay. Therefore, PLED operation involves charge injection, charge transport, exciton formation and light emission, which is schematically illustrated in Fig. 1.4.

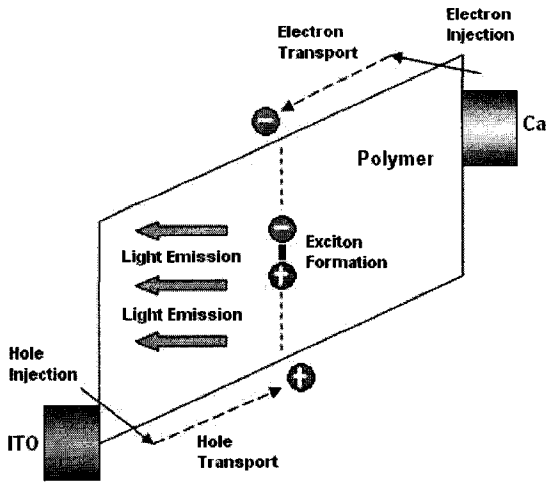

Fig. 1.4 Schematic band diagram of a PLED under forward bias.

1.2.1 Charge Injection

When carriers are injected, there is typically a roughly triangular barrier for both hole and electron penetration from electrodes. In the lower-current regime, the current is determined by charge injection that is realized via two possible mechanisms, Schottky thermal injection and Fowler-Nordheim tunneling injection (shown in Fig. 1.5).

In Schottky emission process, the current flow is described by

$$J = \frac{4\pi qmk}{h^3} T^2 \exp(-\frac{q\Phi_{Bn}}{kT})[\exp(\frac{qV}{kT}) - 1], \qquad (1\text{-}1)$$

where m is the effective mass of the electron (hole), k is Boltzmann's constant, h is Planck's constant, T is the temperature, q is the elementary charge, Φ_{Bn} is the barrier height, and V is the applied voltage [2].

However, the typical energy barrier between polymer and metal electrode was estimated to be 1.0 eV. A large current density could not be achieved over such a high-energy barrier of 1 eV via Schottky emission. Actually, the activation energy of typical PLEDs was found to be only ~0.03 eV. A possible explanation for this is through the localized levels induced by structural defects and unexpected impurities, which is shown in Fig. 1.5 (a).

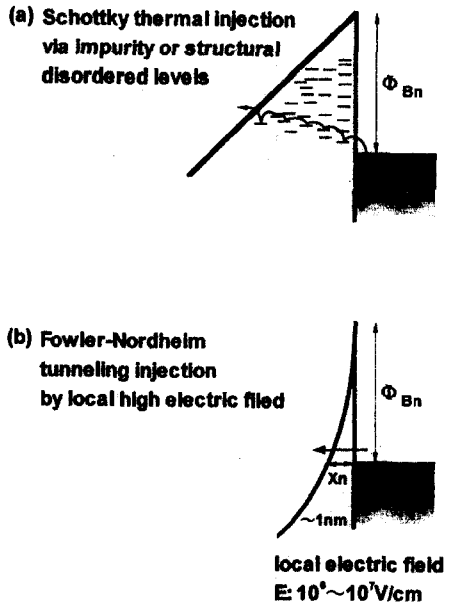

Fig. 1.5 Two possible carrier injection mechanisms at the polymer-electrode interface: (a) Schottky-type carrier injection by impurity or structural disordered levels with thermal assistance, and (b) Fowler-Nordheim tunneling injection with the aid of a local high electric field (10^6-10^7 V/cm) (Ref.[3]).

In the Fowler-Nordheim tunneling mechanism (Fig. 1.5 (b)), a charge carrier is injected with the assistance of a local high electric field (10^6-10^7 V/cm). The current flow is described by

$$J = (\frac{q^3 V^2 m_0}{8\pi h \Phi_{Bn} m^*}) \exp(-\frac{4(2m^*)^{0.5} \Phi_{Bn}^{1.5}}{3\hbar q V}), \qquad (1\text{-}2)$$

where m_0 is the mass of the free electron and m^* is the effective mass [2].

1.2.2 Charge Transport

Most electroluminescent polymers are low-conductance materials with a typical hole mobility of 10^{-7}-10^{-3} cm^2/Vs and typical electron mobility lower by a factor of 10-100 [3]. The low mobility in these materials results from the disorder in the amorphous or polycrystalline materials. It is known that charge carrier mobility μ in conjugated polymers is field-dependent, which is described by

$$\mu = (\mu_* e^{-\Delta / kT}) e^{\gamma \sqrt{E}}, \qquad (1\text{-}3)$$

where Δ is the activation energy, k the Boltzmann's constant, μ_* the mobility prefactor, and γ the electric-field coefficient to the mobility due to the interaction between charge carriers and randomly distributed permanent dipoles in semiconducting polymers [4]. The coefficient γ can be written according to the empirical relation:

$$\gamma = (\frac{1}{kT} - \frac{1}{kT_0}) B, \qquad (1\text{-}4)$$

where B and T_0 are constants [4].

With an applied electric field of over 10^5 V/cm and an injected current density larger than the polymer intrinsic charge density, the injected charge carriers accumulate near the polymer-electrode interface to form space charges by virtue of low carrier

mobility (Fig. 1.6) [3]. As a result, the internal electric field increases, and the current density J is determined by the Space Charge Limited Current (SCLC). For a single-carrier PLED device, the trap-free SCLC density is given by Child's law:

$$J = \frac{9}{8}\varepsilon\mu\frac{E^2}{L}, \qquad (1\text{-}5)$$

where ϵ is the permittivity of the polymer, μ is the charge carrier mobility, E is the electric field across the device, and L is the thickness of the active polymer [5]. Eq. (1-5) is derived as follows:

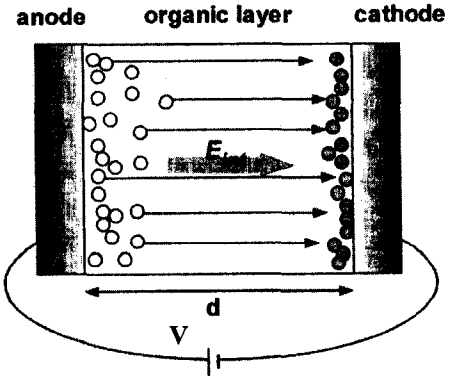

Fig. 1.6 Schematic view of space charge limited current in PLEDs (Ref.[3]): Open symbols (○) represent excess holes, and closed symbols (●) correspond to excess electrons. Besides an external electric field (V/d), there is an additional internal field (E_{int}) that is generated by injected excess charge carriers. As a result, the total electric field greatly improves current flow. E_{int} makes a significant contribution to the achievement of high current density.

In structures where carriers can readily enter the insulator and freely flow through the insulator, the resulting current and carrier densities are found to be very high. The density of free carriers generates a field gradient limiting the current density, which is referred to as space-charge effects. This situation takes place in low doped semiconductors and vacuum tubes [6].

For the case shown in Fig. 1.7, we begin with equations for the drift current and Gauss's law (Eqs. (1-6) and (1-7), respectively). Here we assume that the insulator contains no free carriers, if no current flows.

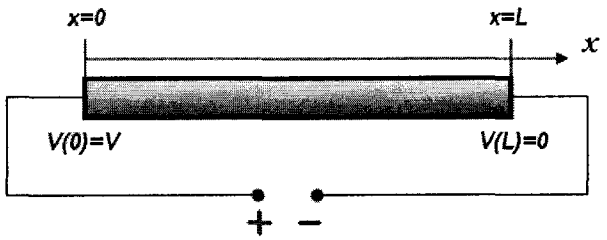

Fig. 1.7 A one-dimensional representation of a low doped semiconductor or a vacuum tube to which a voltage is applied.

$$J = qn\mu E, \tag{1-6}$$

where n is carrier density.

$$\frac{dE}{dx} = \frac{qn}{\varepsilon} \tag{1-7}$$

Eliminating n, we have

$$\frac{J}{\varepsilon\mu} = E\frac{dE}{dx}. \tag{1-8}$$

Let's assume that the electric field is equal to zero at x = 0, and that $J(x)$ is constant J. After integrating this equation from 0 to x, we obtain

$$\frac{Jx}{\varepsilon\mu} = \frac{E^2}{2} \text{ or } E(x) = \sqrt{\frac{2xJ}{\varepsilon\mu}}. \tag{1-9}$$

Integrating once again from $x = 0$ to $x = L$ with $V(0) = V$ and $V(L) = 0$, we find

$$V = \int_0^L E dx = \sqrt{\frac{2J}{\varepsilon\mu}}\frac{d^{3/2}}{3/2} \tag{1-10}$$

Therefore,

$$J = \frac{9\varepsilon\mu V^2}{8L^3}, \tag{1-11}$$

from which we obtain Eq. (1-5), the expression for the space-charge-limited current.

1.2.3 Carrier Recombination and Light Emission

The carrier capture in PLEDs is very important to device operation. When one of charge carriers has very low mobility, a high local charge density can be created, which will facilitate collision capture of the other charge carrier [7]. In this way efficient capture in the polymer film can be realized.

The conversion of electrical energy into light is mediated by excitons, whose properties are the primary determinant of the overall luminescent efficiency. An exciton can be considered two-electron systems: one electron is excited into an unfilled orbital of a given molecule or polymer, while the second remains in a partially filled ground state. The total spin of a two-electron system is either S = 0, or S = 1. The S = 0 spin wavefunction is antisymmetric under particle exchange:

$$\sigma_- = \frac{1}{\sqrt{2}}\{\uparrow(1)\downarrow(2) - \downarrow(1)\uparrow(2)\}, \tag{1-12}$$

where ↑ and ↓ represent the possible spin states of each electron. The electrons are signified by (1) and (2), and σ is spin wavefunction. There are three possible spin wavefunctions with S = 1, all symmetric under particle exchange:

$$\sigma_+ = \frac{1}{\sqrt{2}}\{\uparrow(1)\downarrow(2) + \downarrow(1)\uparrow(2)\} \tag{1-13}$$

$$\sigma_+ = \uparrow(1)\uparrow(2) \tag{1-14}$$

$$\sigma_+ = \downarrow(1)\downarrow(2) \tag{1-15}$$

The degeneracy of each state is reflected in its title: the S = 0 state is known as a singlet, and the S = 1 is a triplet.

Carrier recombination produces singlet (S_1) and triplet excitons (T_1). Radiative emission (fluorescence) originates from emissive transitions from singlet excitons to ground states. In carrier recombination, singlet and triplet excitons are created at a ratio of 1 to 3:

$$4\,(e + h) \rightarrow S_1 \text{ (direct)} + 3\ T_1 .$$

However, the T_1-T_1 annihilation produces both S_1 and T_1:

$$4\,(T_1 + T_1) \rightarrow S_1 \text{ (indirect)} + 3\ T_1 .$$

Therefore, in summary,

$$20\,(e + h) \rightarrow 5\ S_1 \text{ (direct)} + 3\ S_1 \text{ (indirect)},$$

which indicates that the maximum EL quantum efficiency reaches only 40% even if the fluorescence efficiency is 100%.

Fig. 1.8 displays the elementary process for charge recombination that begins with the recombination of holes and electrons, and ends with light emission.

The internal quantum efficiency η_{int}, defined as the ratio of the number of photons produced within the device to the number of electrons flowing in the external circuit, is given by:

$$\eta_{\text{int}} = \gamma\, r_{st}\, q , \qquad (1\text{-}16)$$

where γ is the ratio of the number of exciton formation events within the device to the number of electrons flowing in the external circuit, r_{st} is the fraction of excitons which are formed as singlets, and q is the efficiency of radiative decay of these singlet excitons.

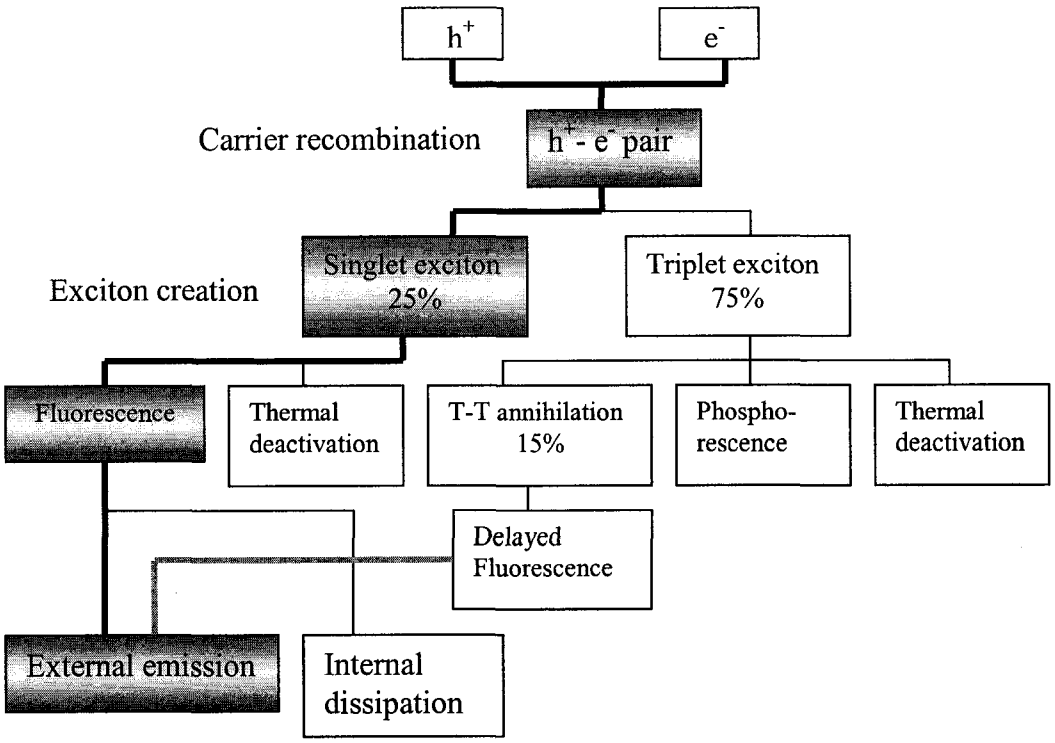

Fig. 1.8 The elementary processes for charge carrier recombination, creation of excitons, emission, and external emission (Ref.[3]).

1.3 Device Characterization

1.3.1 Luminance

Luminance is a measure of the brightness of a surface. To give the precise definition of luminance, it is necessary to describe some closely related quantities. Table 1.1 lists some photometric quantities (that correlate with what the visual sensation is to a normal human observer exposed to the radiation) and radiometric quantities (which concern physical measurement of optical radiation as a function of its wavelength), with units and symbols.

The candela is defined as an SI (Système International) base unit. Luminous flux (lumen) is perhaps the most fundamental photometric quantity, as luminous intensity and luminance are defined in terms of the lumen with appropriate geometric factors.

Table 1.1 Some quantities and units used in photometry and radiometry (Ref.[8]).

Photometric quantity	Unit	Relationship with lumen	Radiometric quantity	Unit
Luminous flux	lm (lumen)		Radiant flux	W (watt)
Luminous intensity	cd (candela)	lm sr^{-1}	Radiant intensity	W sr^{-1}
Luminance	cd m^{-2}	lm sr^{-1} m^{-2}	Radiance	W sr^{-1} m^{-2}

Luminous flux (Φ_v) is the rate of transmission of luminous energy. Radiometric flux is weighted by $V(\lambda)$. Luminous flux is defined as

$$\Phi_v = K_m \int_\lambda \Phi_{e,\lambda} V(\lambda)\, d\lambda, \qquad (1\text{-}17)$$

where K_m is the maximum spectral luminous efficacy (of radiation) for photopic vision; $\Phi_{e,\lambda}$ is the spectral concentration of radiant flux in (W/nm) as a function of wavelength λ in nm; $V(\lambda)$ is the spectral luminous efficiency function for photopic vision.

The constant, K_m, relates the photometric quantities and radiometric quantities. It is normally rounded to 683 lm/W with negligible errors. V(λ) describes the relative spectral responsivity of the human eye, which is defined in the domain 360 nm to 830 nm, and is normalized to one at its peak, 555 nm (Fig. 1.9).

$\Phi_{e,\lambda}$ can be defined as

$$\Phi_{e,\lambda} = \frac{P\, I(\lambda)}{\int_\lambda I(\lambda)\, d\lambda}, \qquad (1\text{-}18)$$

where P is radiant flux or light power in watts; $I(\lambda)$ is intensity in the EL spectrum.

Luminous intensity (I_v) is the luminous flux (from a point source) emitted per unit solid angle in a given direction. It is defined as

$$I_v = \frac{d\Phi_v}{d\Omega}, \tag{1-19}$$

where $d\Phi_v$ is the luminous flux leaving the source and propagating in an element of solid angle $d\Omega$ containing the given direction. The solid angle (Ω) in steradians (sr), is equal to the spherical surface area (A) divided by the square of the radius (r) (Fig. 1.10).

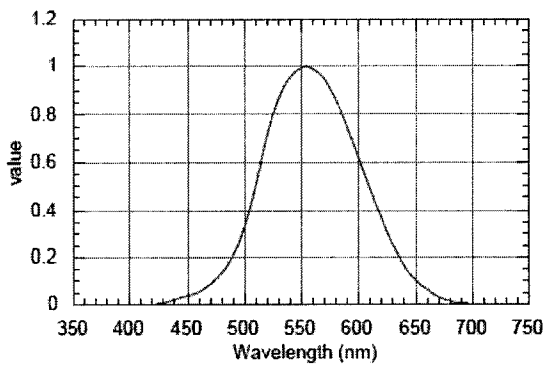

Fig. 1.9 CIE (Commission Internationale de l'Éclairage) V(λ) Function (Ref.[8]).

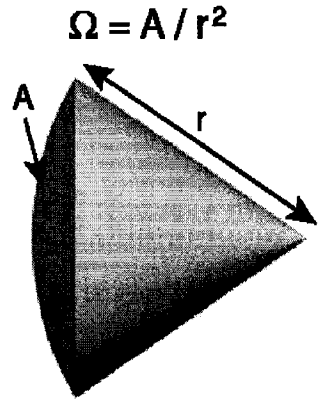

Fig. 1.10 The definition of solid angle (Ref.[9]).

Luminance (L_v) (unit: cd m^{-2}) is the luminous flux from an element of a surface surrounding a given point, emitted into a small solid angle containing the given direction, per unit area of the element projected on a plane perpendicular to that given direction. It is defined as

$$L_v = \frac{d^2\Phi_v}{d\Omega\, dA\cos\theta}, \tag{1-20}$$

where $d\Phi_v$ is the luminous flux emitted (reflected or transmitted) by an elementary beam passing through the given point and propagating in the solid angle $d\Omega$ containing the given direction; dA is the area of a section of that beam containing the given point; θ is the angle between the normal to that section and the direction of the beam.

The emission from organic LEDs is often assumed to be Lambertian, i.e. the flux per solid angle varies as the cosine of the angle from the normal [10]. Therefore, the brightness of a Lambertian source is independent of viewing angle. Usually light output is measured over a small solid angle in the forward direction, normal to the plane of the device [10].

1.3.2 EL Efficiencies

EL efficiencies are important characteristics of PLEDs, among which are External Quantum Efficiency (EQE), luminance efficiency, and luminous efficiency.

1. **External Quantum Efficiency (EQE)**: It gives the ratio of the number of useful light particles to the number of injected charge particles. EQE is calculated using

$$EQE = \frac{\pi e}{K_m h c} \frac{L_v}{J} \left[\frac{\int I(\lambda)\, d\lambda}{\int (1/\lambda)\, I(\lambda)\, V(\lambda)\, d\lambda} \right], \qquad (1\text{-}21)$$

where L_v is the luminance (cd/m^2) of the device at a current density of J (A/m^2).

2. **Luminance Efficiency**: It is given by

$$\Phi_{luminance} = \frac{L_v(cd/m^2)}{J\,(A/m^2)}. \qquad (1\text{-}22)$$

3. **Luminous Efficiency**: It is the luminous flux of the light source divided by the electrical input power. Luminous efficiency is defined as

$$\Phi_{luminous} = \frac{\Phi_v}{IV}, \qquad (1\text{-}23)$$

where the product $I V$ is the electrical input power of the device.

1.3.3 Other Properties

1. Threshold Current Density for Light Emission: It is defined as the minimum current density at which the resulting light power can be detected.

2. Turn-on Voltage for the Current: It is defined as the applied bias at which the current reaches $\sim 8.5 \times 10^{-5}$ A.

CHAPTER 2

LITERATURE OVERVIEW OF POLYFLUORENE-BASED LIGHT-EMITTING DIODES

2.1 Introduction

Since the report on blue emission from poly(alkylfluorene) in 1991 [11], polyfluorenes (PFs) have attracted considerable interest in the application of Light-Emitting Diodes (LEDs) due to their unique combination of high photoluminescence (PL) and electroluminescence (EL) efficiencies, good photo stability and thermal stability, easy processability, and emission covering the entire visible region at low operating voltages (Fig. 2.1). In order to make PF-based LEDs satisfy commercial requirements, enormous effort has been devoted to the improvement of EL performance, the suppression of low energy emission bands (a primary drawback of blue PFs), and the realization of desired characteristics such as white EL, among which are the synthesis of new PFs, refinement of device structure, modification of substrate or electrode, and blending (Fig. 2.2). In this chapter, we carry out a literature overview of PF-based LEDs via giving a general outline of each of the above four strategies, as well as briefly describing the typical devices.

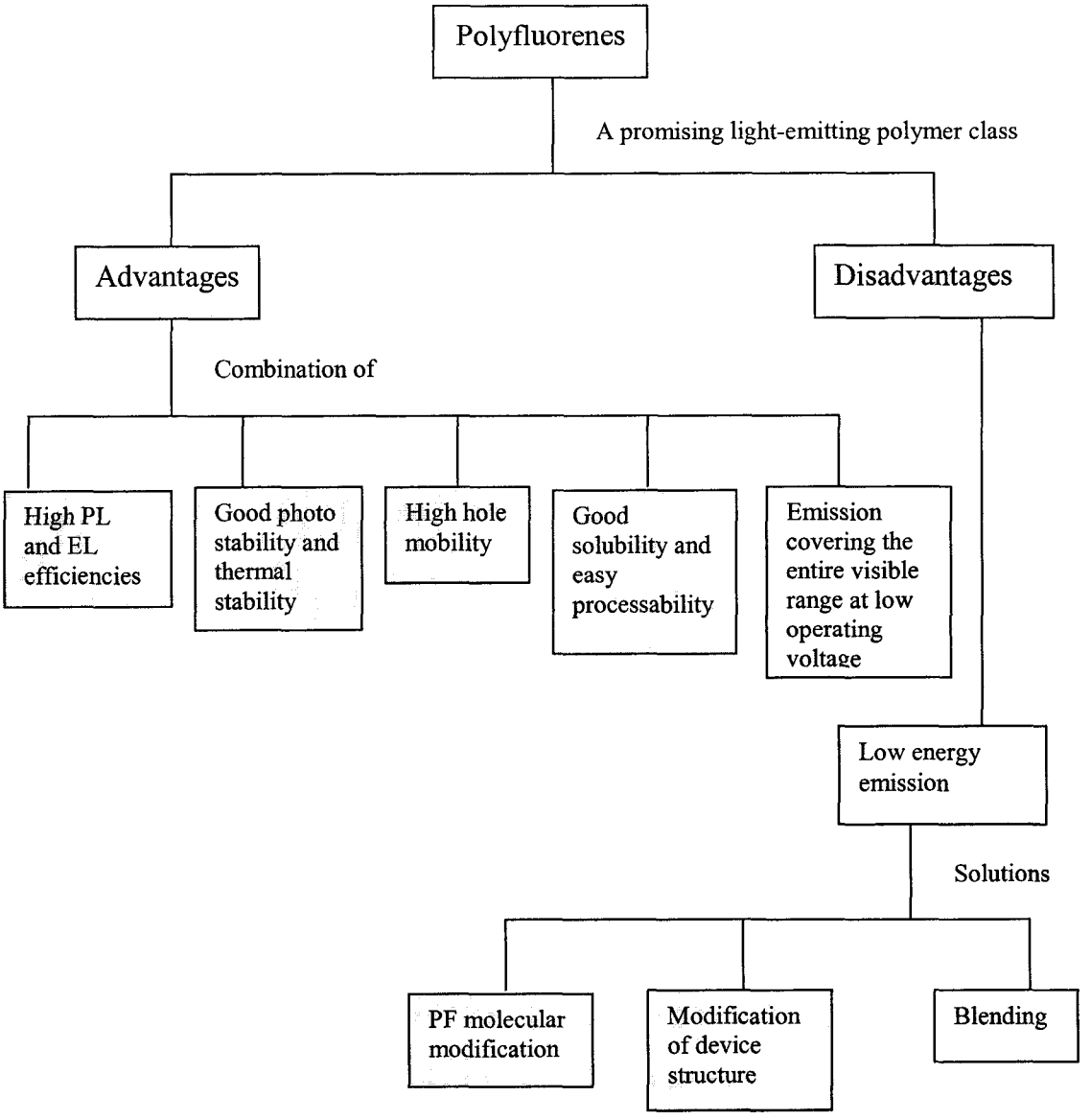

Fig. 2.1 Advantages and disadvantages of polyfluorenes.

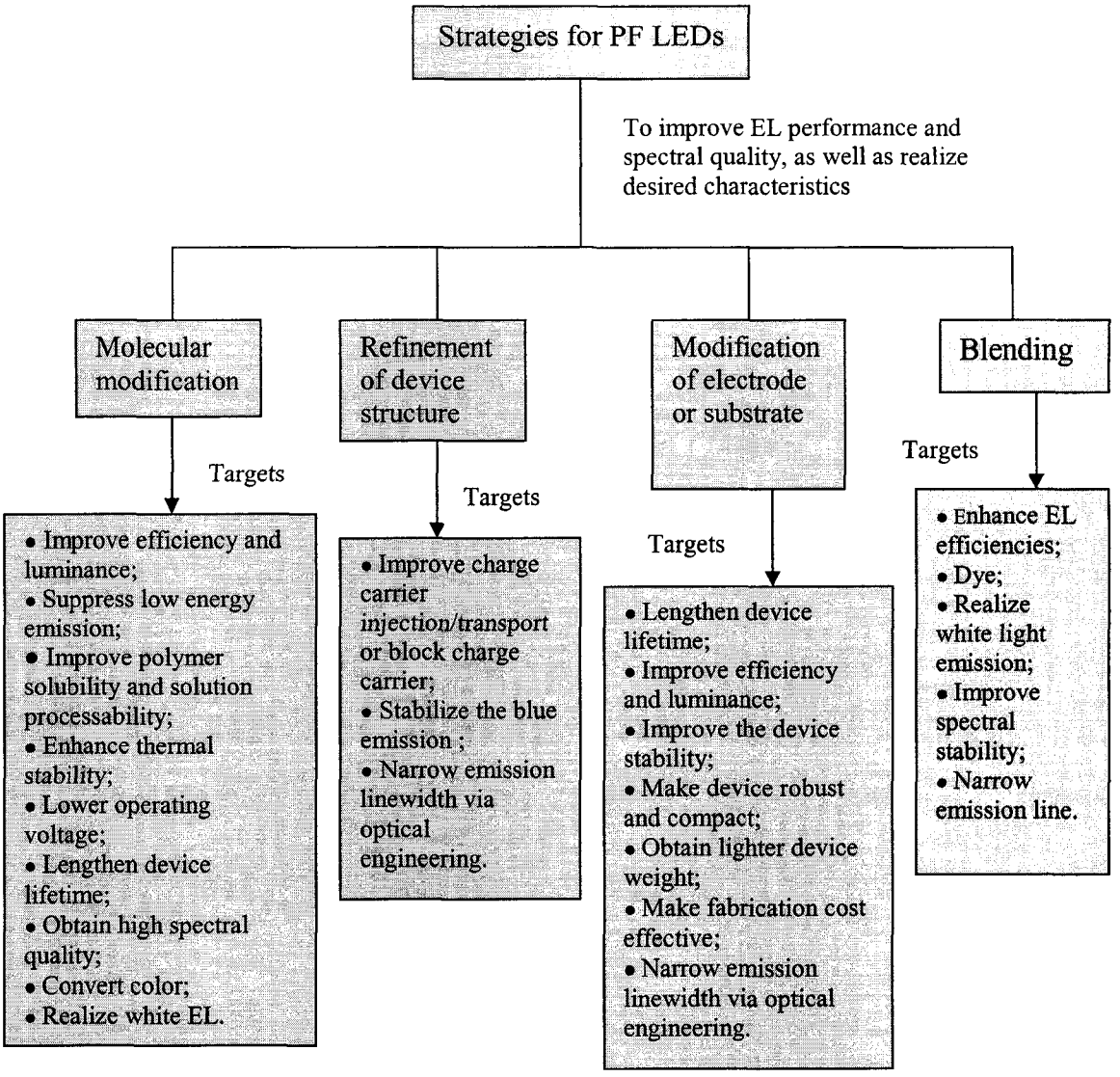

Fig. 2.2 The strategies for PF-based LED devices.

2.2 Molecular Modification

PFs contain a rigid biphenyl unit (which leads to a large band gap with efficient blue emission), and the facile substitution at the remote C9 position provides the possibility of improving the solubility and processability of polymers without significantly increasing the steric interactions in the polymer backbone. PF molecules can be modified to synthesize new polymers by copolymerization, end-capping, introducing

substituents at the C-9 position of fluorene, and so on. In order to increase efficiency, electron-transporting moieties and/or hole-transporting units are incorporated into the side chain or backbone of the conjugated polymers so as to improve the charge balance between electrons and holes [12]-[19]. A typical example is PF-TPA-OXD (Fig. 2.3) [12]. The formation of aggregates, excimers, or keto defects is suppressed to achieve stable blue emission via the introduction of bulky side chains or dendronization, using spiro-linked or cross-linked structure, copolymerization to induce disorder, and improving oxidative stability of pendant groups or chain ends [12][14][16][18][20]-[31]. In addition, PF macromolecular engineering is also aimed at improvement of polymer solubility and solution processability [23][27][32][34], enhancement of thermal stability [16][18][20][23]-[25][27][29][32]-[36], lowering operating voltage [13][17][28][35], lengthening device lifetime [13], procurement of high spectral quality [18][19][25][34][35], color conversion [13][21][34][33], as well as the realization of white EL emission [37].

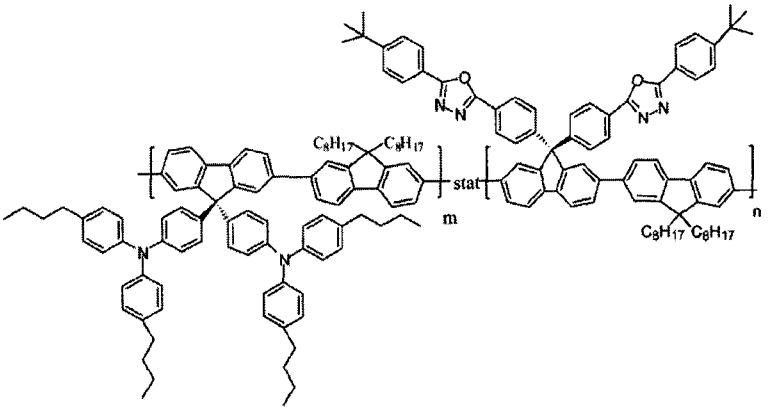

Fig. 2.3 Chemical structure of PF-TPA-OXD, which contains both electron-transporting OXD segments and hole-transporting triphenylamine (TPA) units that are functionalized at the C-9 position of fluorene. After Ref. [12].

2.3 Refinement of Device Structure

In PLEDs, holes and electrons are injected from anode and cathode, migrate toward the opposite electrode under applied electric field, recombine with each other, and form excitons. The radiative decay of the excitons then generates emission. To optimize the charge carrier injection/transport, hole-transporting and electron-transporting layers are often employed in PLED devices [38]-[44]. This modification results in better device performance than observed for simple single-layer PLEDs, not only because charge injection is facilitated by lowering the Schottky barriers at the electrodes, but also because charges are confined at the organic interfaces. For example, the hole transporting layer (HTL) acts as an electron blocker and the electron transporting layer (ETL) as a hole blocker. Thus, the charge densities are increased near the center of the device, both enhancing the recombination rate and ensuring that excitons primarily form far from the metallic electrodes, which may quench the luminescence.

In some cases, a multilayered hetero-structure of PLEDs can be used to stabilize the blue emission from the PFs by depressing the long wavelength bands (> 500 nm) which is typical in blue PF-based LEDs [43][44]. Fig. 2.4 shows that the introduction of CF_3 OXD layer significantly decreases the weight of low energy emission in the EL. The improvement was ascribed to the prevention of interaction between PF and Ca due to the insertion of CF_3 OXD. In addition, the incorporation of a polymer distributed Bragg reflector (DBR) into the PLED structure can lead to a narrowed linewidth of emission [45].

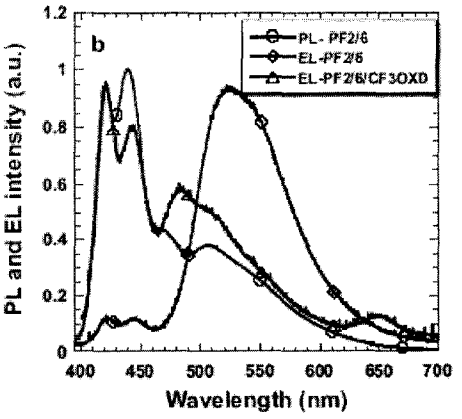

Fig. 2.4 The PL and EL spectra of PF2/6-based LEDs: Lines with circles for PL spectra, lines with diamonds for EL spectra, device with the ITO/PEDOT/PF2/6/Ca/Ag configuration; and lines with triangles for EL spectra, device with the (ITO)/PEDOT/PF2/6/ CF_3 OXD/Ca/Ag configuration. After Ref. [44].

2.4 Modification of Substrate or Electrode

In some devices like full-color graphic displays, the high purity of the individual red, green, and blue pixels is necessary for attaining a full color palette since the spectrally broad sources will reduce the range of colors that can be obtained by mixing. For conjugated polymers, the emission spectra are generally wide because of strong inhomogeneous broadening and vibronic progression. Molecular design [46][47] and doping [48][49] have been explored to address this problem. Another solution to the issue of poor color saturation for conjugated polymers is to employ a DBR substrate instead of a glass substrate, which is expected to optimize the emission properties via optical engineering of the LED structure (Fig. 2.5) [50].

Compared to glass substrates, the flexible plastic substrate has some distinct advantages (more robust and compact, lighter weight and cost effective). High EL performance (a maximum brightness of 13,000 cd/m^2 and a maximum external quantum efficiency of 16.2 %) can be realized for PLED fabricated on the plastic substrate with

proper layer design for minimizing the oxygen and moisture penetration rate through the substrate and maximizing the ITO conductivity [51].

Although the blend poly(3,4-ethylenedi-oxythiophene):poly(styrenesulfonate) (PEDOT:PSS) is commonly exploited to serve as the hole injection/transport layer between the ITO anode and the emissive polymer to enhance hole injection and thereby PLED device properties [16][17][24][36], it is not ideal due to its strong absorption in the visible range and the unstable interface it forms with ITO [52][53]. An alternative is to modify the anode with Self-Assembled Monolayers (SAMs). There have been some reports on SAM-based anode modification specifically directed to increasing hole injection, brightness, and quantum efficiency in blue PLEDs [54]-[56].

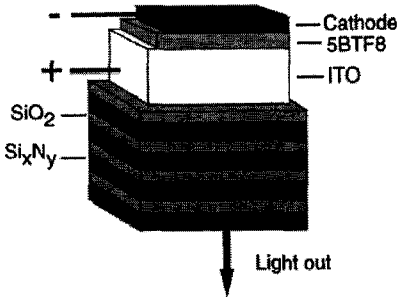

Fig. 2.5 Schematic diagram of PLED with a DBR substrate consisting of four repeat pairs of high index (n =1.95) Si_xN_y and low index (n=1.45) SiO_2 : The device with a structure of DBR substrate/ITO/emissive layer/Ca-Al, emitted EL with a linewidth of only 12 nm. After Ref. [50].

A high device efficiency is not sufficient to ensure device longevity in some cases. Even in the presence of a highly doped PEDOT layer, the properties of the ITO are still crucial to device lifetime. It has been shown that with the ITO anode subjected to an oxygen-plasma treatment, half-brightness (100 cd/m^2) lifetimes were two to five times longer than for untreated samples [57][58]. This may result from inhibition of chemical

processes between the HTL and the ITO, ensured by the treatment, or from physical interaction between the ITO and the HTL, capable of influencing the HTL film forming properties.

For the cathode of PLED devices, Ca is a desirable material. It has a low work function of 3.0 eV, which can lead to a high electron injection level. However, Ca is subject to oxidation because of its reactive characteristics and unstability in air. On the other hand, devices using air-stable metals, e.g., Al with a higher work function of 4.2 eV, suffer from high operating voltages and low efficiencies, which results from poor electron injection. Therefore, composite cathodes such as Ca-Al and Ca-Ag, are commonly used, in which air-stable Al or Ag acts as the protecting layer [12][24][34]. In addition, some other cathode structures like LiF/Ca/Ag and LiF/Al are also regarded as efficient cathodes [35][43][59].

2.5 Blending

In polymer technology, blending is a technique that takes advantage of the processibility of polymers to produce new solid materials or composites with specific structural and physical properties, distinct from those of their components. For PLED application, blending opens a way to improve device performance by enabling both selection of the optimum material for each relevant process (charge transport, charge injection, and luminescence), and also fine tuning of the overall device performance by control of the concentration.

Phase separation commonly exists in polymer blending systems on account of the generally low entropy of the mixing of polymers (Fig. 2.6). During spin-coating, lateral phase domains are formed [60][61]. They either protrude out of the surface (islands) or

form wells into the surface, which has been explained as being driven by the solubility differences of the components in the common solvent [62]. Two separate coexisting phases have different compositions, each consisting dominantly of one of the blend components. There are certain relationships between the morphology of phase separation and PLED device properties.

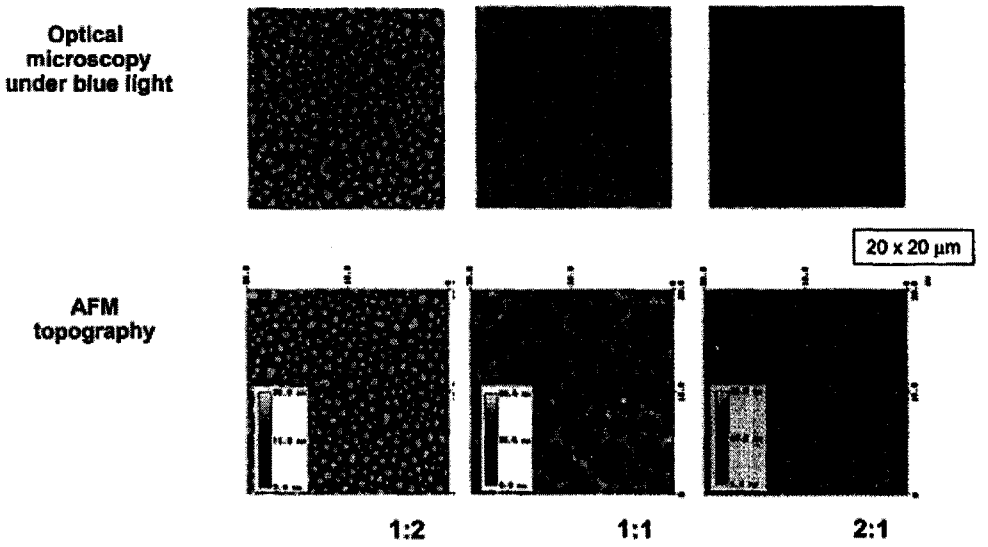

Fig. 2.6 The phase separations observed in optical microscope images and AFM images for various blend ratios in a two-PF system. After Ref. [71].

As an important strategy for improving PLED performance, blending has been exploited extensively in PF-based EL devices. Compared to pure polymers, bend devices displayed strongly enhanced EL efficiencies. Cina, et al. reported an efficient PLED based on a blend of two PFs with the peak efficiencies of 16 lm/W and 11 cd/A, and a high luminance of 100,000 cd/m^2 at about 5.5 V [71]. Dye doping [16][74]-[77], white light emission [24][78][79], improvement of spectral stability [63][73][80], and emission line narrowing [63][73] are other benefits that can be procured from PF blends.

2.6 Recent Progress in the Study of PF-Based LEDs

Recent progress in the study of PF-based LEDs is summarized as follows:

1. **Synthesis of New PFs**: For example, the Dow Chemical Company synthesized new fluorene-based polymers with optimized performance by modifying the polymer compositions so as to increase charge mobilities and to improve the carrier injection balance [13]. A device made of a Dow green emitting polymer has a low turn-on voltage of 2.25 V, and exhibits a peak efficiency of 10.5 cd/A at 6600 cd/m^2 at 4.85 V. This kind of device maintains an efficiency of greater than 10.0 cd/A up to 50,000 cd/m^2, and demonstrates very good stability as exemplified by a device half-life of greater than 1500-h starting from 1100 cd/m^2.

2. **Depression of Low-Energy Emission Band**: The application of blue PF-based LEDs is hampered by a well-documented strong low-energy emission band that converts the desired blue color to blue-green or even yellow. In many reports, the cause has been assigned to aggregates and/or excimers [25][81]-[87], or keto defect [44][88]-[93]. More recently Gamerith, et al. showed that, in addition to the bulk keto emission at 2.3 eV, a second type of defect emission between 2.45 and 2.6 eV can also affect the color purity of PF-based LEDs [94][95]. Although the origin of this long-wavelength emission is the subject of considerable debate in the literature, it has been reported that the spectral stability of PFs can be improved by utilizing molecular modification, refinement of device structure, or blending to suppress the low-energy emission band.

3. **Application in White PLEDs**: In recent reports, PF-based white PLEDs were realized by blending or chemically doping [24][37][78][96]-[101]. Ho, et al. demonstrated white light emission in conjugated polymer homojunctions, i.e., a junction

between two layers with the same host material [78]. One layer is poly(9,9-dioctylfluorene-2,7-diyl) (PFO) host blended with a small amount of MEH-PPV. Another layer is either pure PFO or PFO host blended with green-emitting Dow Chemical LUMATION Green-B PF copolymer. Such homojunction devices were solution processed and showed efficient white light emission. The peak luminance 3000 cd/m^2 is reached at 10 V with CIE coordinate (0.34, 0.34).

4. Combination with Nano Materials: Park, et al. reported stabilized blue emission from polymer-dielectric nanolayer nanocomposites [102]. Blue PF/dielectric nanolayer nanocomposites were prepared by the solution intercalation method and employed in an EL device. By reducing the probability that the excitons initially generated on the PFs will find keto-defects, both the color purity and the luminescence stability were improved.

5. Utilization of SAM-Modified ITO Anode: SAM is used to modify the ITO surface in PF-based LED devices [54]-[56]. In terms of operating voltages, efficiency and luminance, the devices with SAM-modified ITO anode are comparable to, or even better than devices with commonly used PEDOT:PSS as the hole injection layer. Therefore, to modify the anode by depositing SAM opens a way to manufacture high-performance PLEDs with simpler device structures.

CHAPTER 3

MORPHOLOGY AND ELECTROLUMINESCENCE PERFORMANCE OF PF2/6 AND ITS BLENDS WITH PFB

3.1 Introduction

Blending is a common technique used in PF-based light emitting diodes. Thanks to its advantages in processing and many potential applications in PLEDs, blending has been attracting considerable academic interest.

An important physical phenomenon in PF blend systems is phase separation, which results from the low entropy of the mixing of polymers. Many research reports show that the phase-separated morphology of the blends will affect LED device performance [63][65][71][103]-[106]. In order to achieve the desired device properties through control over the phase separation in a blend, understanding the relation between film morphology and device performance is highly desirable. As a rule, charge injection is favored when phase separation perpendicular to the film surface has a configuration such that the phase rich in an electron transporting polymer is close to the cathode, and the phase rich in a hole transporting polymer is close to the anode.

Compared to neat materials, LEDs made of PF blends have shown strongly enhanced EL efficiencies [66]-[70][72][107]. However, the mechanism behind the

improved EL efficiency is not entirely clear. In many reports it is explained by efficient energy transfer through the Forster mechanism [69][77][107]-[109]. Sometimes the EL enhancement is ascribed to increased exciton stability and electron-hole recombination efficiency arising from spatial confinement of excitons [63][110]. Some research groups assign the enhanced EL to a combination of two mechanisms [70][24]. In some cases, it is proposed that improved charge carrier injection is responsible for EL enhancement [67][111]. Recently, Casasanta, et al. suggested that ameliorated aggregate luminescence quenching leads to the improved EL efficiency of their devices [68].

Long wavelength PL and EL band is well documented for blue PF-based LEDs, which changes the expected pure blue emission into an undesired blue-green color. This emission band has been assigned to aggregates and/or excimers [82][85][87], or to an emissive keto defect generated by virtue of thermo-, photo-, or electro-oxidative degradation [91][93]. Recently, Gamerith, et al. showed that in addition to the bulk keto emission at 2.3 eV (around 530 nm), there is another defect emission between 2.45 and 2.6 eV originating from a chemical defect located close to the cathode [95]. Although the origin of this low energy emission is still in debate, many efforts have been made to improve the blue emission of PFs. Blending is one possible solution. Blends of a dilute concentration of hole-transporting molecules with a PF copolymer have been explored to obtain pure blue emission [73]. Blending PF with a high glass transition temperature charge transport or charge blocking polymer also results in increased spectral stability of blue-emitting PFs [63].

Here, we conduct systematic investigations via scanning electron microscopy (SEM) on the film morphology of a PF, poly[9,9-di-(2'-ethylhexyl)fluorenyl-2,7-diyl]

known as PF2/6 [44] or PFE [113], blended with a hole transporting polymer, poly[(9,9-dioctylfluorenyl-2,7-diyl)-co-(N,N'-bis(4-butylphenyl-1,1'-biphenylene-4,4'-diamine))] (PFB). The research results show that the morphology changes significantly with the blend ratio. The polymer solution concentration, substrate and film thickness possibly have an effect on the morphology as well. We also report the use of PF2/6 and its blend with PFB, as a light emitting layer in polymer LEDs with the configuration ITO/PEDOT:PSS/PF2/6 or PF2/6:PFB/Al. Improved brightness and efficiency were observed for the blend based devices. Blending also changes the EL spectrum. Phase separation in the blend film was investigated. The effect that film morphology has on the device performance is tentatively explained. Furthermore, it was noticed that the film thickness of the emissive layer dramatically influences device properties.

3.2 Device Fabrication and Testing

3.2.1 Fabrication

Device structures were fabricated on indium-tin-oxide (ITO) coated glass substrates with a dimension of 25×25×1.1mm and a sheet resistance of 5~15 Ω/□ (Delta's Technologies Limited, Stillwater, MN). The schematic of the devices is shown in Fig. 3.1. The devices have structures sandwiched between Al cathodes and ITO anodes as displayed in Fig. 3.1 (b).

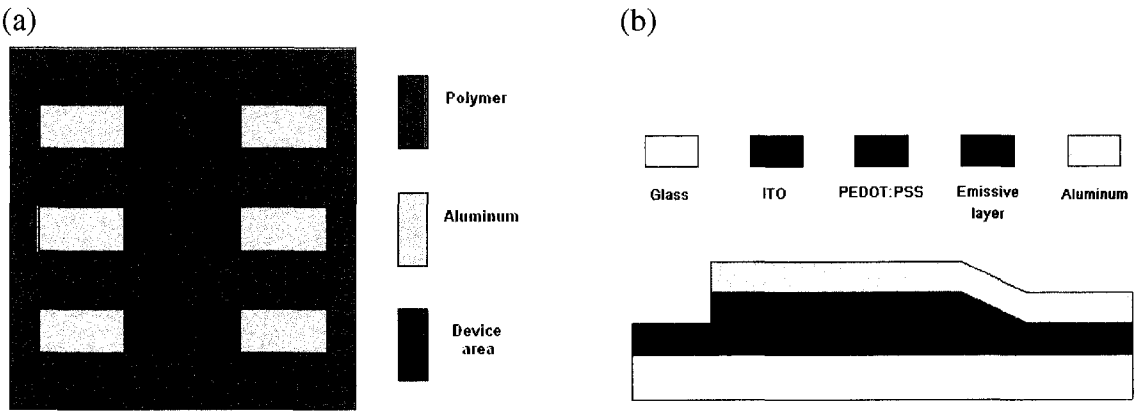

Fig. 3.1 The schematic of PLED devices: (a) the device layout on substrate, and (b) the cross section of the layers of devices.

The device fabrication was carried out under ambient laboratory conditions. The patterned ITO substrates were precleaned by two successive ultrasonic baths in acetone and isopropyl alcohol. After drying them with a nitrogen gun, a 45-nm thick film of poly(3,4-oxyethyleneoxythiophene) doped with poly(styrene sulfonate) (PEDOT:PSS, obtained from Sigma-Aldrich Co., United States) was spin coated over the substrate from a 1.3 wt.% water dispersion. This 50-second spin-coating was done at a speed of 4000 rpm with a ramp of 1000 r/s. The film thickness was measured by an Alpha-Step IQ surface profiler (KLA-Tencor, Mountain View, CA). This film layer can mitigate the roughness of the ITO film, which may lead to electrical contact between anode and cathode. Furthermore, it can lower operating voltages, increase luminescence efficiency, and enhance device lifetimes. These improvements might be due to the reduction of the hole injection barrier at the anode, as well as the formation of a higher built-in field across the emissive layer [112]. Doping PEDOT with PSS increased the conductivity of the film. The emission layer was spin coated from polymer toluene solutions (10 mg/mL) at 2000 rpm for 50 seconds. The filters having a pore size of 0.45 μm (Millipore

Corporation, Bedford, MA) were used to purify the polymer solutions prior to spin-coating. Devices were dried in a vacuum chamber at room temperature for over 24 h before the deposition of the Al film. The manufacturing was completed with thermal evaporation of the aluminum cathode (~200 nm) at 2×10^{-6} Torr through a shadow mask. The equipment used was a DV-502A vacuum evaporator (Denton Vacuum, Moorestown, NJ). The overlap between the two electrodes gave device active areas of 9 mm^2.

The chemical structures of the light emitting material PF2/6 and the hole transporting material PFB are shown in Fig. 3.2. PF2/6 was purchased from Sigma-Aldrich Corporation, United States. It is a yellow-green crystal-like particulate material which is soluble in common organic solvents such as toluene, xylene, $CHCl_3$, and THF. PFB was purchased from American Dye Source, Inc., Canada. This polymer is a light yellow powder and soluble in chloroform, THF, toluene, $CHCl_3$, and dichloroethane. Its molecular weight is 20,000-70,000 as determined by gel permeation chromatography in THF using polystyrene standards.

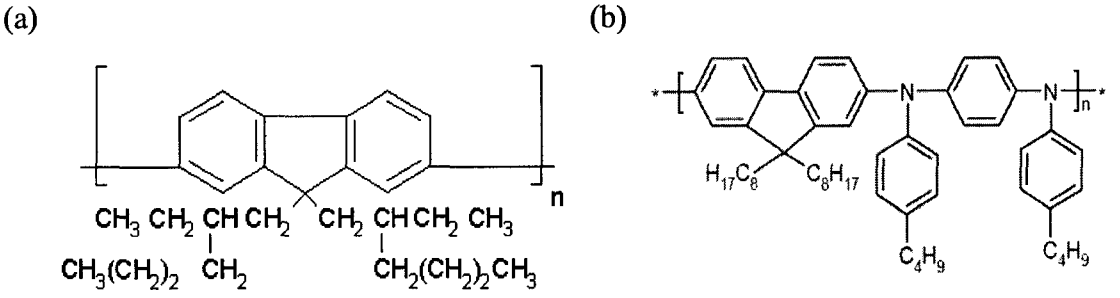

Fig. 3.2 Chemical structures of light emitting polymer and hole transporting polymer: (a) PF2/6, (b) PFB.

PF2/6:PFB blend films for morphology studies were formed by spin casting onto substrates of bare ITO or ITO precoated with 45 nm PEDOT:PSS (the processing details

for preparation of PEDOT:PSS film are described above) from polymer toluene solutions with varied weight ratio. The films on bare ITO have a thickness of 30 nm (that were formed by a 50-second spin-coating at 2000 rpm with a ramp of 1000 r/s), and those on ITO precoated with PEDOT:PSS film have a thickness of 50 nm (which were formed by a 50-second spin-coating at 2000 rpm with a ramp of 500 r/s). EL devices with a configuration of ITO/PEDOT:PSS/emissive layer/Al, were prepared from PF2/6 and its blend with PFB at weight ratio 5 to 1. Two film thicknesses, 40 nm (formed by a 50-second spin-coating at 2000 rpm with a ramp of 1000 r/s) and 50 nm (the processing details were described above), were used for the emissive layer.

3.2.2 Testing

All device testing was implemented in air at room temperature. Current-voltage characteristics were measured on a Keithley 236 source-measure unit (Fig. 3.3 (a)). The power of the EL emission was measured using an ILX Lightwave OMM-6810B equipped with a silicon power/wave head (OMH-6722B) (Fig. 3.3 (b)). The light power testing principle is demonstrated in Fig. 3.4. Electroluminescence (EL) spectra were obtained with a USB 2000 spectrometer (Ocean Optics Inc., Dunedin, FL). By assuming Lambertian distribution of the EL emission, luminance (cd/m^2) was calculated utilizing the forward output light power and the EL spectra of the devices.

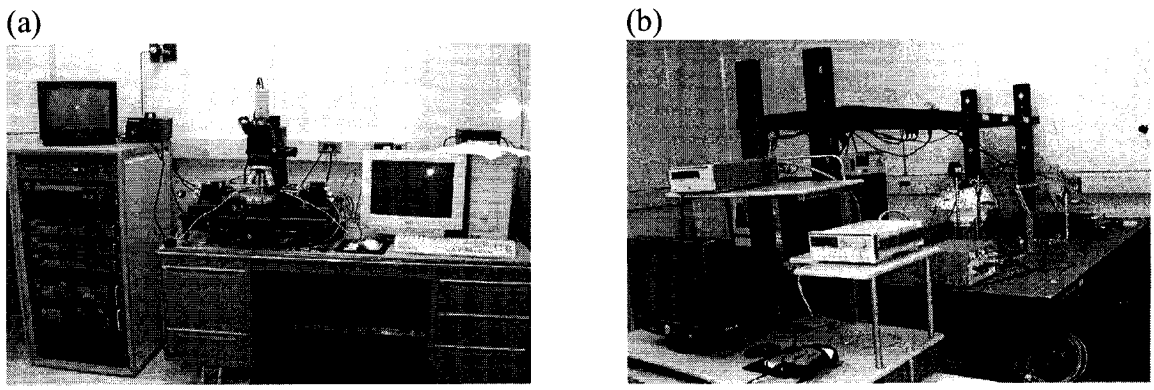

Fig. 3.3 Some testing equipments: (a) Keithley test system, (b) ILX lightpower testing system.

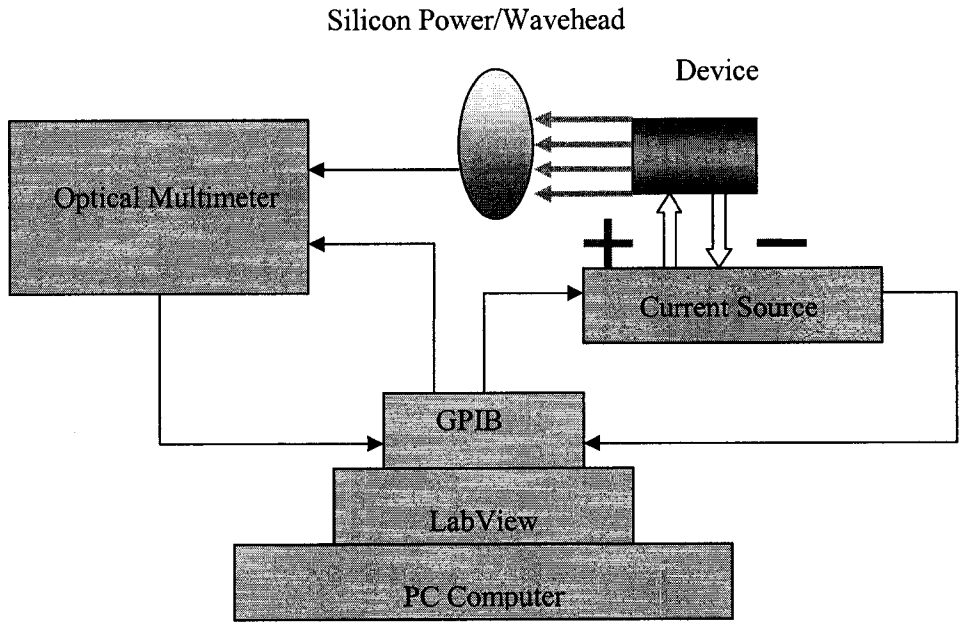

Fig. 3.4 The measurement principle of light power.

The OMH-6722B head, having a power measurement accuracy of ±3.5%, is specified with an NA (numerical angle) of <= 0.3, which means that the collection solid angle ($d\Omega$ in Eq. (1-19)) of ILX testing system is about 35 degrees, that is, 0.2907 sr (Fig. 3.5). In addition, the cosine of the maximum angle from the normal to the plane of the

device ($Cos\frac{35^0}{2}$) is close to unity which corresponds to the direction normal to device plane. The value of dA in Eq. (1-20) is the device area which is 9 mm^2.

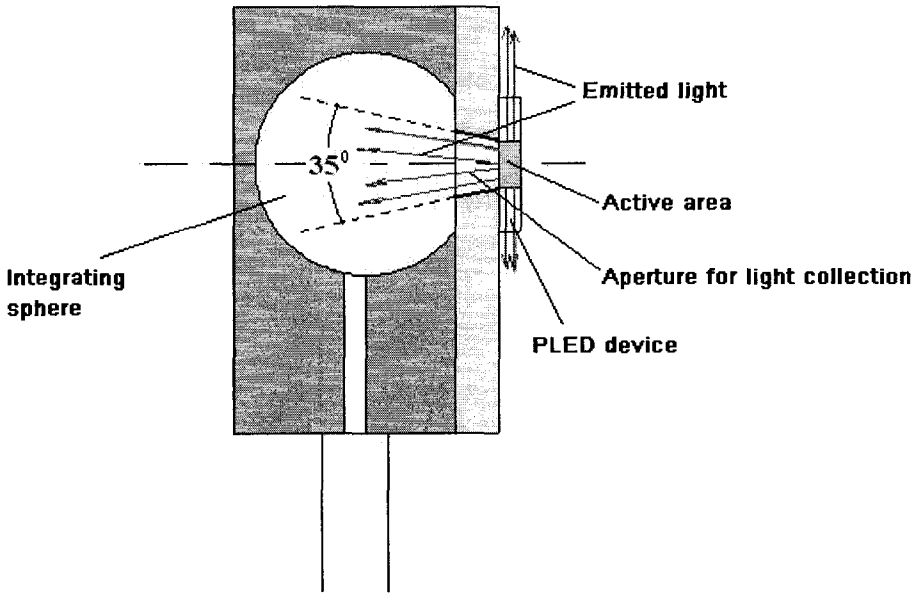

Fig. 3.5 Schematic cross section of the OMH-6722B head.

To prepare samples for optical absorption (UV-Vis) measurements, polymer thin films were spin cast onto quartz plates from polymer toluene solutions (14 mg/mL). The optical absorption (UV-Vis) spectra were recorded with an Agilent-8453 UV-visible spectrophotometer.

The current-voltage characteristics were recorded in a forward sweep mode with a voltage stimulus and an integration of 60 Hz. The light power was measured in a current sweep mode with a wait time of 1200 ms/sample. And the EL spectra were recorded with an integration time of 300 ms.

3.3 Results and Discussion

3.3.1 Energy Band Diagrams of the Materials Used in the PLEDs

Fig. 3.6 shows the energetic positions (eV, below vacuum) of the polymers' frontier levels and electrodes' work functions. The energy levels of PFB are unknown since we have not found them by literature searching. They are represented here by the energy levels of poly((9,9-dioctylfluorene)-alt-bis-N, N'-(4-butylphenyl)-bis-N, N'-phenyl-1, 4-phenylenediamine) (S-PFB) whose chemical structure is similar to that of PFB [65].

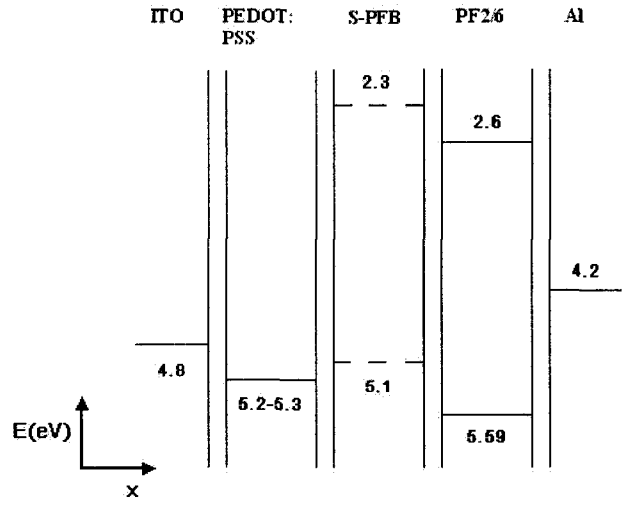

Fig. 3.6 Energetic position, relative to the vacuum level, of the frontier levels of the materials used in the LED structures: The energy levels of PFB are represented by those of S-PFB whose chemical structure is similar to that of PFB.

3.3.2 Morphology of PF2/6:PFB Blends

When two different materials are mixed together, the miscibility between them is determined by the change in the Gibbs free energy of the system, which includes both enthalpic and entropic contributions. In the case of polymer blending, the mixing system does not gain a negative free energy of mixing due to small mixing entropy. As a result,

the separate coexisting phases are produced in the polymer blend film during the spin-coating process and have different compositions, consisting dominantly of one of the blend components. Because of the solubility difference of the components in the common solvent, the film surface undulates, resulting in some domains sticking out of the surface and others falling into the surface [65]. There are many factors which can influence the blend film morphology, including blend ratio, polymer molecular weight, solvent, polymer solution concentration, spin-coating conditions like spin speed and temperature, and so on.

Fig. 3.7 shows the SEM images of the PF2/6:PFB blend films on the bare ITO substrates with varied blend ratio. Snowflake-like bright phase domains, over the length range of 1 μm – 20 μm, are distributed in the dark phase matrix, which may indicate the nucleation and growth type [63]. In general, the separated phases are not made up of a pure component of the blend. The PF2/6-rich phase should contain a trace of PFB, and the PFB-rich phase should include a small proportion of PF2/6. In order to find out which phase is enriched in PF2/6, and which phase is enriched in PFB, further investigations using fluorescence optical microscopy are necessary, in which the difference in PL quantum yield between PF2/6 and PFB is utilized [63]. It is found that the blend ratio strongly affects the film morphology. Both the shape and size of the bright phase domains change with the blend ratio. For the (1:10) and (1:2) ratios, the domains have a larger length in one dimension than in the other dimension. However, for the (1:1) and (2:1) ratios, the length and width of the domains are comparable to each other and the domain length increases with the PFB concentration in the blend. The film surface should be undulant, but the SEM images do not show the height difference between the phase

domains. However, the raised features can be seen by using atomic force microscopy (AFM) [65].

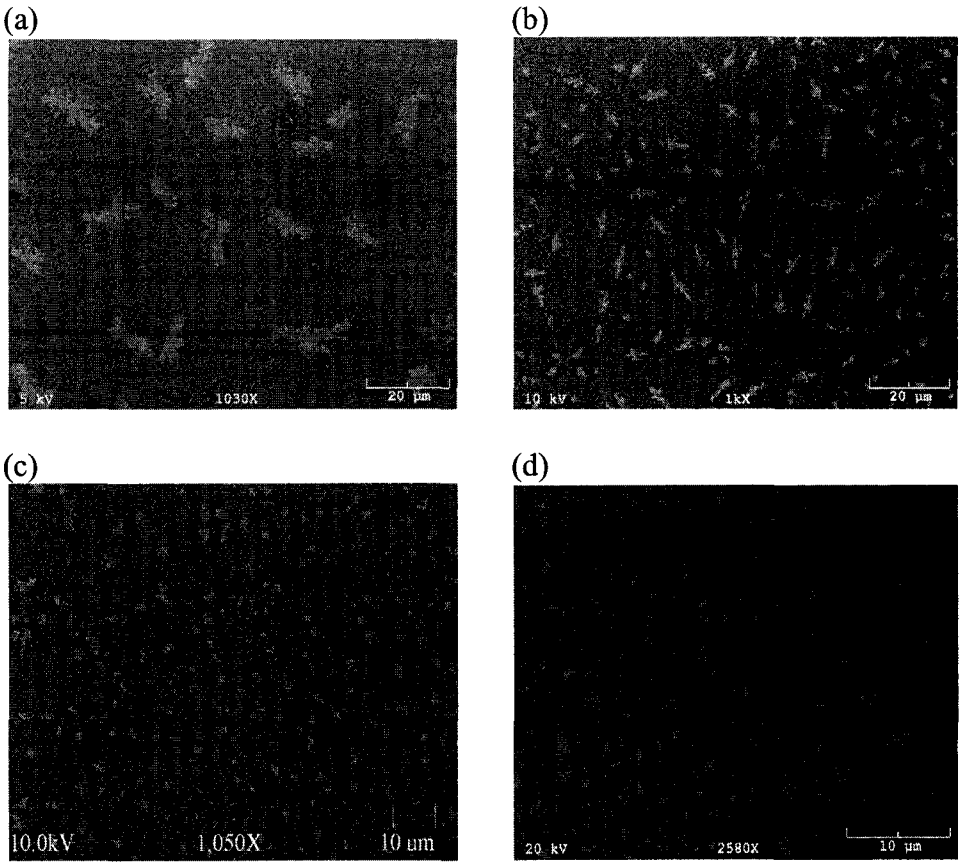

Fig. 3.7 SEM images (Amray-1830, Amray, Inc., Bedford, MA, USA) of the 30 nm-thick thin films of the PF2/6:PFB blends spin-cast from 5 mg/mL solutions in toluene with varied blend ratio over the substrates of bare ITO. The PF2/6: PFB blend ratios are: (a) 1:10, (b) 1:2, (c) 1:1, and (d) 2:1.

Similar to the PF2/6:PFB blend films on the plain ITO substrates, the phase separated morphology of the PF2/6:PFB blend films on the PEDOT:PSS-coated ITO substrates (Fig. 3.8) changes significantly with the blend ratio. However, for all of blend ratios, the length and width of the bright phase domains are nearly equal to each other. Particularly, the bright phase domains for the (5:1) ratio bear a hollowed-out structure. The length of the domains ranges from a few microns to around thirty microns. Contrary

to the films on the bare ITO substrates, the domain length decreases with the PFB concentration in the blend. Furthermore, compared to the (1:1) film on the plain ITO substrate, the morphology of the (1:1) film on the PEDOT:PSS-coated ITO substrate is quite different. These suggest that polymer solution concentration, substrate and film thickness may have an influence upon the film morphology.

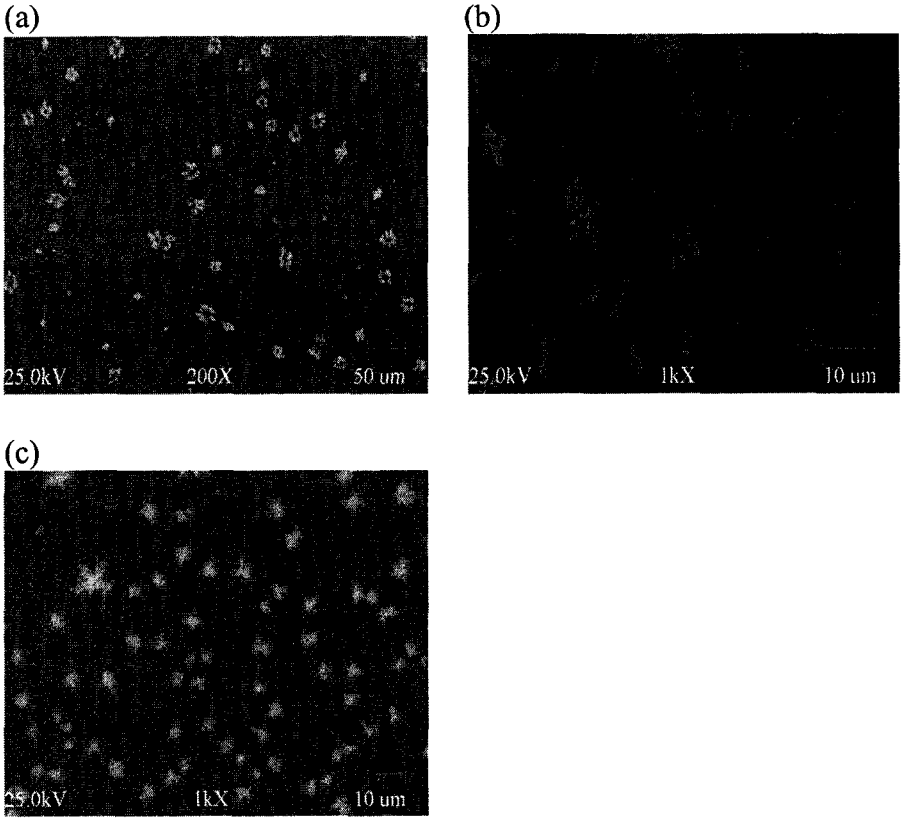

Fig. 3.8 SEM images of the 50 nm-thick thin films of the PF2/6:PFB blends spin-cast from 10 mg/mL solutions in toluene with various blend ratios onto the substrates of ITO precoated with 45 nm PEDOT:PSS. The PF2/6:PFB blend ratios are: (a) 5:1, (b) 1:1, and (c) 1:5.

The way the phase separated morphology affects the device performance is still in debate. Cina, et al. proposed that the ideal morphology corresponding to the best performance perhaps gives rise to a more balanced ratio between the electron and the

hole currents because the changes in morphology are related to changes in the total area in which the two polymers are contiguous to each other [71]. It was reported that in the ideal morphology, the confinement of one phase to a very thin area likely generates locally a very high electric field which helps the charges of one type to overcome the barrier at the polymer-polymer interface and recombine [65]. Kulkarni, et al. believed that the isolated island-like phase domains help confine the excitons in the blends, which is responsible for the observed improvement in the device performance [63].

3.3.3 Electroluminescence Properties

Fig. 3.9 shows the optical absorption (UV-Vis) spectra of thin films of PF2/6 and PFB. The absorption of PF2/6 exhibited an onset at 415 nm and a peak at 362 nm, while the absorption of PFB exhibited an onset at 428 nm and a peak at 399 nm. In addition, PFB UV-Vis spectrum has a shoulder at around 350 nm. The band-gap energies were determined from the optical absorption spectra to be 3.0 eV for PF2/6 and 2.9 eV for PFB, respectively.

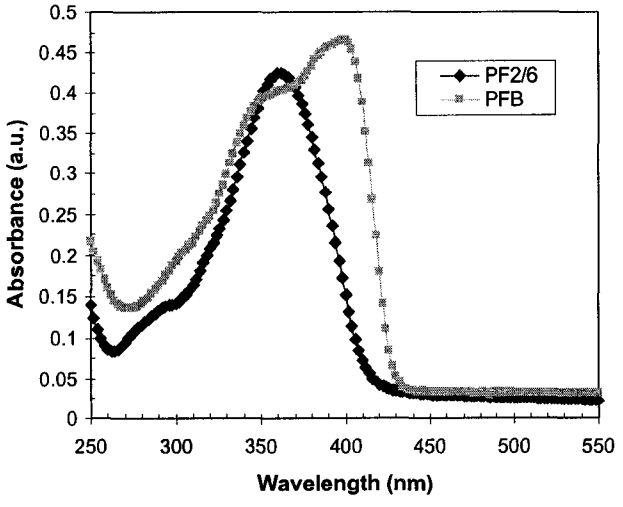

Fig. 3.9 Optical absorption (UV-Vis) spectra of thin films of PF2/6 and PFB.

In comparison with other blend ratios, the devices based on PF2/6:PFB blend at weight ratio 5 to 1 displayed relatively good performance. In addition, according to our research results, the thickness of the emission layer greatly influences the device properties. In our work, the thickness of ~ 40 nm seems to be a relatively ideal one for the active layer. We therefore concentrated the investigations on the EL devices based on the (5:1) PF2/6:PFB blend with a 40 nm-thick emissive layer.

The current-voltage characteristics of the devices are presented in Fig. 3.10. The turn-on voltages, for both the PF2/6 based device and for the device based on PF2/6 blended with PFB, are approximately the same at 2 V. However, compared to the pure PF2/6, the current density is clearly decreased for the case of the blend emission layer, which gives rise to increased efficiency.

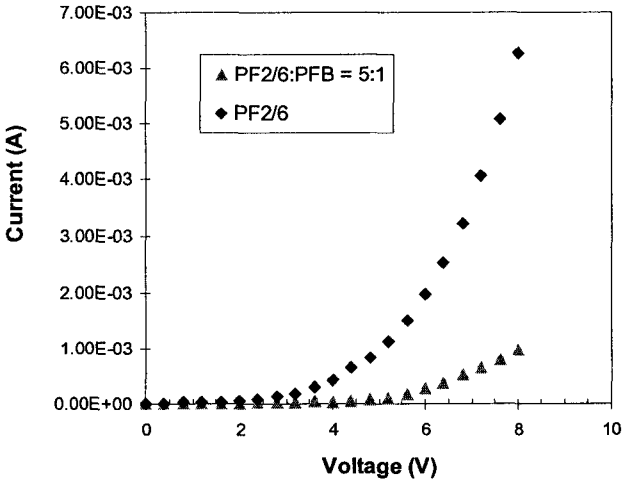

Fig. 3.10 Current-voltage characteristics of the LEDs based on PF2/6 and its blend with PFB.

Fig. 3.11 compares the current dependence of light power for the two device types. The introduction of hole transporting polymer PFB into the emitting layer reduces the threshold current density for light emission from about 96.9 mA/cm^2 to 8 mA/cm^2.

This indicates a better hole/electron balance within the emissive layer, because excessive population of either charge carrier over the other will bring about an increase in current but no emission increase. For the pristine PF2/6 active layer, the maximum brightness is 179 cd/m^2 at 19.22 mA, corresponding to a current density of 214 mA/cm^2. The maximum luminance efficiency and maximum external quantum efficiency were calculated to be 0.084 cd/A and 0.03% at 214 mA/cm^2, respectively. When PF2/6 was blended with PFB, the device performance was enhanced. The luminance reaches 884 cd/m^2 at 38.97 mA, corresponding to a current density of 433 mA/cm^2. The maximum luminance efficiency and maximum external quantum efficiency were 0.21 cd/A and 0.1% at 428 mA/cm^2, improved by a factor of 2.5 and 3.3, respectively. The shoulders in the lightpower-current curves were also observed at around 15.22 mA (pure PF2/6) and 27.22 mA (PF2/6 blend), respectively.

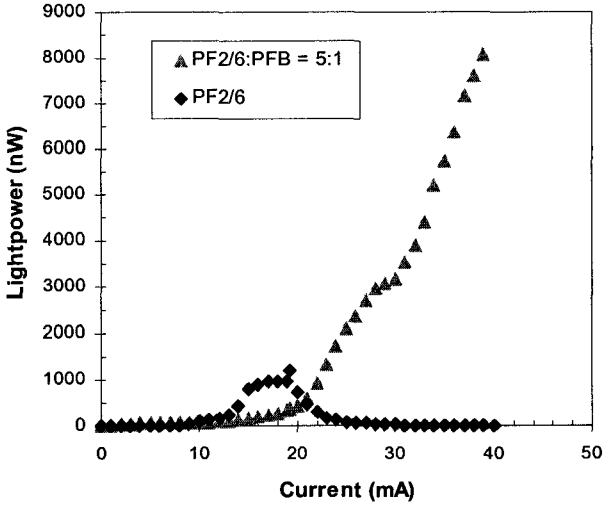

Fig. 3.11 Lightpower-current characteristics of the LEDs based on PF2/6 and its blend with PFB.

The EL spectra are displayed in Fig. 3.12 (a) and (b). For the pristine PF2/6 device, the emission maximum was found to be at 537 nm. For the blend, three main peaks can be identified at 430 nm, 504 nm, and 624 nm. The EL emission maximum was at 504 nm, blueshifted 33 nm in comparison with pure PF2/6.

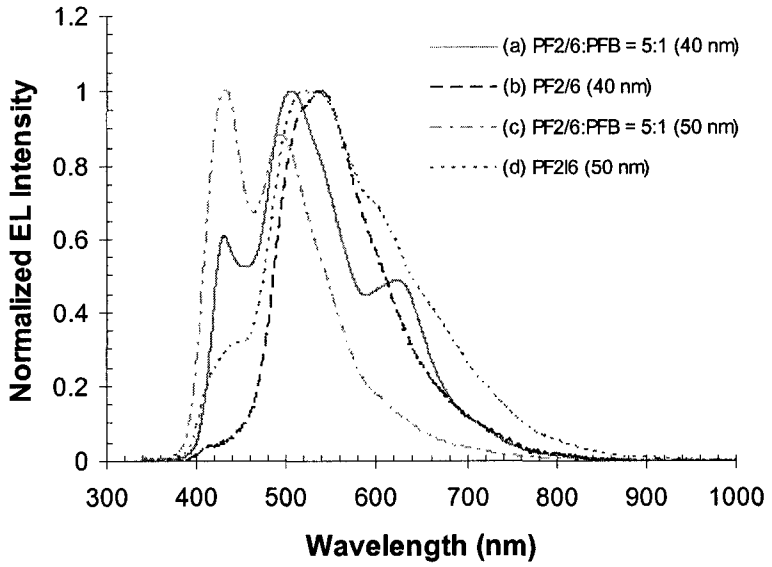

Fig. 3.12 Electroluminescence spectra of the LEDs based on PF2/6 and its blend with PFB: (a) PF2/6:PFB = 5:1, 40 nm-thick active layer, (b) PF2/6, 40 nm-thick active layer, (c) PF2/6:PFB = 5:1, 50 nm-thick active layer, (d) PF2/6, 50 nm-thick active layer.

Generally, large bandgap differences between two polymers are beneficial for energy transfer [65]. The bandgap difference between PF2/6 and PFB is very small (0.1 eV). Furthermore, contrasting the PL spectrum of PF2/6 [44] with the absorption spectrum of PFB, it is found that the overlap between them is poor. As a result, the energy transfer efficiency is expected to be very low. Fig. 3.10 clearly shows that blend devices have lower currents than pure PF2/6 devices, which reveals an increased electron-hole recombination efficiency. Exciton confinement might be an important reason for the improved device performance. On the other hand, as a hole-transporting material, the presence of PFB improves the hole-injection from the anode and the hole

transport through the layer. Moreover PFB is likely to act as hole traps in the host PF2/6. Hole trapping can generate a hole space charge near the anode, which can cause a redistribution of the internal electric field to facilitate the electron injection from the cathode [63][72]. We therefore propose that the enhancement of device properties may be due to both exciton confinement and enhanced charge carrier injection.

The change in the EL spectra is noticeable. Both spectra are dominated by the low-energy emission. However, it is observed that the EL emission band of the blend is blueshifted relative to that of neat PF2/6. The possible reason for this blueshift is a reduction in the interchain interactions which result from the dilution effect of blending [24]. The contribution from the PFB emission might affect the EL spectrum as well. Actually in addition to a hole transporting polymer, PFB is also a light emitting polymer and it is possible that some energy was transferred from PF2/6 to PFB.

The SEM images in Fig. 3.13 (a) and (b) show the lateral phase-separated morphology in the present 40 nm-thick film of the PF2/6 blend with PFB. Some bright phase domains take on a leaf-like shape, which are formed in the homogeneous dark background of the other phase. Other snowflake-like bright phase domains disperse between the "leaves" or inside the "leaves". The morphology of conjugated polymer blends is known to have an effect on the device properties of PLEDs. The film morphology might affect device performance by influencing the effectiveness of the exciton spatial confinement effects [63]. It is also likely that one phase (PFB) is confined to a very thin region, which produces a very high local electric field [65]. Thanks to this high electric field, the holes can surmount the energy barrier at the polymer-polymer interface to recombine with electrons, and thus resulting in emission. Here snowflake-like

phase domains might act to confine excitons, while "leaves" may facilitate the creation of a high local electric field.

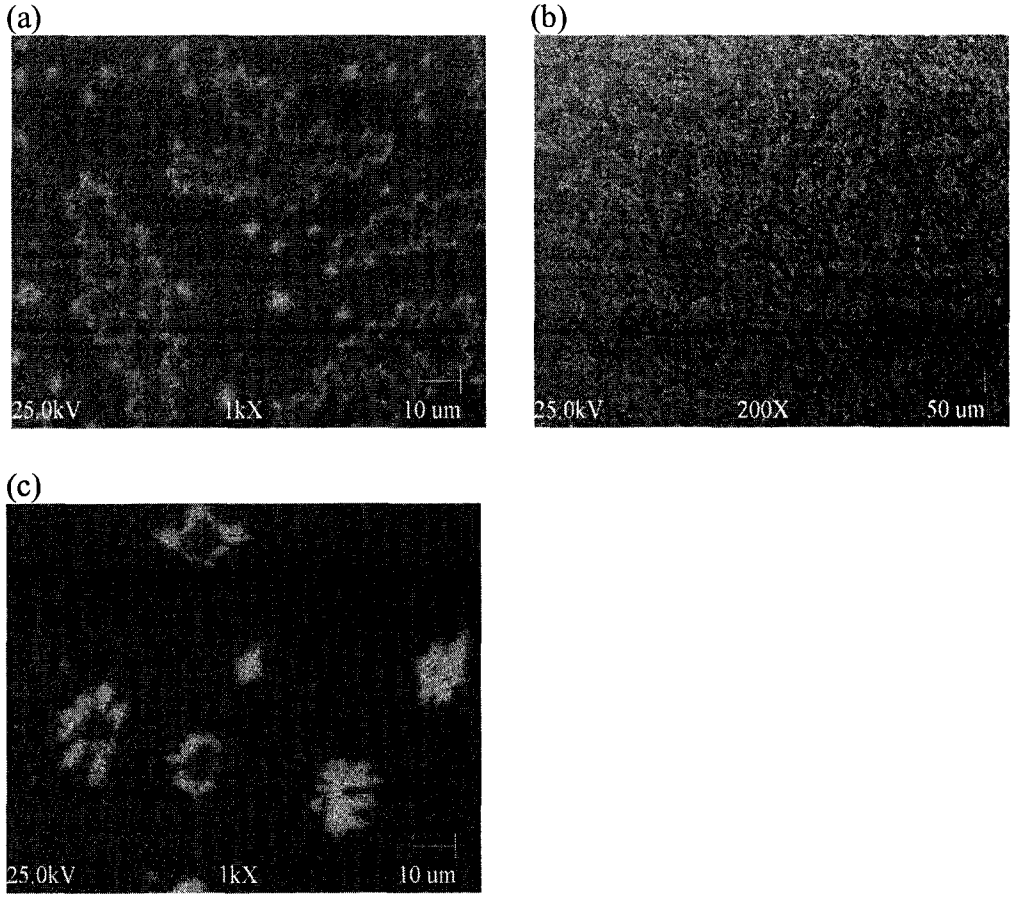

Fig. 3.13 (a) SEM image of a 40 nm-thick thin film of the blend PF2/6:PFB (5:1) spin-coated from 10mg/mL solution in toluene on a substrate of ITO, precoated with 45 nm PEDOT:PSS, (b) SEM image of the same thin film of the blend PF2/6:PFB (5:1) as in (a), (c) SEM image of the same thin film of the blend PF2/6:PFB (5:1) as in Fig. 3.8 (a).

Compared with the devices with a 40 nm-thick emissive layer, the performance of the devices that have an active layer of 50 nm is very poor, which implies that the thickness of the emission layer can strongly influence the device properties. The film morphology is perhaps one of the reasons that made the great difference since the phase separated morphology of the 50 nm film (Fig. 3.13 (c)) is quite dissimilar to that of the 40

nm film (Fig. 3.13 (a) and (b)) even though all other conditions are the same. However, very intriguingly, the bright phase domains in both films present a hollowed-out structure, which were not seen in the films of the other blend ratios.

Although the devices with a 50 nm active layer exhibited very poor performance, the low energy emissions from them were ameliorated significantly in comparison with the devices with a 40 nm emissive layer. This is especially evident for the blend based devices. As shown in Fig. 3.12 (c), their EL spectrum peaks at 431 nm and 494 nm. The EL intensity reaches the maximum at 431 nm, which is blueshifted 73 nm relative to the 40 nm emission layer. For the neat PF2/6 devices with a 50 nm active layer, the EL emission maximum is at 521 nm (Fig. 3.12 (d)), blueshifted 16 nm in comparison with the 40 nm emissive layer. Two shoulders are identified at around 444 nm and 605 nm.

EL intensity-current characteristics of the blend based devices with 40 nm and 50 nm active layer is shown in Fig. 3.14. For the 40 nm emission layer, the threshold current for light emission is 0.72 mA, the same as the 50 nm active layer. However, its EL intensity reached a maximum at 38.97 mA, while for the 50 nm active layer the EL maximum was at only 6.47 mA. This indicates that the devices with a 50 nm emissive layer operate under much lower current than those with a 40 nm emission layer. The great variance in operating current suggests that the increased current may possibly have deteriorated the long wavelength emissions. This is in agreement with what was reported in some publications, in which the long wavelength EL bands are partly attributed to electro-oxidative degradation.

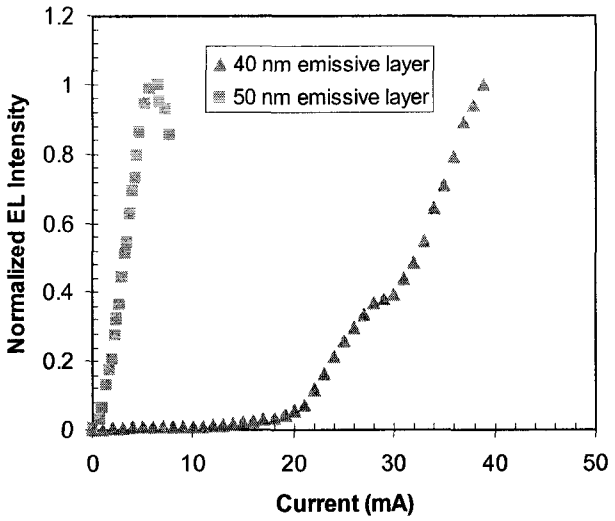

Fig. 3.14 EL intensity-current characteristics of the PLEDs based on (5:1) PF2/6:PFB blend.

3.4 Summary

In this chapter, we investigated the film morphology of the PF2/6:PFB blends. The blend ratio is a very important factor that influences the blend film morphology. It is likely that the polymer solution concentration, substrate and film thickness affect the morphology as well. We demonstrated light-emitting diodes based on PF2/6 and its blend with PFB. Adding a hole-transporting polymer to the emissive layer causes an improvement in device performance. At a current density of 433 mA/cm^2, the blend based device showed a maximum luminance of 884 cd/m^2. The maximum external quantum efficiency reached 0.1% at 428 mA/cm^2, increased by a factor of 3.3 compared to pure PF2/6. The long wavelength emission was suppressed to a certain extent in the blend LEDs. We propose that the morphology of phase-separated domains in the blended film has an influence on the enhancement of device properties. The research also showed that the film thickness of the emissive layer has a great effect on the device performance.

CHAPTER 4

DEVICES BASED ON PF2/6 WITH END CAPPERS

4.1 Introduction

End-capping is one of the strategies in macromolecular engineering which can be exploited to modify polymer properties to satisfy specific application requirements. For PLED applications, end-capping has been directed toward improving device efficiency [15][114]-[117], stabilizing blue emission [15][117][118][119], as well as tuning the emission color [114][115]. As a means for increasing PLED device performance, end-capping will not result in phase separation (a common phenomenon in polymer blend systems) with time and does not alter the electronic properties of the polymer backbone [15]. Furthermore, when end-capped with some hole transport moieties, polyfluorenes can become more resistant to oxidation [120].

In some literature sources, the enhancement in PLED device efficiency is ascribed to the improved charge carrier injection resulting from polymer end-capping [15][116][117]. Miteva, et al. reported PLED devices made from PF2/6 end-capped with N,N-bis(4-methylphenyl)-N-phenylamine (TPA) [15]. Compared to the devices made from PF2/6, the improved device performance (a maximum luminance of 1600 cd/m^2

with an efficiency of 1.1 cd/A) was observed from the end-capped PF2/6 devices. It was proposed that most holes in the layers of the end-capped PF2/6 might be directed to the end-capper groups instead of sites with less efficient emission, which subsequently recombined the electrons on the PF main chain. However, Nakazawa, et al. believed that the position of the exciton recombination zone has an effect on light emission and device efficiency [117]. They suggested that end-capping gives rise to improved hole injection, which moves the recombination zone away from the polymer/anode interface. In addition to the end-capped polymers used as light emitting materials, the polymers with end-cappers can also act as Hole Transport Layers (HTL) to increase device efficiency via improving charge carrier injection. Jikei, et al. synthesized hyperbranched poly(triphenylamine)s with end functional groups that were examined as hole transporting materials for Organic Light Emitting Diodes (OLEDs) [116]. When the polymer end-capped with alkyl chlorides was used as the HTL, the devices composed of ITO/ hyperbranched poly(triphenylamine)s with end capper/ Alq_3/Mg-Al exhibited the best performance (a maximum luminance of 1110 cd/m^2 and a current efficiency of 0.63 cd/A at a current density of 100 mA/cm^2). There is a small energy difference between Alq_3 and HTL, which could cause the efficient hole injection from ITO electrode to Alq_3. Energy transfer is another mechanism behind the enhanced efficiency resulting from end-capping. Polyfluorene derivatives endcapped with 1,8-naphthalimide dye have been synthesized [115]. Their EL emission is predominantly composed of the contribution from the 1,8-naphthalimide unit. The NFP50 based devices with a configuration of ITO/PEDOT/polymer/Ca/Al displayed the current efficiency of 7.40 cd/A, the power efficiency of 2.89 lm/W, and the maximum brightness of 19280 cd/m^2, which is about 30

times more efficient than that of non-end-capped polyfluorene. Energy transfer and charge trapping from polyfluorene backbone to 1,8-naphthalimide dye should be responsible for the enhancement in device performance.

It has been observed that end-capping can be employed to significantly suppress troublesome green emission in PFs. Many end-cappers have been found to have a great influence upon prevention of PF long wavelength emission, among which are mono-functional fluorene derivatives [84], anthracene [121], crosslinkable moieties [122][39], hole-trapping groups [15], sterically hindered groups [26][123], polyhedral oligomeric silsesquioxanes [124], and so on. A few mechanisms have been proposed to explain the role end-capping plays in reducing the low energy emission band. Miteva, et al. suggested that, in the devices based on the end-capped PFs, the chain ends, rather than aggregates and excimer forming sites, preferably become the places where the electron-hole recombinations occur [15]. Nakazawa, et al. assigned the suppression of green emission to the shift of the recombination zone away from the polymer/anode interface, since the PF molecules only have strong interchain interactions near the anode interface but not in the bulk [117]. Recently Kadashchuk, et al. found that PFs end capped with certain hole-transporting molecules, like triphenylamine derivatives, demonstrate high stability against oxidation, which gives rise to considerably decreased concentration of keto defects (another possible origin of green emission).

Color conversion is another effect that has been observed in end-capped polymers. MEH-PPV end-capped with coumarin has been synthesized [114]. PLED devices based on these MEH-PPV derivatives demonstrated yellow EL with its maximum emission at 560 nm, blueshifted by around 40 nm with respect to that of MEH-PPV. As

mentioned above, for the devices fabricated with the polyfluorene derivatives endcapped with 1,8-naphthalimide dye as the emitter, EL emission was dominated by the contribution from the 1,8-naphthalimide unit due to energy transfer from polyfluorene backbone to 1,8-naphthalimide dye [115].

In this work, we fabricated and characterized PLED devices based on PF2/6 end capped with Dimethylphenyl (DMP) and TPA. Compared to PF2/6 based devices, end-capped PF2/6 devices displayed improved properties in terms of luminance and efficiency. Predominant long wavelength emission observed in PF2/6 was significantly suppressed in end-capped PF2/6. The role played by end-capping on the enhancement of device performance and color stability is discussed.

4.2 Experimental

The chemical structures of the end-capped polymers used in our study are shown in Fig. 4.1. Both PF2/6 end-capped with DMP and TPA were synthesized by American Dye Source, Inc. They are a light yellow powder, and highly soluble in toluene and tetrahydrofuran. Their molecular weight ranges from 40,000 to120,000.

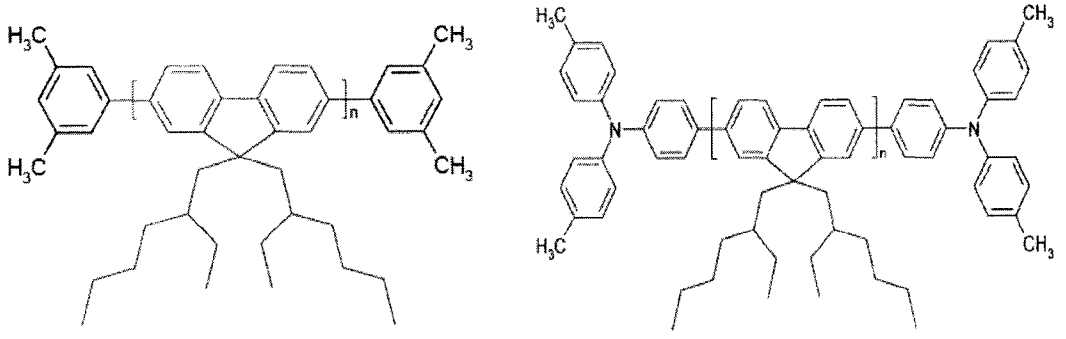

PF2/6 end-capped with DMP PF2/6 end-capped with TPA

Fig. 4.1 The chemical structures of PF2/6 end capped with DMP and TPA.

The preparation of the films for the measurement of optical absorption spectra was described in detail in Chapter 3. The EL devices were fabricated at ambient conditions on glass substrates covered by patterned ITO electrodes. The ITO substrates were precleaned by two successive ultrasonic rinses in acetone and isopropyl alcohol. After drying them with a nitrogen gun, a 45-nm thick film of PEDOT:PSS was spin coated over the substrate from a 1.3 wt.% water dispersion. The spin-coating was done at a speed of 4000 rpm with a ramp of 1000 r/s for 50 seconds. The emissive layers consisted of PF2/6 end-capped with DMP or TPA. They were formed at the top of PEDOT:PSS films by a 50-second spin casting from polymer toluene solutions (10 mg/mL) at a speed of 2000 rpm that was reached via a ramp of 1000 r/s. The filters having a pore size of 0.45 μm (Millipore Corporation, Bedford, MA) were used to purify the polymer solutions prior to spin-coating. The thickness of the DMP-end-capped PF2/6 film is 70 nm, and that for TPA-end-capped PF2/6 film is 80 nm. Devices were dried in a vacuum chamber at room temperature for a minimum of 24 hrs before the deposition of the Al film. The manufacturing was completed with the thermal evaporation of the aluminum cathode (~200 nm) at 2×10^{-6} Torr through a shadow mask. The overlap between the two electrodes gave device active areas of 9 mm^2.

The equipment used for the measurement of current-voltage characteristics, light power, EL spectra and optical absorption spectra were described in Chapter 3. The current-voltage characteristics were recorded in a forward sweep mode with a voltage stimulus and an integration of 60 Hz. The light power was measured in a current sweep mode with a wait time of 1200 ms/sample. It was observed that the devices began to

degrade after the maximum light power levels were reached. The EL spectra were recorded with an integration time of 300 ms.

4.3 Results and Discussion

Fig. 4.2 shows the energetic positions (eV, below vacuum) of the polymers' frontier levels and electrodes' work functions. The energy levels of end-capped PF2/6s are unknown since we have not found these values by literature searching. They are represented here by the energy levels of PF2/6 [113] whose chemical structure is similar to those of end-capped PF2/6s.

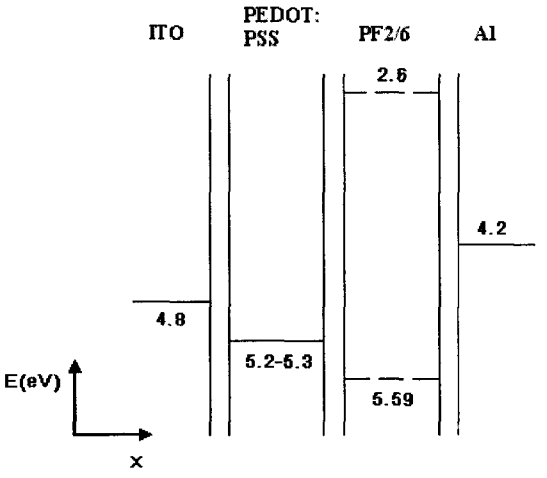

Fig. 4.2 Energetic position, relative to the vacuum level, of the frontier levels of the materials used in the LED structures: The energy levels of end-capped PF2/6s are represented by those of PF2/6 whose chemical structure is similar to those of end-capped PF2/6s.

The optical absorption (UV-Vis) spectra of thin films of PF2/6 and end-capped PF2/6 are shown in Fig. 4.3. The UV-Vis spectra of DMP- and TPA-terminated PF2/6 are very similar to each other. The absorption of DMP-terminated PF2/6 had an onset at 425 nm, the same as that of TPA-terminated PF2/6. And both spectra exhibited a peak at

nearly the same wavelength. However, the optical absorption spectra of PF2/6 with end-capper groups were clearly red-shifted compared to that of PF2/6. Table 4.1 summarizes the film optical absorption properties of PF2/6 and PF2/6 end-capped with DMP and TPA.

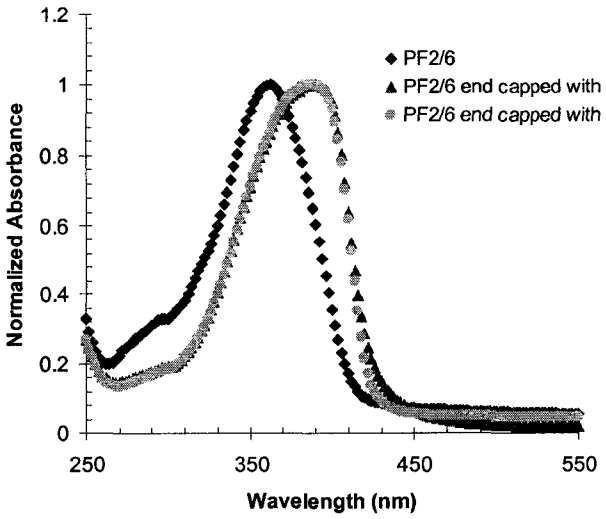

Fig. 4.3 UV-Vis spectra of PF2/6, and PF2/6 end-capped with DMP and TPA.

Table 4.1 Film optical absorption properties for PF2/6 and end-capped PF2/6.

Polymers	PF2/6	PF2/6 end capped with DMP	PF2/6 end capped with TPA
λ_{onset} (nm)	415	425	425
$E_{band-gap}$ (eV)	3.0	2.92	2.92
λ_{peak} (nm)	362	389	387

λ_{onset} : Onset wavelength.
$E_{band-gap}$: Band-gap energy.
λ_{peak} : Peak wavelength.

Fig. 4.4 shows the current density-electric field characteristics of PLEDs based on PF2/6 and PF2/6 end-capped with DMP and TPA (electric fields are calculated by using

applied bias divided by the thickness of the emissive layer). The turn-on voltage of PF2/6 based devices was around 2 V, while those for end-capped PF2/6 devices were around 5 V. It was observed that, in the low field region, the current density passing through the PF2/6 device is slightly higher than that through the end-capped PF2/6 devices. However it seems that for the end-capped PF2/6 devices the current densities increase faster with electric field than that for the PF2/6 device. And it is especially notable that the current density through the device based on PF2/6 end-capped with TPA increases drastically at high fields.

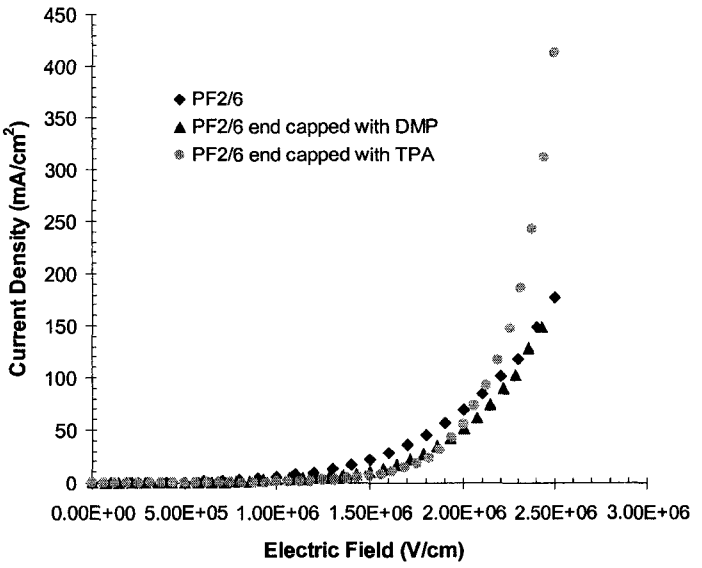

Fig. 4.4 Current density-electric field characteristics of EL devices based on PF2/6 and end-capped PF2/6.

Fig. 4.5 displays light power as a function of the current for the three types of devices under study. Using the data shown in Fig. 4.5, we calculated brightness, luminance efficiency, and external quantum efficiency at different currents. Table 4.2 presents a comparison of the EL performance of the three kinds of devices. End -capping decreases the threshold current for light emission from 96.9 mA/cm^2 to 2.4 (DMP-end-

capped PF2/6) and 1.2 mA/ cm^2 (TPA-end-capped PF2/6), which suggests that there is better balance between holes and electrons within the end-capped PF2/6 emission layer. The charge balance between holes and electrons significantly affects the device efficiency because a surplus of either of the charge carriers results in a current increase that does not enhance the emission, but raises Joule heating which causes more rapid polymer degradation [73][125]. In comparison with the devices based on non-end-capped polymer, end-capping improves EL properties in light of luminance and efficiency. The best performance is observed for DMP-end-capped PF2/6 devices with a maximum luminance of 381 cd/m^2 at 122 mA/cm^2, a maximum luminance efficiency of 0.319 cd/A at 117 mA/cm^2, and a maximum external quantum efficiency of 0.16 % at 117 mA/cm^2, which is higher than the PF2/6 devices by a factor of 2.1, 3.8 and 5.3, respectively. Efficient hole trapping at the end-capper groups may be a reason for the observed performance improvement. The end-cappers may show preference for the sites with less efficient emission when they compete with each other with respect to hole trapping in the active layer [15]. On the other hand, trapping of holes will create a space charge field, which brings about a redistribution of the internal field, and thus an improved charge carrier balance [73][63]. Another possible explanation is the shift of the position of the exciton recombination zone, which is believed to have an influence on the device efficiency [117]. End-capping possibly increases hole injection, which will move the exciton recombination zone from the polymer/anode interface into the bulk of the light emitting polymer.

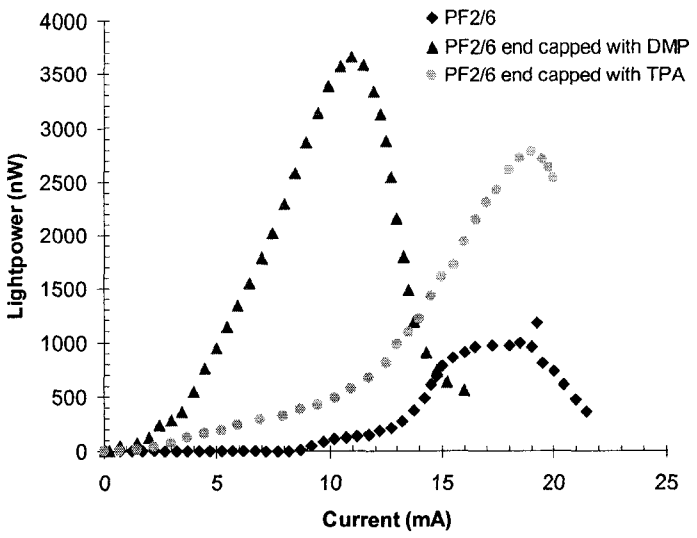

Fig. 4.5 Light power-current characteristics of EL devices based on PF2/6 and end-capped PF2/6.

Table 4.2 EL performance for the devices based on the three kinds of Light Emitting Polymers (LEPs).

LEPs	*PF2/6*	*PF2/6 end capped with DMP*	*PF2/6 end capped with TPA*
d_{EL} (nm)	40	70	80
$J_{threshold}$ (mA/cm^2)	96.9	2.4	1.2
V_{on} (V)	2	5	5
B_{max} (cd/m^2)	179	381	327
η_{max} (%)	0.03	0.16	0.069
LE_{max} (cd/A)	0.084	0.319	0.156
λ_{peak} (nm)	537	420, 445, 485 (maximum)	422, 443, 512 (maximum)

d_{EL} : Thickness of emissive layer.

$J_{threshold}$: Threshold current density for light emission.

V_{on} : Turn-on voltage for the current at which the current reaches $\sim 8.5\times10^{-5}$ A.

B_{max} : Maximum luminance.

η_{max} : Maximum external quantum efficiency.

LE_{max} : Maximum luminance efficiency.

λ_{peak} : EL peak wavelength.

As shown in Fig. 4.6, end-capping significantly suppresses the long wavelength emission that is overwhelming in the PF2/6 EL spectrum. The blue excitonic emission bands that display the intrinsic characteristics of PFs become predominant in EL emission from end-capped PF2/6. It is especially pronounced for DMP-end-capped PF2/6. Its EL peaks at 420 nm, 445 nm, and 485 nm, which all fall into violet-blue region. The maximum intensity is at 485 nm, blue shifted by 52 nm relative to that of PF2/6. There are a few possible reasons for the greatly improved blue emission. In the end-capped PF2/6 emissive layer, the main body of holes may be trapped by the end-cappers, which leads to much fewer electron-hole recombinations taking place at aggregates or excimer forming sites than those in the PF2/6 active layer [15]. Another possible explanation is that the improved hole injection resulting from end-capping shifts the exciton recombination zone away from the polymer/anode interface, where the PF molecules are believed to have strong interchain interactions [117]. It is also likely that end-capping enhances the resistance of PFs to oxidation, hence considerably decreasing concentration of keto defects [120].

Miteva, et al. reported PLEDs based on TPA-end-capped PF2/6 that displayed a maximum luminance of 1600 cd/m^2 with an efficiency of 1.1 cd/A [15]. There are a few reasons for the better performance figures from Miteva, et al. The TPA-end-capped PF2/6 they used had an optimized monomer/end-capper feed ratio of 4 mol-% and Ca/Al composite cathodes were used. The device characterization was carried out in an evacuated sample chamber. The difference in device area (5 mm^2 in their case) could also affect properties.

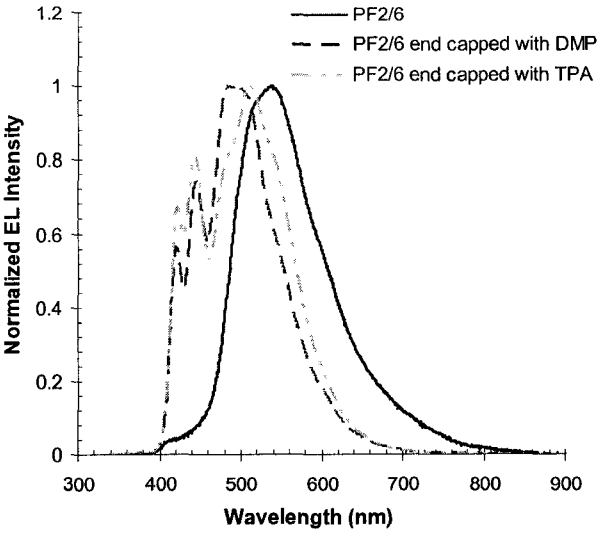

Fig. 4.6 EL spectra of the LEDs based on PF2/6 and end-capped PF2/6.

4.4 Summary

We used end-capped PF2/6 as active layers to fabricate PLED devices. Investigation results demonstrate that end-capping PF2/6 with DMP and TPA clearly improves device properties, significantly suppressing green emission bands. The best performance is observed for devices with a DMP-end-capped emissive layer which exhibited a maximum luminance of 381 cd/m^2, a maximum luminance efficiency of 0.319 cd/A, and a maximum external quantum efficiency of 0.16 %, which is 2-6 times higher than those of the PF2/6 LEDs. All three EL peaks belong to the violet-blue zone with a maximum emission at 485 nm, having a blue shift of 52 nm with respect to that of the PF2/6 based devices. The role played by end-capping in the enhancement of device properties and blue emission is discussed.

CHAPTER 5

DEVICES BASED ON F8BT AND ITS BLENDS WITH PPB

5.1 Introduction

There are much fewer n-type polyfluorenes (PFs) than p-type ones because of the susceptibility of polymers to oxidation and the typically smaller injection barriers at the anode/polymer interface [13]. Chemically some modifications have been carried out to improve electron transport in PFs, which include the incorporation of electron-transporting moieties into the PF polymer chain [126], as well as end-capping the polymer with electron-transporting moieties [127]. The green-emitting alternating copolymer poly(9,9'-dioctylfluorene-alt-benzothiadiazole) (F8BT) is a known electron transporting polyfluorene copolymer. It combines high electron mobility with high electron affinity, which leads to easy electron injection [40]. In recent years, F8BT has attracted considerable academic interests in PLED applications. Although PLEDs featuring neat F8BT displayed good EL performance [38][45], more commonly F8BT was blended with other polymers such as Poly(9,9-dioctylfluorene) (PFO) and poly((9,9-dioctylfluorene)-alt-N-(4-butylphenyl)diphenylamine) (TFB) to act as the active layer in EL devices because the device properties were greatly enhanced upon

doping [111][65]. Some researchers conducted investigations on film morphology of F8BT blends, trying to find out the relationship between PLED device performance and the phase-separated morphology of the blends [65][103][104][106][128][129].

Here, we report on the fabrication and characterization of LEDs based on poly[(9,9-dioctylfluorenyl-2,7-diyl)-co-(1,4-benzo-{2,1'-3}-thiadiazole)] (F8BT). The light emitting polymer thin film layer was either pristine F8BT or the polyfluorene copolymer blended with the hole transport material poly(N,N'-bis(4-butylphenyl)-N,N'-bis(phenyl)benzidine) (PPB). Although doping did not affect the EL spectrum, an enhancement in device properties was observed for blend based devices. The origin of the EL improvement is discussed.

5.2 Experimental

Molecular structures of F8BT and PPB used in our study are shown in Fig. 5.1. Both polymers were obtained from American Dye Source, Inc., Canada. F8BT is yellow powder, while PPB is light yellow powder. They are highly soluble in toluene and tetrahydrofuran. Their molecular weights are around 44,000 and 12,000, respectively, as determined by gel permeation chromatography using polystyrene standards.

The preparation of the films for the measurement of optical absorption spectra was described in detail in Chapter 3. The EL devices were fabricated at ambient conditions on glass substrates covered by patterned ITO electrodes. The ITO substrates were precleaned by two successive ultrasonic baths in acetone and isopropyl alcohol. After drying them with a nitrogen gun, a 45-nm thick film of PEDOT:PSS was spin coated over the substrate from a 1.3 wt.% water dispersion. The spin-coating was done at a speed of 4000 rpm with a ramp of 1000 r/s for 50 seconds. The emissive layers

consisted of pure F8BT and its blends with PPB at varied weight ratio. They were formed on top of the PEDOT:PSS films by a 50-second spin casting from polymer/toluene solutions (10 mg/mL) at a speed of 2000 rpm that was reached via a ramp of 1000 r/s. The filters having a pore size of 0.45 μm (Millipore Corporation, Bedford, MA) were used to purify the polymer solutions prior to spin-coating. The achieved film thicknesses were around 55 nm. Devices were dried in a vacuum chamber at room temperature for a minimum of 24 hrs before the deposition of Al film. The fabrication was completed with the thermal evaporation of the aluminum cathode (~200 nm) at 2×10^{-6} Torr through a shadow mask. The overlap between the two electrodes gave device active areas of 9 mm^2.

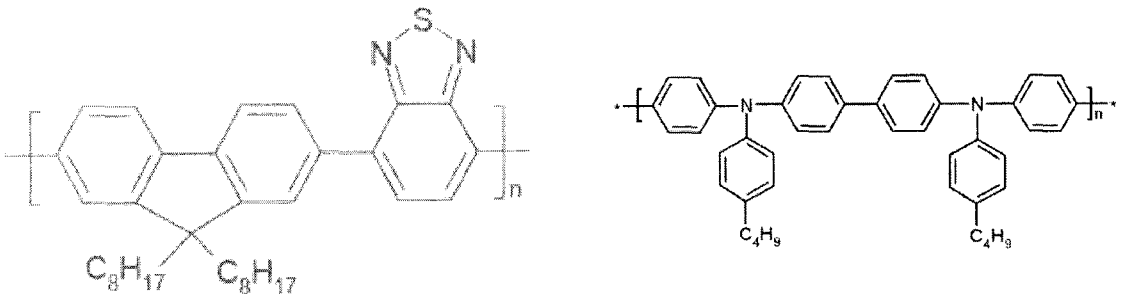

F8BT PPB

Fig. 5.1 Molecular structures of F8BT and PPB used in this study (refer to the webpage of American Dye Source, Inc.).

The equipment for the measurement of current-voltage characteristics, light power, EL spectra and optical absorption spectra were described in Chapter 3. The current-voltage characteristics were recorded in a forward sweep mode with a voltage stimulus and an integration of 60 Hz. The light power was measured in a current sweep mode with a wait time of 1200 ms/sample. It was observed that the devices began to

degrade after the maximum light power levels were reached. The EL spectra were recorded with an integration time of 300 ms.

5.3 Results and Discussion

Fig. 5.2 shows the energetic positions (eV, below vacuum) of the polymers' frontier levels and electrodes' work functions. The energy levels of PPB were not published in the available literature and they are represented here by the energy levels of TPTE [73] whose chemical structure is similar to that of PPB.

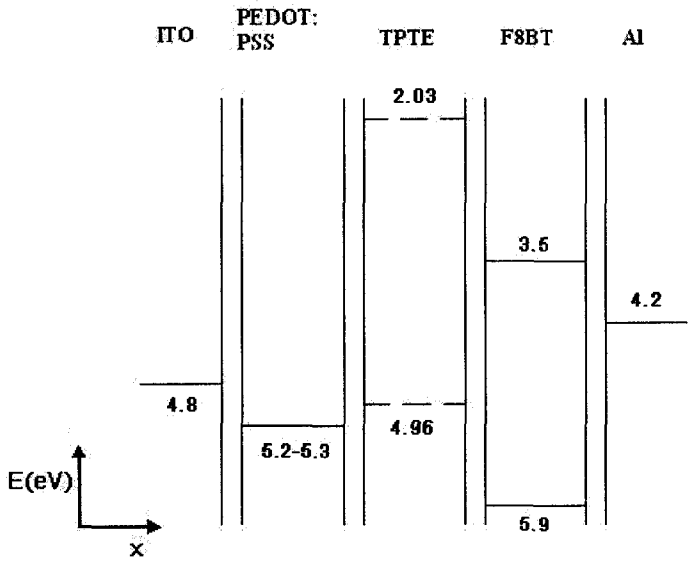

Fig. 5.2 Energetic position, relative to the vacuum level, of the frontier levels of the materials used in the LED structures: The energy levels of PPB are represented by those of TPTE whose chemical structure is similar to that of PPB.

Fig. 5.3 shows the UV-Vis spectra for thin films of F8BT and PPB. The optical absorption of F8BT had three peaks at 209, 322, and 464 nm with two shoulders at 254, and 340 nm. From the extrapolation of the optical absorption spectrum, the band-gap energy of F8BT was calculated to be 2.38 eV (λ_{onset}= 520 nm), which is close to the value

reported in Ref.[65]. The UV-Vis spectrum of PPB exhibited peaks at 214 and 372 nm. Its band-gap energy was determined to be 2.88 eV (λ_{onset}=430 nm).

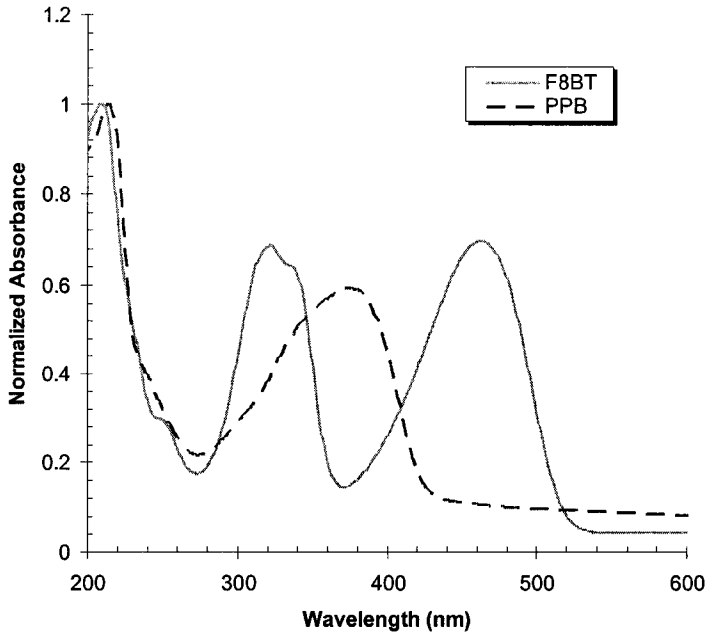

Fig. 5.3 Optical absorption spectra of thin films of F8BT and PPB.

Fig. 5.4 displays the current-voltage characteristics of PLEDs based on F8BT and its blends with PPB with varied blend ratio. In comparison with the pure F8BT, the turn-on voltage is decreased for all blend cases and it is shown that although below 17.5 V the current through pure F8BT device is lower than those though the blend emission layers, it increases faster with voltage.

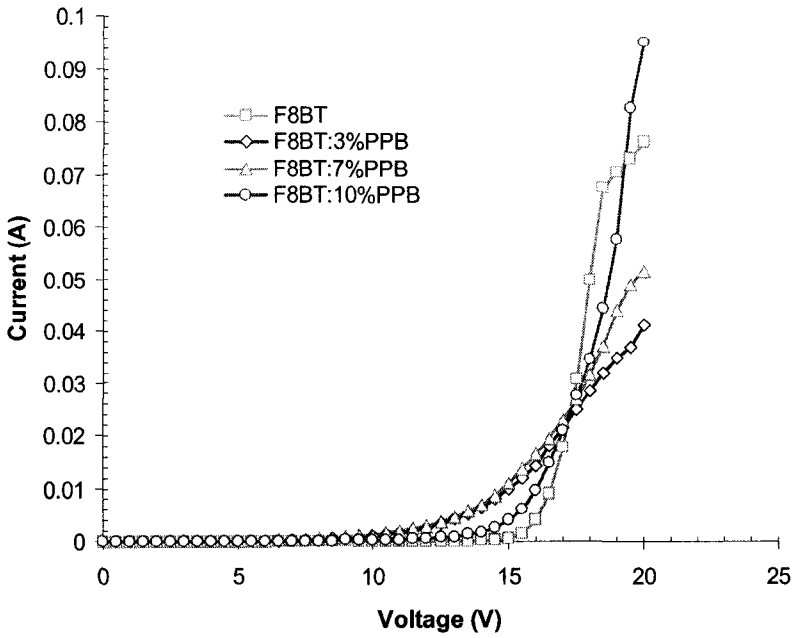

Fig. 5.4 Current as a function of the applied voltage for LEDs based on F8BT and its blends with PPB with varied blend ratio.

Fig. 5.5 compares the light power-current characteristics of the LEDs fabricated with F8BT and its blends with PPB. By utilizing the data shown in Fig. 5.5, we calculated brightness, luminance efficiency, and external quantum efficiency which are summarized in Table 5.1. The introduction of PPB into the emissive layer reduces the threshold current for light emission, which is indicative of an improved hole/electron balance within the active layer. Enhanced performance was found in the blend devices with a maximum brightness of 1078 cd/m^2, a maximum luminance efficiency of 0.207 cd/A, and a maximum external quantum efficiency of 0.055% for the 7% PPB blend. There are a few possible reasons for the improved EL properties seen in the blend cases. Since the band-gap difference in F8BT:PPB is 0.5 eV, it is likely that some energy was transferred from the higher band gap PPB to F8BT [65]. However, the efficiency of energy transfer might be low because of weak EL observed from the neat PPB devices we fabricated

(PPB is a hole transport polymer, as well as a light emitting polymer) [63]. More possibly, the improvement of device performance may be due to enhanced charge carrier injection and transport. As a hole transporting component, PPB that is added to the emissive layer can improve the hole injection from the anode and the hole transport through the layer. On the other hand, F8BT has a high electron affinity, and exhibits strong electron transport. The combination of both is advantageous to EL enhancement. Another possibility is that spatial confinement of excitons made some contributions to the improvement of device properties. Phase-separated domains in the thin film morphology of the 7% PPB blend were observed in the SEM micrograph (Fig. 5.6). The isolated domains may help confine the excitons in the blends [63]. The possible reason why the best performance was found in the 7% PPB blend may be that this blend ratio corresponds to a more balanced ratio between the electron and hole currents, and/or that this blend ratio produces a phase separation morphology that can give rise to a better spatial confinement effect.

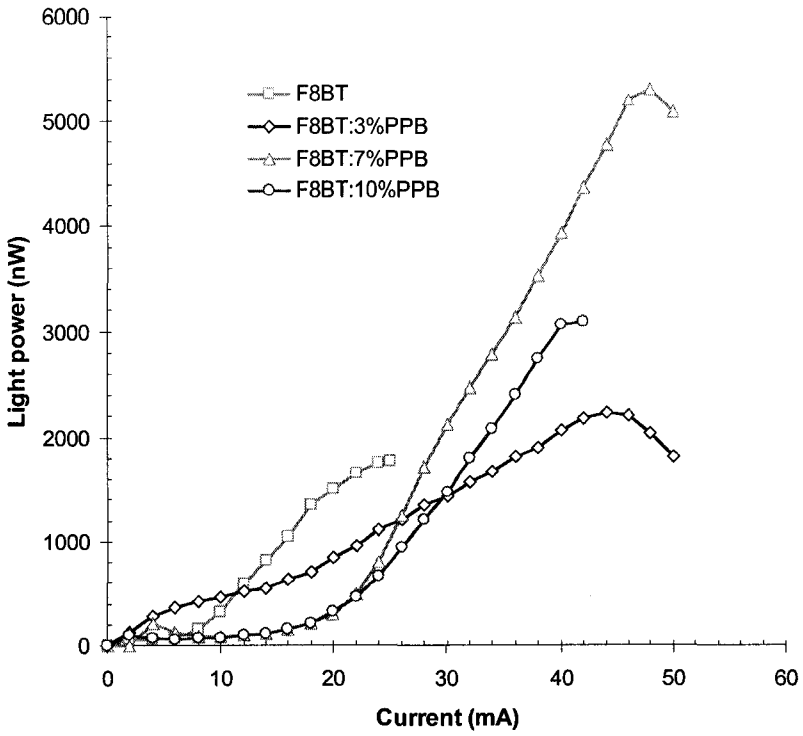

Fig. 5.5 Variation of the light power with current for LEDs based on F8BT and its blends with PPB with varied blend ratio.

Table 5.1 EL performance for the LEDs based on F8BT and its blends with PPB.

Emission layers	F8BT	F8BT:3% PPB	F8BT:7% PPB	F8BT:10% PPB
d_{EL} (nm)	55	55	55	55
$J_{threshold}$ (mA/cm^2)	16.6	10.9	10.9	11
V_{on} (V)	13.5	6	5.5	8
B_{max} (cd/m^2)	360	455	1078	627
η_{max} (%)	0.037	0.038	0.055	0.037
LE_{max} (cd/A)	0.138	0.143	0.207	0.14

d_{EL} : Thickness of emissive layer.

$J_{threshold}$: Threshold current density for light emission.

V_{on} : Turn-on voltage for the current at which the current reaches $\sim 8.5\times10^{-5}$ A.

B_{max} : Maximum luminance.

η_{max} : Maximum external quantum efficiency.

LE_{max} : Maximum luminance efficiency.

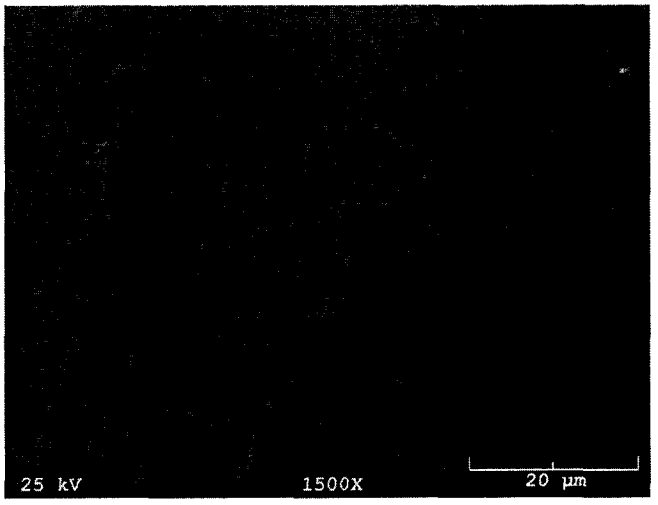

Fig. 5.6 SEM image of a thin film of F8BT:7% PPB blend spin-cast from 10mg/mL solution in toluene onto a PEDOT:PSS-covered ITO substrate.

Doping F8BT with PPB had no effect on the EL spectrum. For all devices under study, EL emission exclusively came from the contribution of F8BT. EL peaks at 541 nm (Fig. 5.7), which is close to the value reported in Ref.[38]. The light intensity increased with an increasing of the applied voltage, and the EL spectrum was reproducible and remained stable during device characterization.

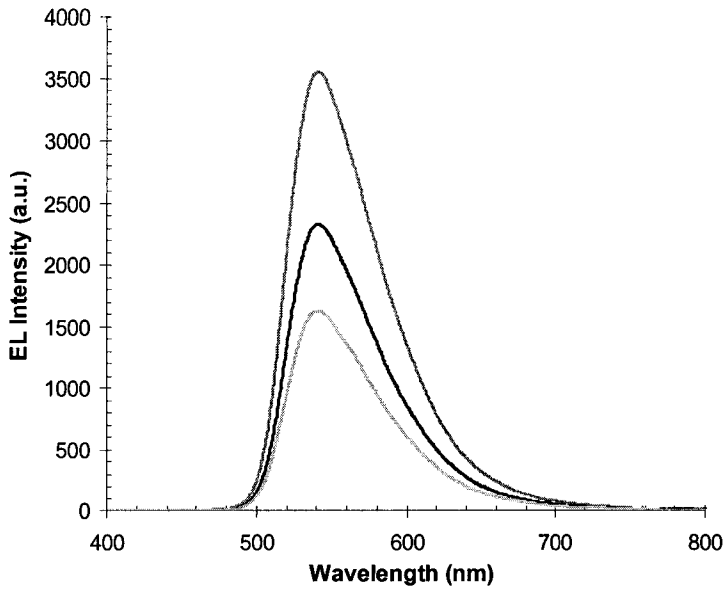

Fig. 5.7 EL spectra of the pristine F8BT devices under different forward bias.

5.4 Summary

Addition of hole transporting polymer PPB to F8BT is shown to bring about an increase in PLED device properties. The devices with the 7% PPB blend as the emissive layer exhibited the best performance in light luminance and efficiency. The maximum brightness reached 1078 cd/m^2 at a current density of 528 mA/cm^2, which is three times higher than that of the pristine F8BT LEDs. EL spectrum was not influenced by blending. A few possible reasons are given to explain the enhanced performance observed from the blend devices.

CHAPTER 6

DEVICES BASED ON END-CAPPED PF2/6 BLENDS WITH F8BT

6.1 Introduction

The blend of Poly(9,9'-dioctylfluorene) (PFO) with poly(9,9'-dioctylfluorene-alt-benzothiadiazole) (F8BT) is a well-known and popular PF blend system, which has been used as active materials for EL devices in many investigations related to PLED that were aimed at a variety of research objectives [40][50][55][65][103][111][128]. Blue emitter PFO exhibits a relatively high hole mobility [130] and a high solid state PL efficiency (~60%). And F8BT couples a high electron mobility with a high electron affinity of around 3.5 eV below vacuum [65] that brings about easy electron injection. As a result, doping PFO with F8BT gives rise to EL devices with high efficiency, high brightness, and low turn-on voltage [111]. Optimal LED performance has been observed for the devices based on the blends containing 95% PFO and 5% F8BT [104][106]. Due to a good spectral overlap between the host PFO blue emission and the guest F8BT absorption [40][128], efficient energy transfer takes place from PFO to F8BT, which produces an emission spectrum that is essentially that of neat F8BT. However, upon the treatment of the blend film with acetone, a very poor solvent for the PF components, or upon the incorporation of a Hole-Blocking Layer (HBL), 2-(4-biphenylyl)-

5-butylphenyl-1,3,4-oxadiazole (PBD), between the cathode and the emissive blend film, the blue emission from the PFO host arose in the PL and EL spectra [128][103].

As demonstrated by the results described in Chapter 4, end-capped PF2/6s are efficient blue emitting polymers. It is likely that in these materials, the hole mobility is much greater than the electron mobility as in many other PF materials [130][130]. Enlightened by PLEDs based on PFO blends with F8BT, we conducted research on EL properties of the devices prepared from end-capped PF2/6s blended with F8BT. DMP-end-capped PF2/6 or TPA-end-capped PF2/6 doped with F8BT at varied blend ratio was used as the light-emitting layer. Blend based devices displayed better performance in terms of luminance and efficiency than those made from either of the pure components. Efficient energy transfer from host end-capped PF2/6 to guest F8BT should be responsible for the improvement. However, the energy transfer was incomplete since EL emission did not exclusively come from F8BT. Although the EL spectra were dominated by the emission of F8BT, the blue emission from the end-capped PF2/6 contributed to the spectra with the weight of the blue component changing with the blend ratio. Therefore, we have tentatively explained the reason for the existence of the blue component in the EL spectra.

6.2 Experimental

Molecular structures of end-capped PF2/6s and F8BT we used here are shown in Fig. 4.1 and Fig. 5.1. The other details related to these materials are described in Chapter 4 and Chapter 5, respectively.

The devices were fabricated at ambient conditions on glass substrates covered by patterned Indium-Tin-Oxide (ITO) electrodes. The ITO substrates were precleaned by

two successive ultrasonic baths in acetone and isopropyl alcohol. After drying them with a nitrogen gun, a 45-nm thick film of poly(3,4-oxyethyleneoxythiophene) doped with poly(styrene sulfonate) (PEDOT:PSS) was spin coated over the substrate from a 1.3 wt.% water dispersion. The spin-coating was done at a speed of 4000 rpm with a ramp of 1000 r/s for 50 seconds. The emissive layers consisted of end-capped PF2/6 blends with F8BT at a varied blend ratio. They were formed on top of PEDOT:PSS films by a 50-second spin casting from polymer toluene solutions (10 mg/mL) at a speed of 2000 rpm that was reached via a ramp rate of 1000 r/s. Filters having a pore size of 0.45 μm (Millipore Corporation, Bedford, MA) were used to purify the polymer solutions prior to spin-coating. The thicknesses of DMP-end-capped PF2/6 blend films are 70 nm, and those for TPA-end-capped PF2/6 blend films are 80 nm. Devices were dried in a vacuum chamber at room temperature for a minimum of 24 hrs before the deposition of the Al film. The manufacturing was completed with the thermal evaporation of the aluminum cathode (~200 nm) at 2×10^{-6} Torr through a shadow mask. The overlap between the two electrodes gave active device areas of 9 mm^2.

The equipment used for the measurement of current-voltage characteristics, light power, EL spectra and optical absorption spectra were described in Chapter 3. The current-voltage characteristics were recorded in a forward sweep mode with a voltage stimulus and an integration of 60 Hz. The light power was measured in a current sweep mode with a wait time of 1200 ms/sample. It was observed that the devices began to degrade after the maximum light powers were reached. The EL spectra were recorded with an integration time of 300 ms.

6.3 Results and Discussion

6.3.1 Energy Band Diagrams of the Materials Used in the PLEDs

Fig. 6.1 shows the energetic positions (eV, below vacuum) of the polymers' frontier levels and electrodes' work functions. The energy levels of end-capped PF2/6s are not published in the available literature. Therefore, they are represented by the energy levels of PF2/6 whose chemical structure is similar to those of end-capped PF2/6s.

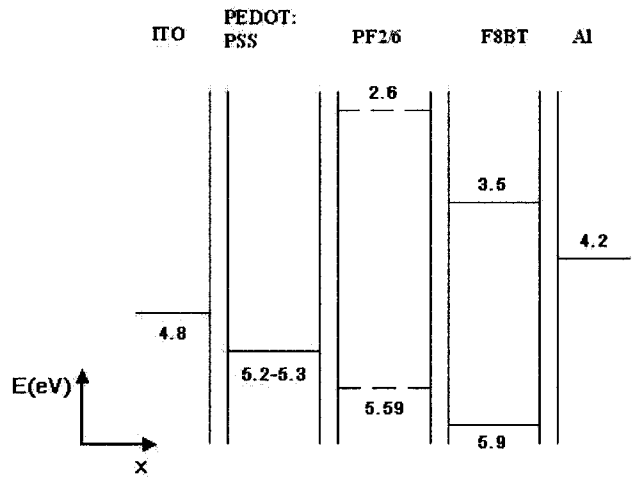

Fig. 6.1 Energetic position, relative to the vacuum level, of the frontier levels of the materials used in the LED structures: The energy levels of end-capped PF2/6s are represented by those of PF2/6 whose chemical structure is similar to those of end-capped PF2/6s.

6.3.2 Electroluminescence of DMP-End-Capped PF2/6 Blends with F8BT

Fig. 6.2 displays current density as a function of the electric field for devices with DMP-end-capped PF2/6, F8BT and their blends as active layers. The F8BT device operates under higher electric fields than any other devices and it has the highest turn-on voltage of ~13.5 V. The devices based on DMP-end-capped PF2/6 and its blends with 7% and 10% F8BT have approximately the same turn-on voltages at ~5 V. Although, under

low electric field, the current passing through the DMP-end-capped PF2/6 device is higher than that through the 10% F8BT and 20% F8BT devices, the latter increase faster with electric field. However, the current through the 7% F8BT device is always lower that that through DMP-end-capped PF2/6 device.

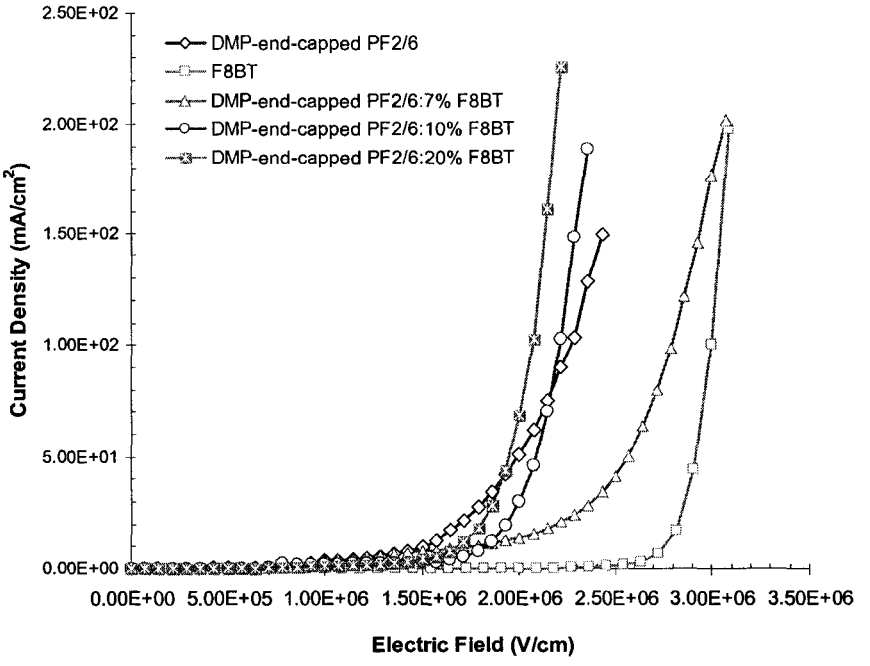

Fig. 6.2 Current density-electric field characteristics of PLEDs based on DMP-end-capped PF2/6, F8BT and their blends.

The variation of the light power with current for the LEDs under study is presented in Fig. 6.3. By using the data shown in Fig. 6.3, we calculated performance including threshold current density for light emission, luminance, external quantum efficiency, and luminance efficiency, which are summarized in Table 6.1. Compared to the devices based on either of the components, blend based devices exhibited better properties in light for brightness and efficiencies. The best performance was observed from the blend containing 10% F8BT with a maximum luminance of 1074 cd/m^2 at 213.6

mA/cm^2, a maximum external quantum efficiency of 0.16% and a maximum luminance efficiency of 0.514 cd/A at 205.2 mA/cm^2.

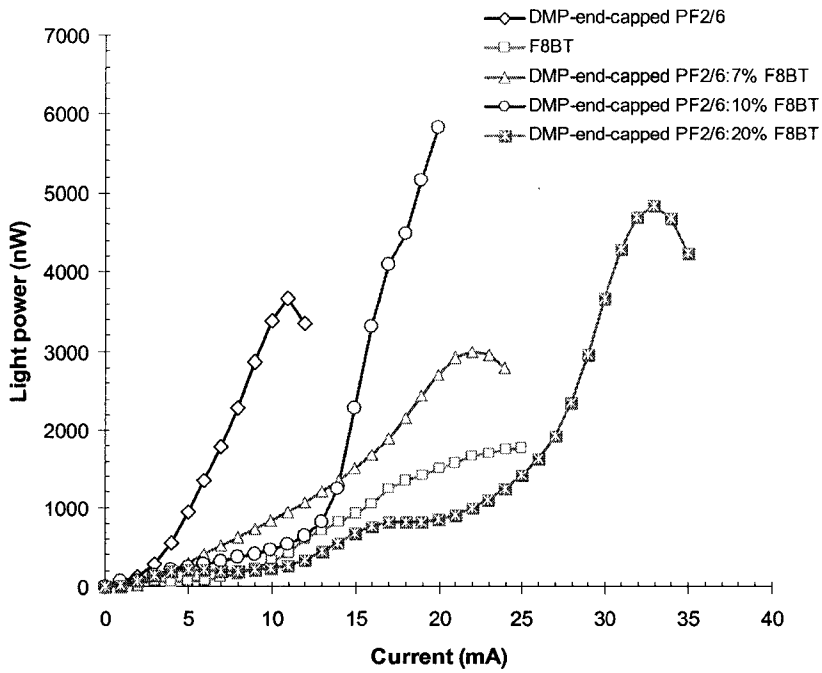

Fig. 6.3 Light power as a function of current for the devices constructed of DMP-end-capped PF2/6, F8BT and their blends.

Table 6.1 EL performance for the LEDs based on DMP-end-capped PF2/6, F8BT and their blends.

Emission layers	DMP-end-capped PF2/6	F8BT	7% F8BT	10% F8BT	20% F8BT
	70	55	70	70	70
	2.4	16.6	16.3	8	10.7
	5	13.5	5	5	6
	381	360	515	1074	816
	0.16	0.037	0.066	0.16	0.07
	0.319	0.138	0.215	0.514	0.225
	420, 445, 485 (maximum)	541	420, 442, 527 (maximum)	420, 442, 528 (maximum)	419, 438, 525 (maximum)

d_{EL} : Thickness of emissive layer.

$J_{threshold}$: Threshold current density for light emission. It is defined as the minimum current density at which the resulting light power can be detected.
V_{on} : Turn-on voltage for the current at which the current reaches $\sim 8.5 \times 10^{-5}$ A.
B_{max} : Maximum luminance.
η_{max} : Maximum external quantum efficiency.
LE_{max} : Maximum luminance efficiency.
λ_{peak} : EL peak wavelength.

Fig. 6.4 shows the EL spectra for the devices made from DMP-end-capped PF2/6, F8BT and their blends at varied blend ratios ranging from 7% F8BT to 50% F8BT. Although the emission of F8BT dominates the EL spectra of the blends, that of DMP-end-capped PF2/6 contributes to them as well. Two emission peaks representing the blue component obviously correspond to those at 420 nm and 445 nm in the EL spectrum of DMP-end-capped PF2/6. In general, the weight of the blue component increases with the decrease of F8BT content in the blends except that the blue emission from 7% F8BT blend is not the most intense one of all blends. The maximum emission peaks are found to be at ~527 nm, which are blue-shifted by 14 nm relative to that of pure F8BT. A similar phenomenon was observed from other blends [24]. This could be due to the reduced interchain interactions between the F8BT chains arising from the dilution effect of the host DMP-end-capped PF2/6.

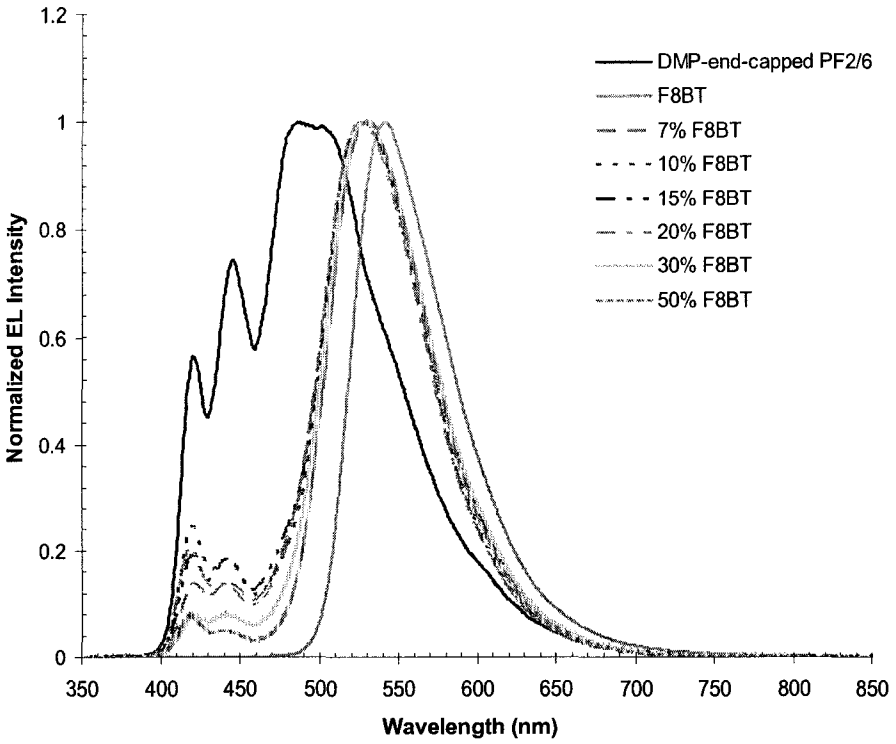

Fig. 6.4 EL spectra of the devices based on DMP-end-capped PF2/6, F8BT and their blends.

6.3.3 Electroluminescence of TPA-End-Capped PF2/6 Blends with F8BT

Fig. 6.5 shows current density as a function of the electric field for device structures using TPA-end-capped PF2/6, F8BT and their blends as emissive layers. Of all LEDs, the F8BT based device operates under the highest electric field and the operating electric fields for the blend devices are lower than those for the devices based on either of the pristine components. The working field regions for 5% F8BT and 20% F8BT devices are similar to each other, which are the lowest ones among all devices. The turn-on voltage for F8BT device is ~13.5 V, while those for TPA-end-capped PF2/6 and blend devices are ~5 V.

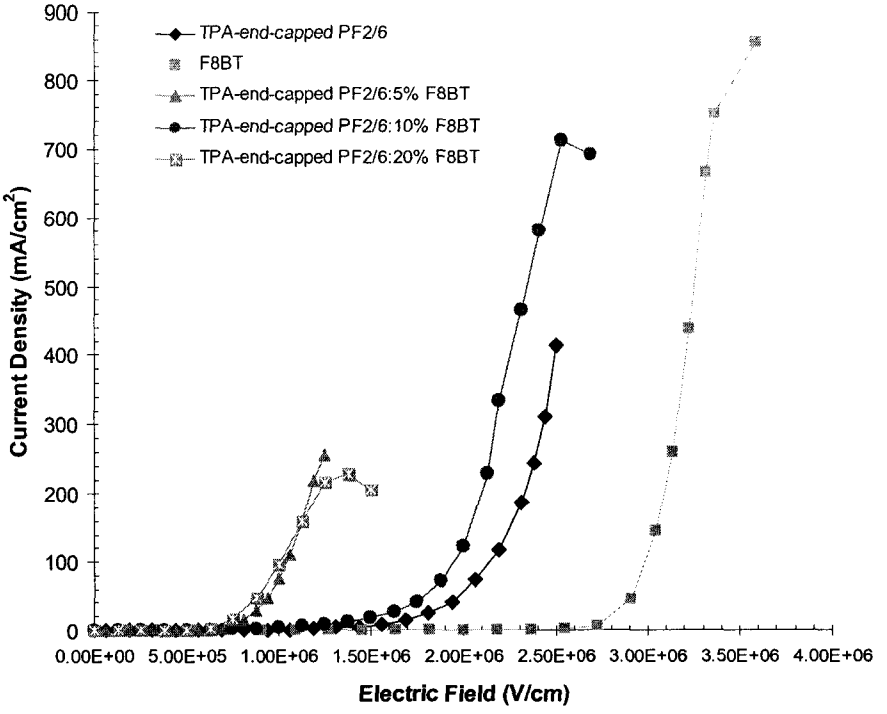

Fig. 6.5 Current density-electric field characteristics of LEDs based on TPA-end-capped PF2/6, F8BT and their blends.

Fig. 6.6 compares the current dependence of light power for the devices based on TPA-end-capped PF2/6, F8BT and their blends. EL performance, like threshold current density for light emission, luminance, external quantum efficiency, and luminance efficiency, is calculated by utilizing the data displayed in Fig. 6.6. Table 6.2 summarizes these properties. The 5% F8BT device exhibited a maximum external quantum efficiency of 0.103%, and a maximum luminance efficiency of 0.308 cd/A at 124.7 mA/cm^2. The maximum brightness of 518 cd/m^2 was achieved with an active layer of 10% F8BT blend.

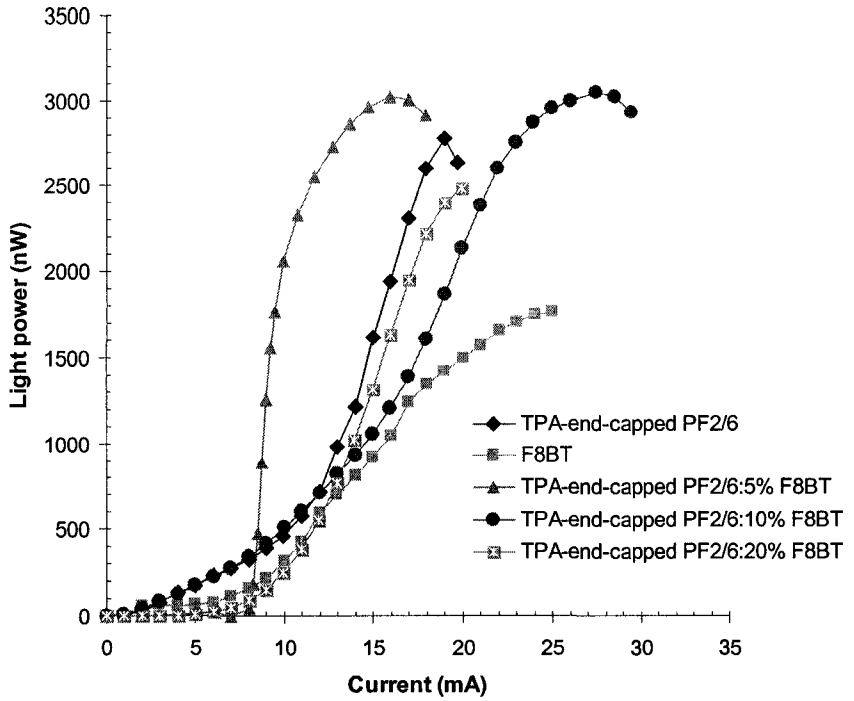

Fig. 6.6 Light power-current characteristics for the LEDs made from TPA-end-capped PF2/6, F8BT and their blends.

Table 6.2 EL performance for the LEDs based on TPA-end-capped PF2/6, F8BT and their blends.

Emission layers	TPA-end-capped PF2/6	F8BT	5% F8BT	10% F8BT	20% F8BT
d_{EL} (nm)	80	55	80	80	80
$J_{threshold}$ (mA/cm^2)	1.2	16.6	30.2	10.8	44.1
V_{on} (V)	5	13.5	5	5	5
B_{max} (cd/m^2)	327	360	474	518	426
η_{max} (%)	0.069	0.037	0.103	0.057	0.060
LE_{max} (cd/A)	0.156	0.138	0.308	0.184	0.195
λ_{peak} (nm)	422, 443, 512 (maximum)	541	420, 441, 520 (maximum)	421, 441, 526 (maximum)	420, 440, 526 (maximum)

d_{EL} : Thickness of emissive layer.

$J_{threshold}$: Threshold current density for light emission. It is defined as the minimum current density at which the resulting light power can be detected.

V_{on} : Turn-on voltage for the current at which the current reaches $\sim 8.5 \times 10^{-5}$ A.

B_{max} : Maximum luminance.
η_{max} : Maximum external quantum efficiency.
LE_{max} : Maximum luminance efficiency.
λ_{peak} : EL peak wavelength.

As shown in Fig. 6.7, the EL spectra of TPA-end-capped PF2/6 blends with F8BT are similar to those of DMP-end-capped PF2/6:F8BT blends. Although the F8BT emission is predominant, that from TPA-end-capped PF2/6 makes contributions to the EL spectra of the blends. Two blue emission peaks evidently originate from the peaks at 422 nm and 443 nm in the EL spectrum of TPA-end-capped PF2/6. Just like DMP-end-capped PF2/6 blends with F8BT, the higher weight of the blue component was observed from the blends with lower F8BT concentration. The maximum emission peaks are blue-shifted compared to that of pure F8BT, which might result from the dilution effect of the host polymer, the same reason as for what causes the blue-shift found in DMP-end-capped PF2/6:F8BT blends.

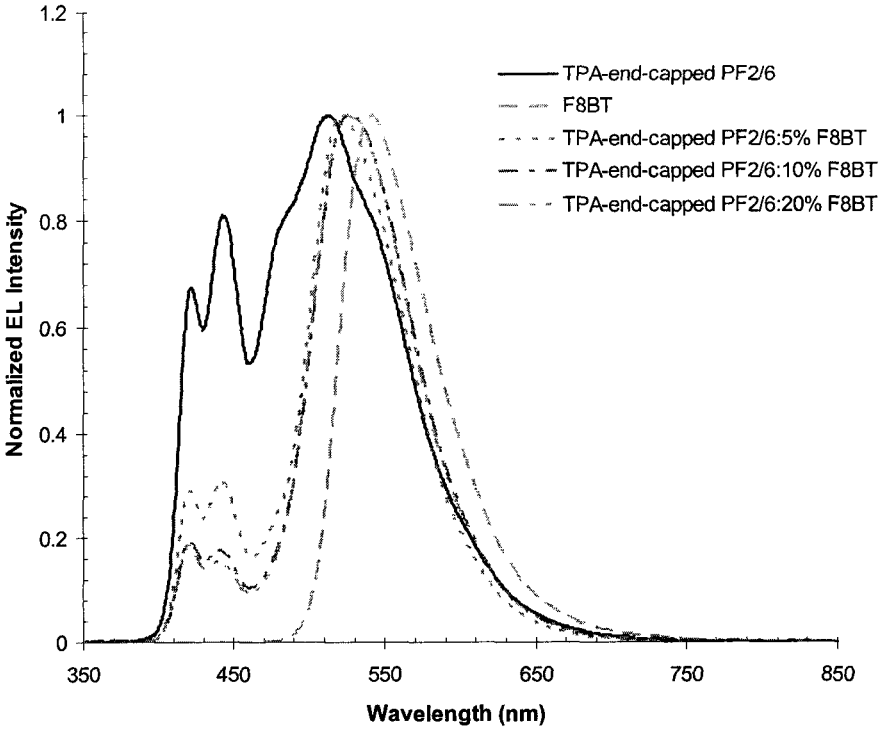

Fig. 6.7 EL spectra of the LEDs made from TPA-end-capped PF2/6, F8BT and their blends.

6.3.4 Origin of EL Enhancement and Blue Emission in End-Capped PF2/6:F8BT Blends

We believe that efficient energy transfer of excitations is the primary reason for the improvement in device luminance and efficiency which was observed from end-capped PF2/6 blends with F8BT. As characterized in Chapter 4, end-capped PF2/6s are efficient blue emitters with a wide energy gap of ~2.92 eV. They can therefore act as an adequate host material to achieve efficient energy transfer to a guest. F8BT possesses a band-gap energy of ~2.38 eV (refer to Chapter 5). The relatively large band-gap difference between end-capped PF2/6 and F8BT favors energy transfer [65]. On the other hand, it is probable that end-capped PF2/6s have a much larger hole mobility than

electron mobility. Doping end-capped PF2/6s with electron transporting F8BT could result in a better balance between the transports of both types of carriers.

Interestingly, the energy transfer from end-capped PF2/6s to F8BT is incomplete because the residual blue component appeared in the blend EL spectra. Actually, blue emission was also observed from PFO:F8BT blends when HBL, PBD, was incorporated between the emissive layer and the cathode, or when the blend film was treated with acetone [103][128]. In the first case, the blue emission was explained by confining the recombination to a region close to the emissive polymer/PBD interface, where the concentration of F8BT was relatively depleted [104]. In the second case, it was suggested that acetone drove the blend system towards further de-mixing. We propose that in the present blend systems the residual blue emission resulted from the presence of depleted regions where the concentration of F8BT is very low and not sufficient for complete quenching of end-capped PF2/6 luminescence. In these regions, relatively complete phase separation of the two components occurs on a larger scale than the exciton diffusion length and the Forster transfer radius.

6.4 Summary

We find that an enhancement in brightness and efficiencies can be realized via doping end-capped PF2/6 with F8BT. In particular, with an active layer of DMP-end-capped PF2/6 blended with 10% F8BT, the EL reached a maximum luminance of 1074 cd/m^2, a maximum external quantum efficiency of 0.16%, and a maximum luminance efficiency of 0.514 cd/A. The improvement is assigned to efficient energy transfer from host end-capped PF2/6 to guest F8BT. However, the energy transfer is incomplete because the blue component is observed in blend EL spectra. We think that the presence

of the regions where the concentration of F8BT is relatively depleted accounts for the residual blue emission.

6.5 Comparison between Devices under Investigation

The principal EL properties of the important devices under study are summarized in Table 6.3. All the devices were fabricated with the same configuration, ITO/PEDOT:PSS (45 nm)/emissive layer/Al (200 nm). The investigation demonstrated that blending is an effective means for improving device properties, and that end-capping can significantly suppress low energy emission, as well as enhance EL performance.

In comparison with pristine PF2/6 LED, the device based on PF2/6 blend with PFB displayed improved EL performance in light brightness and efficiency. The EL reached a maximum luminance of 884 cd/m^2. The maximum external quantum efficiency of the blended device was 0.1%, which is more than three times higher than that of the pure PF2/6 LED. The enhancement of device properties might be due to both exciton confinement and improved charge carrier injection. The phase-separated morphology, which was observed in the SEM images, may play a role in the enhanced device performance as well. In addition, blending suppressed the long wavelength emission to a certain extent.

End-capping can clearly improve device properties. DMP-end-capped PF2/6 based device exhibited a maximum luminance of 381 cd/m^2, a maximum luminance efficiency of 0.319 cd/A, and a maximum external quantum efficiency of 0.16 %, which are 2-6 times higher than those of the PF2/6 based LED. In particular, end-capping can effectively suppress low energy emissions. In the case of DMP-end-capped PF2/6, long

wavelength emission bands were nearly completely suppressed since all EL peaks fall into violet-blue zone. Two possible reasons for the enhancement in EL performance and blue emission are efficient hole trapping at the end-capper groups and the shift of the position of the exciton recombination zone.

Table 6.3 The principal EL properties for the important devices under investigation.

Emission layers	PF2/6	PF2/6: 16.7% PFB	DMP-end-capped PF2/6	F8BT	F8BT: 7% PPB	DMP-end-capped PF2/6: 10% F8BT
d_{EL} (nm)	40	40	70	55	55	70
B_{max} (cd/m^2)	179	884	381	360	1078	1074
η_{max} (%)	0.03	0.1	0.16	0.037	0.055	0.16
LE_{max} (cd/A)	0.084	0.21	0.319	0.138	0.207	0.514
λ_{peak} (nm)	537	430, 504 (maximum), 624	420, 445, 485 (maximum)	541	541	420, 442, 528 (maximum)

d_{EL} : Thickness of emissive layer.
B_{max} : Maximum luminance.
η_{max} : Maximum external quantum efficiency.
LE_{max} : Maximum luminance efficiency.
λ_{peak} : EL peak wavelength.

Compared to neat F8BT, an enhancement in luminance and efficiencies was observed from F8BT blends with PPB. With F8BT doped with 7% PPB as the active layer, the EL reached a maximum brightness of 1078 cd/m^2, a maximum luminance efficiency of 0.207 cd/A, and a maximum external quantum efficiency of 0.055%. The enhanced charge carrier injection and transport may be an important reason for the improved EL properties. Doping did not influence the EL spectra. The EL spectra of the blend devices are the same as that of pure F8BT. As shown in Table 6.3, F8BT devices demonstrated higher maximum brightness than the devices based on PF2/6 or end-capped

PF2/6 since the human eye is more responsive to the EL of F8BT which has a peak wavelength of 541 nm than the blue emission from PF2/6 or end-capped PF2/6.

Another PF blend system under study is end-capped PF2/6 doped with F8BT. The blend devices exhibited better EL performance in terms of brightness and efficiencies than either of the components. The best performance was observed from DMP-end-capped PF2/6 blended with 10% F8BT with a maximum luminance of 1074 cd/m^2, a maximum external quantum efficiency of 0.16%, and a maximum luminance efficiency of 0.514 cd/A. It is proposed that the efficient energy transfer of excitations is responsible for the enhanced EL properties. However, the energy transfer is incomplete since the blue component was observed in the EL spectra of the blends. The residual blue emission might originate from the depleted regions where the concentration of F8BT is very low and not sufficient for complete quenching of end-capped PF2/6 luminescence.

CHAPTER 7

SIMULATION OF CURRENT DENSITY-VOLTAGE CHARACTERISTICS OF PF-BASED LEDS

7.1 Introduction

As one promising new technology for large area display application, PLEDs have attracted intense interest both in academic research and industrial development. In order to optimize device performance, it is important to develop proper models to predict PLED operational characteristics. Presently, PLED numerical study mainly covers current density-voltage (*J-V*) characteristics, efficiency and emission location [131]-[137]. The electroluminescent polymers involved include poly(dialkoxy-p-phenylene vinylene) (PPV), poly[2-methoxy-5-(2'-ethylhexyloxy)-1,4-phenylenevinylene] (MEH-PPV), polyfluorenes and etc..

The operation of PLEDs comprises injection of holes and electrons from electrodes, transport of carriers through the bulk organic layer, formation of excited states, and luminous emission. Numerical simulation requires understanding the mechanism of charge injection at the metal/organic interface, as well as the transport properties of the organic layer.

To simplify the problem, single-carrier devices were introduced into the study, where one of electrodes is deliberately chosen to be an inefficient carrier injector (for

example, Au as cathode or Ca as anode) that does not inject charge carriers (Fig. 7.1). In a single layer device which can conduct only a single type of carrier, the current density is governed by contact injection at low voltage and limited by bulk space-charge effects at higher voltage [133]. It was proposed that holes and electrons are injected from the electrodes by a Fowler-Nordheim tunneling mechanism or by thermionic emission [131][133]. On the other hand, the carrier mobility (and therefore the charge transport) in most organic semiconductors is dependent on electric field and temperature [4].

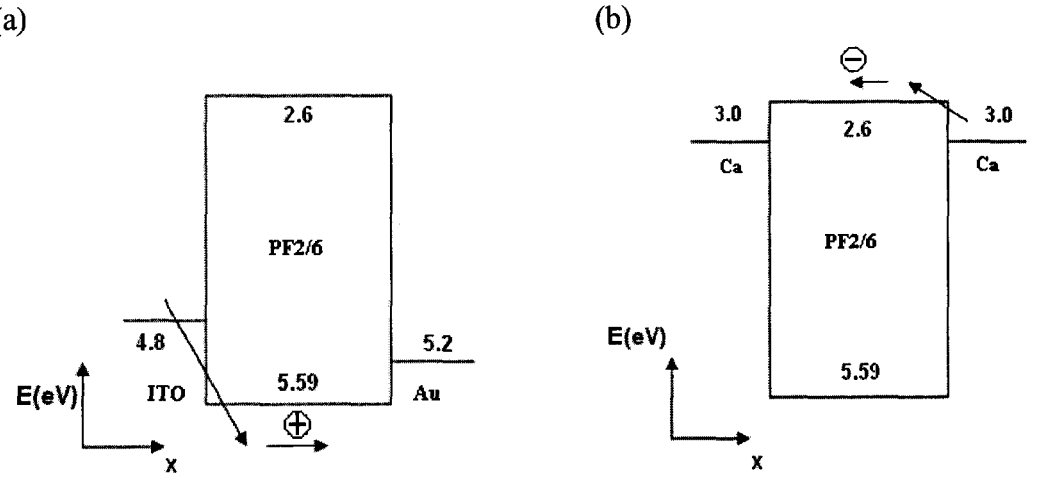

Fig. 7.1 Energy level diagrams of single-carrier devices: (a) Hole-only device. High work function of Au leads to large electron injection barrier between Au and polymer. As a result, carriers in the device are almost exclusively holes, (b) Electron-only device. With an anode having a low work function, an electron-only device results due to the large offset between the Fermi level of the anode and the HOMO of PF2/6 at 5.59 eV.

Compared to single-carrier devices that can be used to help understand the charge injection and transport mechanism, the double-carrier case is of practical significance. Since the charge distribution and flow of one carrier can strongly affect those of the other carrier [130][138]-[140], the current density in a double-carrier device can be much larger than that in a single-carrier device, which is not the simple sum of the two

monopolar currents. It has been shown that the differences between the two types of devices can be well understood via taking into account a bimolecular recombination process, in which the recombination rate is proportional to the product of the electron and hole concentrations [134].

In the present study, we used space charge limited current theory to model a pristine PF2/6 (see Fig. 3.2) based device with the configuration of ITO/ PEDOT:PSS (45 nm)/PF2/6 (40 nm)/Al (200 nm). SAS PROC REG, a widely used software package for fitting regression models, was employed to carry out model calculations and evaluation of simulation results. We also utilized the commercial simulation package TCAD (Synopsys Company) to conduct numerical study on the pristine F8BT (see Fig. 5.1) based device and the above pristine PF2/6 based device.

7.2 Simulation with Space Charge Limited Current Theory

For organic LEDs (OLEDs), both contact injection and space-charge effects have effect on the *J-V* characteristics. However, if an Ohmic contact (shown in Fig. 7.2) is made to a device the current dependence will be controlled by the bulk limit, Space Charge Limited Current (SCLC). In this case, the field produced by neighboring carriers dominates over the field generated by the applied bias. It has been shown that when the barrier to carrier injection is less than around 0.3-0.4 eV, the contact is Ohmic [131][141][142]. The Ohmic injection of holes can be realized with an ITO electrode coated with a film of PEDOT:PSS [143]. The enhancement in OLED properties arising from PEDOT:PSS may be in part due to the improvement of the adhesion of the polymer

to the ITO, since poor adhesion or interface damage can possibly result in a blocking contact [144][145].

In a polymer layer, the transport of holes is found to be governed by space charge effects at low electric fields [5], and by a combination of space-charge effects and a field dependent mobility at high electric fields [146]. On the other hand, the electron current is limited by the traps because electrons are very sensitive to traps formed during processing, atmospheric contamination and molecular diffusion [4][5]. However, if an inefficient cathode like an evaporated Au contact is used, a hole-only device results (Fig. 7.1 (a)).

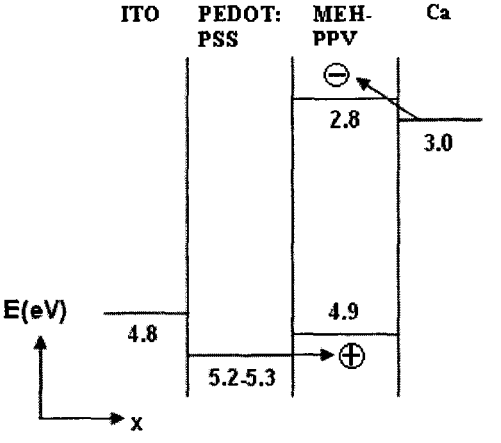

Fig. 7.2 Energy level diagram of a PLED with Ohmic contact: A very small or negative Schottky barrier height of a metal-semiconductor junction will lead to an Ohmic contact, a contact with voltage independent resistance. For an Ohmic contact, the carriers are free to flow in or out of the semiconductor, which results in a minimal resistance across the contact. In the present case, both the ITO/PEDOT anode and Ca cathode form Ohmic contacts. As a result, both hole and electron injections are barrier-free.

In our case, the device under investigation can be regarded as single-carrier hole-only type since Al was used as a cathode to form a hole-dominated device because of the poor electron injection from Al to polymer. As displayed in Fig. 7.3, there is a large

electron injection barrier between Al and polymer of ~1.6 eV compared to the negligible hole injection barrier of ~0.34 eV between PEDOT:PSS and polymer. On the other hand, a PEDOT:PSS coated ITO anode leads to an Ohmic hole injector. We therefore use space charge limited current theory for the single-carrier case to model the present device, taking into account field-dependent hole mobility.

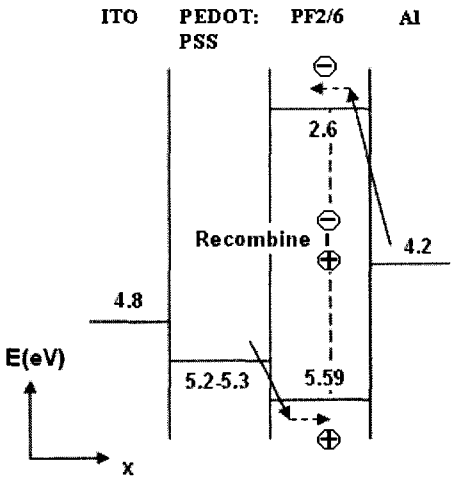

Fig. 7.3 Energetic position, relative to the vacuum level, of the frontier levels of the materials used in the device with a configuration of ITO/PEDOT:PSS/PF2/6/Al.

For the single-carrier hole-only device, the trap-free space-charged-limited current density for hole is given by

$$J = \frac{9}{8}\varepsilon\mu_p \frac{E^2}{L}. \qquad (1\text{-}5)$$

The hole mobility μ_p is described by

$$\mu_p = (\mu_* e^{-\Delta/kT}) e^{\gamma\sqrt{E}}. \qquad (1\text{-}3)$$

The quantity in parenthesis in Eq. (1-3) is field independent and is usually identified as the zero-field mobility μ_0. Therefore the hole mobility μ_p can also be given by

$$\mu_p = \mu_0 e^{\gamma\sqrt{E}}. \qquad (7\text{-}1)$$

Combining Eqs. (1-5) and (7-1), we have

$$\log\frac{J}{E^2} = \log(\frac{9}{8}\varepsilon\frac{\mu_0}{L}) + \gamma\log eE^{1/2} \text{ [4]}. \qquad (7\text{-}2)$$

Eq. (7-2) shows that there is a straight-line relationship between $\log\frac{J}{E^2}$ and $E^{1/2}$.

Actually Eq. (1-5) is true only for a field-independent mobility. However, for a mobility as in Eq. (7-1) at low electric fields, the trap-free space charge limited current can be well approximated by Eq. (7-2) when a factor of 0.89 is considered to properly calculate γ[131][4].

Table 7.1 presents the important parameters used in the simulation of the *J-V* characteristics of PF2/6-based LED with SCLC theory. The variation of $\log\frac{J}{E^2}$ with $E^{1/2}$ for the device under study is plotted in Fig. 7.4. By fitting the data to Eq. (7-2), zero-field mobility μ_0 and electric-field coefficient for the hole mobility γ are calculated to be $2.7646\times10^{-9}\text{cm}^2/\text{Vs}$ and $3.126\times10^{-3}(\text{cm}/\text{V})^{1/2}$, respectively. Linear regression analysis shows that there is a linear relationship between $\log\frac{J}{E^2}$ and $E^{1/2}$ above ~2.6 V (we can reject null hypothesis $H_0 : \beta_1 = 0$), and 99.89% of the variability in $\log\frac{J}{E^2}$ is accounted for by the regression model (the coefficient of determination $R^2 = 0.9989$)). As a result, the regression model is in a very good agreement with the experimental data when the applied bias is larger than ~2.6 V (as demonstrated in Fig. 7.4).

Table 7.1 The important parameters used in the simulation of *J-V* characteristics of PF2/6-based LED with SCLC theory.

Parameter	Symbol	Value used in SCLC simulation
PF2/6 relative permittivity	ε_r	3.0 [143]
Thickness of the active polymer (nm)	L	40 (measurement)
Zero-field mobility (cm^2/Vs)	μ_0	2.7646×10^{-9} (fitting result)
Electric-field coefficient $(cm/V)^{1/2}$	γ	3.512×10^{-3} (fitting result)

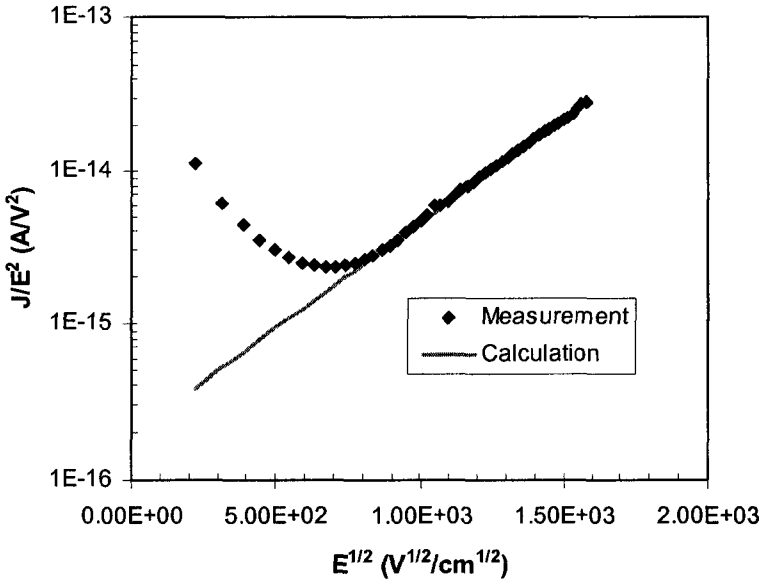

Fig. 7.4 Space charge limited current for the hole-dominated PF2/6-based device at 300K: The current is limited by space-charge effects at bias voltages above ~2.6 V. The line is fit to space-charge-limited behavior.

Fig. 7.5 compares the calculated *J-V* characteristics of PF2/6 based LED with the experimental results. With the values found for μ_0 and γ, the theoretical calculation agrees very well with the *J-V* measurement for bias voltages above 2.6 V. However, it can be seen that they don't fit each other below 2.6 V, which indicates that the current is not space charge limited under 2.6 V. Some neglected effects, such as mobility for hopping transport in disordered systems that are not involved in the model, may be responsible for the variance [141][146][147].

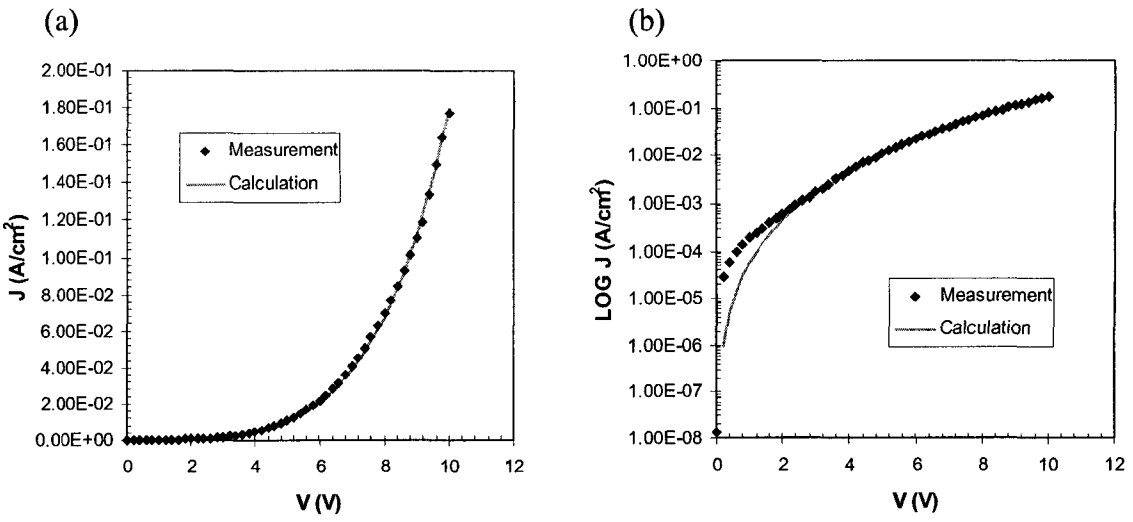

Fig. 7.5 Calculated *J-V* characteristics of PF2/6 based LED for SCLC with a field dependent mobility: (a) linear scale for *J*, (b) logarithmic scale for *J*. Experimental *J-V* characteristics of the same device is also plotted for comparison.

As mentioned above, a factor of 0.89 should be used to properly calculate γ since Eq. (7-2) is only approximately valid at low electric fields. Thus in the present case the value of γ should be $3.512\times10^{-3}(\mathrm{cm/V})^{1/2}$. Fig. 7.6 presents the calculated hole mobility as a function of the applied voltage. The hole mobilities are calculated by using the field-dependent hole mobility equation (Eq. (7-1)). Under the PLED operating voltages, the calculated mobilities are of the order of $\sim10^{-7}\ \mathrm{cm^2/Vs}$.

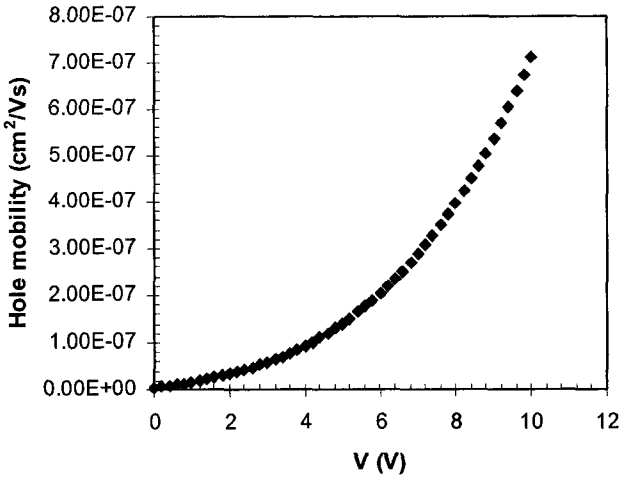

Fig. 7.6 The calculated hole mobility of PF2/6 at 300 K in SCLC simulation as a function of the applied voltage (Eq. (7-1)).

7.3 Simulation with TAURUS

7.3.1 Introduction

As components of TCAD, both MEDICI and TAURUS can be used for the simulation of the electrical characteristics of semiconductor devices [148]. At first, we tried to employ MEDICI to simulate the *J-V* characteristics of polyfluorene-based devices via choosing a proper carrier mobility model which is provided by MEDICI. Although many mobility models (which can be classified into low field mobility, transverse field-dependent mobility, and parallel field-dependent mobility) are available in MEDICI, the simulation calculation indicates that none of them is suitable to the present PF-based LEDs. Since the mobility model can greatly affect the numerical simulation of *J-V* characteristics, selection of a correct mobility model is very important. One advantage of TAURUS over MEDICI is that TAURUS can furnish a Physical Model and Equation Interface (PMEI) that allows users to implement new equations and models which are unavailable in the software. We therefore use TAURUS as a simulation tool to perform the numerical study.

Poisson's equation, continuity equation and Boltzman transport theory are the main theories involved in the simulation calculation in TAURUS, which are as follows:

Poisson's equation

$$\varepsilon\nabla^2\psi = -q(p - n + N_D^{+} - N_A^{-}) - \rho_s \,, \tag{7-3}$$

continuity equation

$$\frac{\partial n}{\partial t} = \frac{1}{q}\vec{\nabla}\cdot J_n - (U_n - G_n) = F_n(\psi, n, p)$$

$$\frac{\partial p}{\partial t} = \frac{1}{q}\vec{\nabla}\cdot J_p - (U_p - G_p) = F_p(\psi, n, p)\,, \tag{7-4}$$

and

Boltzman transport theory

$$\vec{J}_n = q\mu_n n\vec{E}_n + qD_n\vec{\nabla}\cdot n$$

$$\vec{J}_p = q\mu_p p\vec{E}_p - qD_p\vec{\nabla}\cdot p\,. \tag{7-5}$$

The parameters in the equations are presented in Table 7.2.

Table 7.2 The parameters in Poisson's equation, continuity equation, and Boltzman transport theory.

Parameter	Symbol	Unit
Permittivity	ϵ	F/m
Electric potential	ψ	V
Electron charge	q	C
Acceptor concentration	p	number/cm^3
Donor concentration	n	number/cm^3
Donor doping	N_D^+	number/cm^3
Acceptor doping	N_A^-	number/cm^3
Charge density	ρ_s	C/cm^3
Divergence operator	$\vec{\nabla}\cdot$	
Current density of electron	J_n	A/cm^2
Current density of hole	J_p	A/cm^2
Hole recombination rate	U_p	number/cm^3/s
Electron recombination rate	U_n	number/cm^3/s
Hole generation rate	G_p	number/cm^3/s
Electron generation rate	G_n	number/cm^3/s
Hole mobility	μ_p	cm^2/Vs
Electron mobility	μ_n	cm^2/Vs
Electric field for hole	E_p	V
Electric field for electron	E_n	V

As mentioned above, the carrier mobility in polymers is field-dependent, and is commonly described in a Poole-Frenkel-like form ((Eq. (7-1)). However, the mechanism is presently believed not to be Poole-Frenkel (The Poole-Frenkel effect is the decrease of a metal-insulator barrier due to electrode image-force interaction with the field at the metal-insulator interface [149]). Instead, it has been explained as being related to the intrinsic charge transport in disordered materials [150]. We can introduce this mobility model into the numerical calculation by the PMEI in TAURUS.

7.3.2 Simulation of *J-V* Characteristics of PF2/6-Based Device

It is found that the densities of states in valence band (N_V) and conduction band (N_C), the zero-field mobility (μ_0), as well as the electric-field coefficient to the mobility (γ) can significantly influence the calculated *J-V* characteristics. How these important parameters can affect the simulation calculation is shown in Fig. 7.7, Fig. 7.8, and Fig. 7.9. For the same applied voltage, the current density increases proportionally with N_V (N_C) or μ_0 and γ affects the current density exponentially. Therefore the current density is more sensitive to a change in γ.

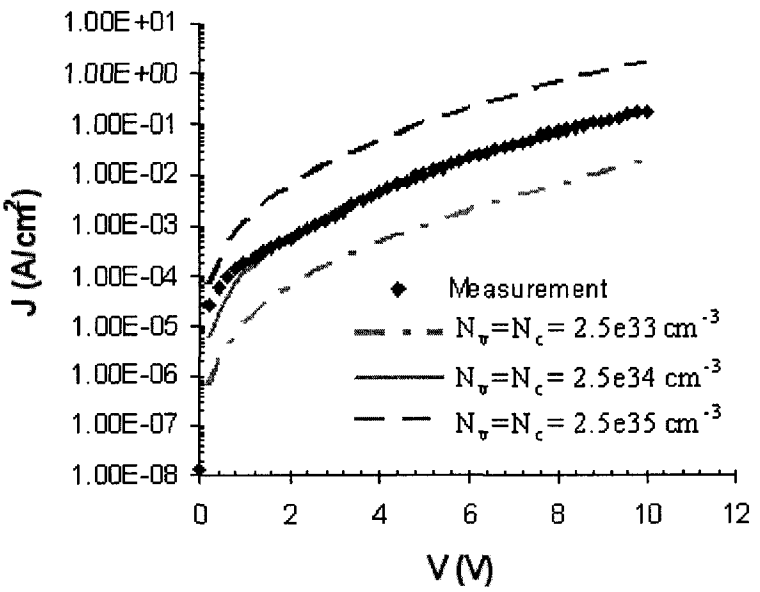

Fig. 7.7 The effect of N_C and N_V of PF2/6 on the calculated J-V characteristics of a pristine PF2/6-based LED in the case of μ_0=0.15 cm^2/Vs, and γ=7.46×10^{-4} $(cm/V)^{1/2}$.

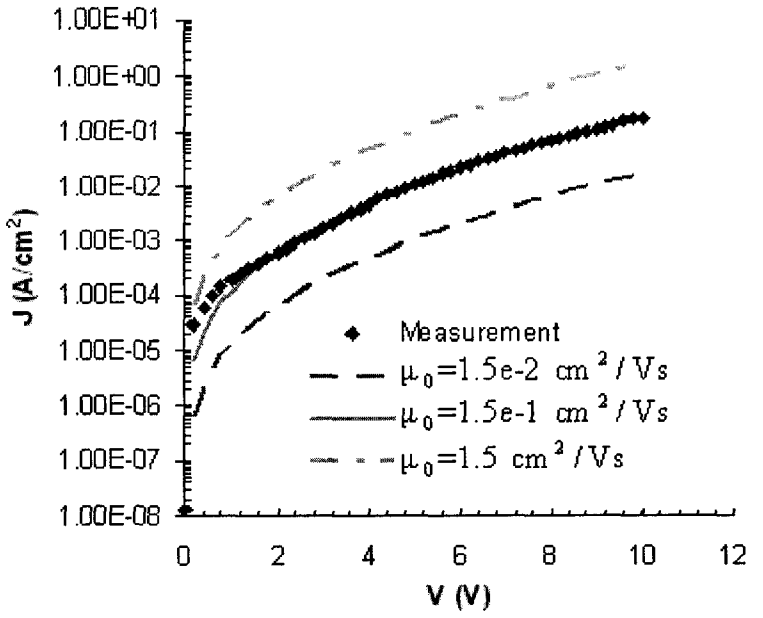

Fig. 7.8 The effect of μ_0 of PF2/6 on the calculated J-V characteristics of a pure PF2/6-based LED in the case of $Nv = Nc = 2.5\times10^{34}$ cm^{-3}, and $\gamma = 7.46\times10^{-4}$ (cm/V)$^{1/2}$.

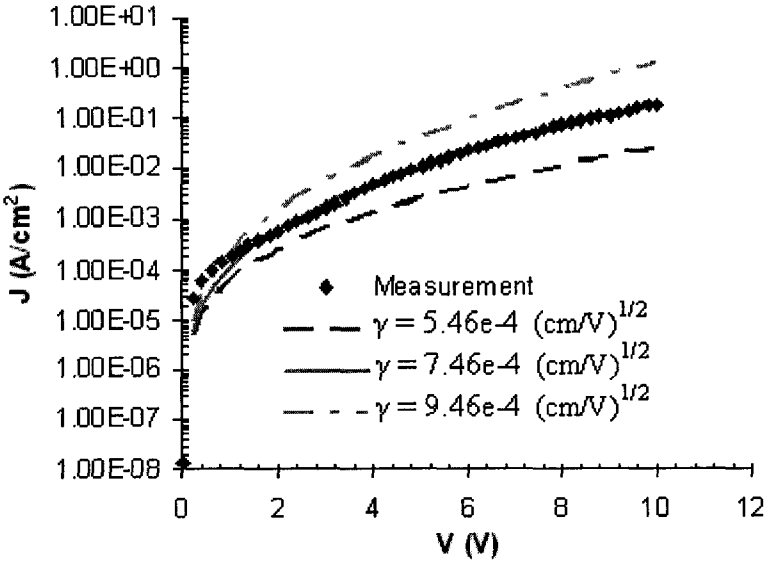

Fig. 7.9 The effect of γ of PF2/6 on the calculated J-V characteristics of a neat PF2/6-based LED in the case of $Nv=Nc=2.5\times10^{34}$ cm^{-3}, and $\mu_0=0.15$ cm^2/Vs.

The simulation calculation can be well fitted to the experimental data above ~1.4 V by properly selecting the important parameters (Fig. 7.10). The values of Nv, Nc, μ_0,

and γ that are used in the numerical calculation are presented in Table 7.3. For comparison the values of μ_0 and γ that are used in the SCLC simulation, as well as the values of *Nv*, *Nc*, μ_0, and γ for polymers that were reported in the literature are also given in the table.

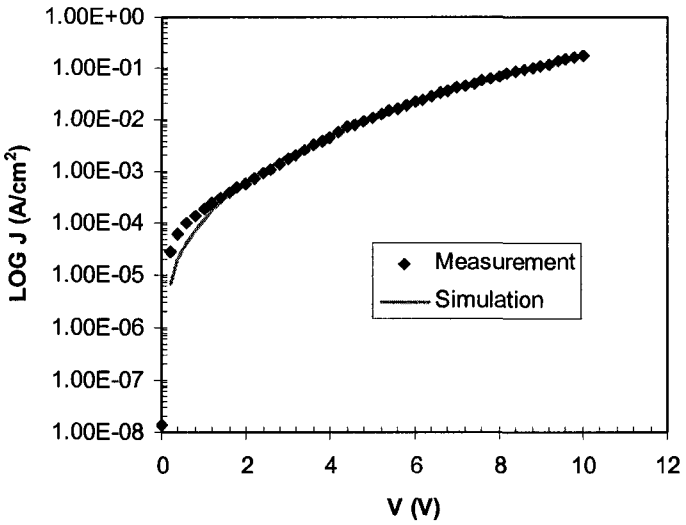

Fig. 7.10 *J-V* characteristics of PF2/6-based LED calculated with TAURUS (*J* is in logarithmic scale). Experimental *J-V* characteristics of the same device are also plotted for comparison.

Table 7.3 The important parameters used in the simulation of *J-V* characteristics of PF2/6-based LED.

Parameter	Symbol	Value used in TAURUS simulation	Value used in SCLC simulation	Values for polymers reported in the literature
Valence band density of states (cm^{-3})	N_V	2.5×10^{34}		10^{19}~10^{21} [134][141][149]
Conduction band density of states (cm^{-3})	N_C	2.5×10^{34}		10^{19}~10^{21} [134][141][149]
Zero-field mobility (cm^2/Vs)	μ_0	0.15	2.7646×10^{-9}	10^{-9} ~ 10^{-5} [4][146][152][153]
Electric-field coefficient $(cm/V)^{1/2}$	γ	7.46×10^{-4}	3.512×10^{-3}	10^{-4} ~ 10^{-3} [4][152]

N_C and N_V have an effect on the *J-V* characteristics by affecting the intrinsic concentration of the polymers ($n_i = \sqrt{N_C N_V} \exp(-\frac{E_g}{2kT})$). It was reported in the literature that for polymers the density of states in the conductance and valence band is estimated to be 10^{19}~10^{21} cm^{-3} [134][141][149]. By contrast, the values of N_C and N_V used in the present case are too large. The zero-field mobility has the same problem compared to the values reported in the literatures (10^{-9} ~ 10^{-5} cm^2/Vs) [4][146][152][153]. As a result, the carrier mobility calculated from Eq. (7-1) is of the order of 10^{-1} cm^2/Vs at the device working voltages (Fig. 7.11), which is much higher than the mobilities the fastest carriers in polymers are known to have (~10^{-3} cm^2/Vs) [111][154][155]. If we use the values of N_V, N_C, μ_0, and γ that are of the ranges reported in the literature and render the numerical calculation as close to the measurement as possible, there is a great difference between calculation and measurement (shown in Fig. 7.12). On the other hand, the parameter values used in the SCLC simulation and the corresponding mobility values calculated from these parameters are much more reasonable. This may be due to fewer fitting parameters in the analytical model. Nevertheless, the calculated mobility values in the SCLC simulation are small (the order of 10^{-7} cm^2/Vs) even if they fall into the range of the mobility values for polymers reported in the literature (10^{-3} cm^2/Vs - 10^{-9} cm^2/Vs) [130][140][154], which perhaps results from device degradation.

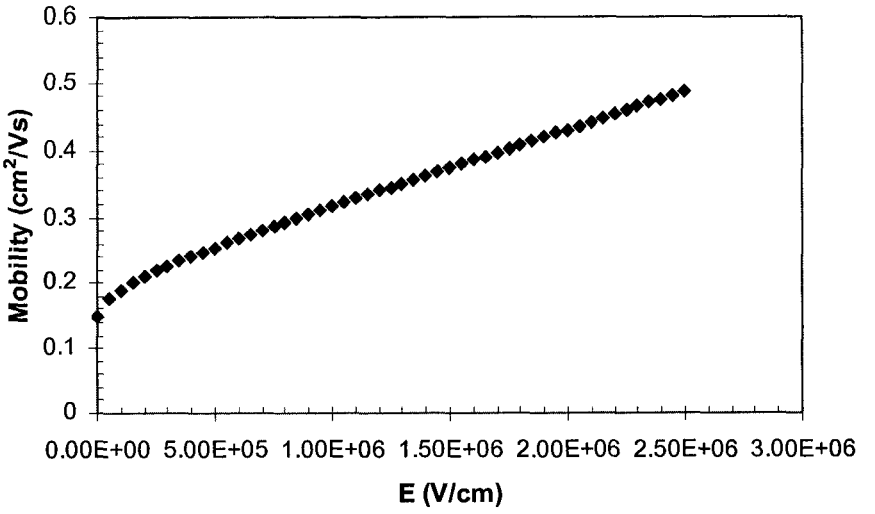

Fig. 7.11 The carrier mobility of PF2/6 at 300 K calculated from Eq. (7-1) in Taurus simulation as a function of the applied electric field.

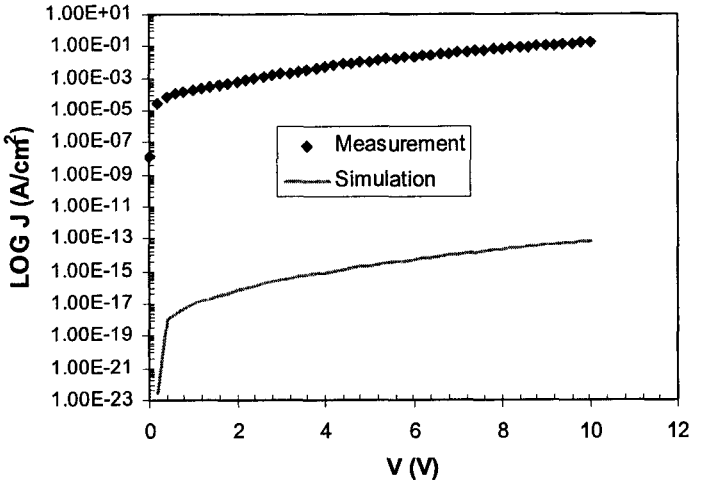

Fig. 7.12 *J-V* characteristics of PF2/6-based LED calculated with TAURUS (*J* is in logarithmic scale) by using values of N_V, N_C, μ_0, and γ that were reported in the literatures ($N_V = N_C = 10^{21}$ cm^{-3}, $\mu_0 = 10^{-5}$ cm^2/Vs, $\gamma = 10^{-3}$ (cm/V)$^{1/2}$). Experimental *J-V* characteristics of the same device are also plotted for comparison.

7.3.3 Simulation of *J-V* Characteristics of F8BT-Based Device

Fig. 7.13 shows the energetic positions (eV, below vacuum) of the polymers' frontier levels and electrodes' work functions in the F8BT-based device. Since the electron injection barrier between Al and F8BT (~0.7 eV) is comparable to the hole

injection barrier between PEDOT:PSS and F8BT (0.6-0.7 eV), we regard the F8BT-based LED as a bipolar device. The SCLC theory (Eq. (1-5)) is applicable to the single-carrier case. Therefore it can not be used for the *J-V* characteristics simulation of the F8BT-based device. In this case, we conduct the numerical simulation with TAURUS, assuming that the electron mobility is equal to the hole mobility in F8BT.

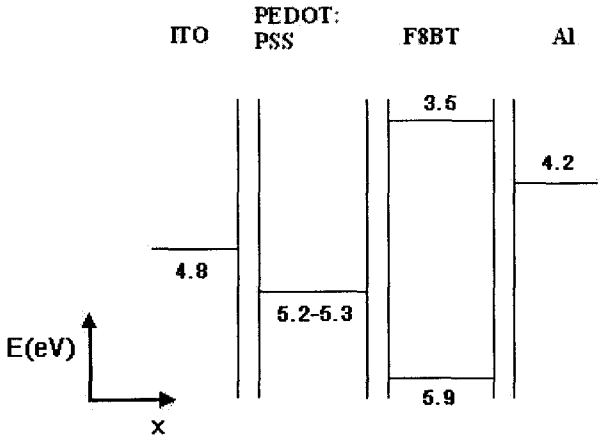

Fig. 7.13 Energetic position, relative to the vacuum level, of the frontier levels of the materials used in the device with a configuration of ITO/PEDOT:PSS/F8BT/Al.

Just like the case of PF2/6, N_V, N_C, μ_0, as well as γ have a great effect on the calculated *J-V* characteristics of the F8BT-based device and these important parameters affect the numerical simulation in a way similar to that for the case of PF2/6. With the proper values of *Nv*, *Nc*, μ_0, and γ, the calculated *J-V* characteristics are in good agreement with the measurements from ~3 V through ~13.5 V (Fig. 7.14). The values of *Nv*, *Nc*, μ_0, and γ that are used in the numerical calculation are presented in Table 7.4. For comparison the values of *Nv*, *Nc*, μ_0, and γ for polymers that were reported in the literature are also given in the table.

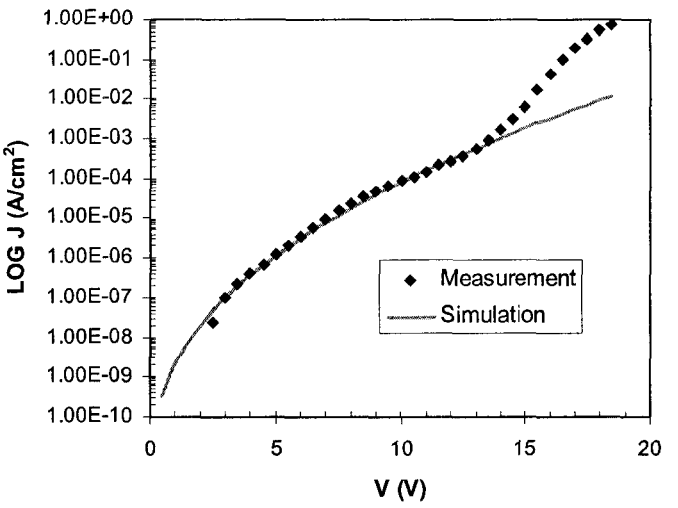

Fig. 7.14 *J-V* characteristics of F8BT-based LED calculated with TAURUS (*J* is in logarithmic scale). Experimental *J-V* characteristics of the same device are also plotted for comparison.

Table 7.4 The important parameters used in the simulation of *J-V* characteristics of F8BT-based LED.

Parameter	Symbol	Value used in TAURUS simulation	Values for polymers reported in the literature
Valence band density of states (cm^{-3})	N_V	3.6×10^{26}	10^{19}~10^{21} [134][141][149]
Conduction band density of states (cm^{-3})	N_C	3.6×10^{26}	10^{19}~10^{21} [134][141][149]
Zero-field mobility (cm^2/Vs)	μ_0	3.18×10^{-4}	10^{-9} ~ 10^{-5} [4][146][152][153]
Electric-field coefficient $(cm/V)^{1/2}$	γ	1.44×10^{-3}	10^{-4} ~ 10^{-3} [4][152]

In comparison with the values for polymers that were reported in the literature (10^{19}~10^{21} cm^{-3}) [134][141][149], the values of N_C and N_V (3.6×10^{26} cm^{-3}) used here are very large although they are much smaller that those used in the case of PF2/6. The value of μ_0 (3.18×10^{-4} cm^2/Vs) is very close to the range of μ_0 values for polymers that were reported in the literature (10^{-9} ~ 10^{-5} cm^2/Vs) [4][146][152][153]. By using the found values of μ_0 and γ, we calculate the carrier mobilities as a function of the applied electric field, which are shown in Fig. 7.15. At the device operating voltages, the calculated

carrier mobilities (in the order of 10^{-3} cm^2 /Vs) are reasonable compared to the carrier mobilities in F8BT reported in the literature (in the order of 10^{-3} cm^2 /Vs at an applied field of 5×10^5 V/cm) [111][154]. We therefore conclude that the theories involved in TAURUS simulation can explain the electrical characteristics of F8BT-based devices to a certain extent.

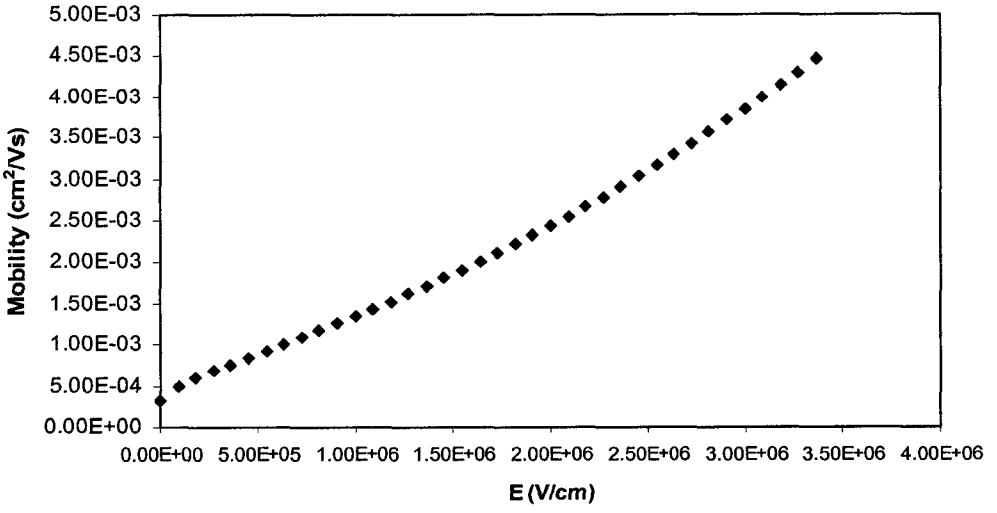

Fig. 7.15 The carrier mobility of F8BT at 300 K calculated from Eq. (7-1) in TAURUS simulation as a function of the applied electric field.

It is noticed that the current density increases sharply with the applied voltage above ~15 V (Fig. 7.14), which leads to the disagreement between calculations and measurements above ~15 V. The possible explanation is that higher voltages cause a rise in the device temperature that can influence the carrier mobilities [134][4].

7.3.4 Simulation of Band Diagrams

The applied forward bias voltage can influence the band bending in a PLED. Fig. 7.16 displays the band diagrams for PF2/6-based LED which were derived from PLED theory [156]. Fig. 7.16 (a) illustrates the case for zero bias. The voltage drop is assumed

to occur across the whole polymer layer due to the absence of charge in the material. When a forward bias is applied to the device, the voltage drop across the polymer is made up. There is typically a triangle barrier for both carriers penetration into the polymer from the electrodes. With an increase in the applied voltage, the width of the potential barrier for charge injection diminishes and, at some critical field, charge injection into the polymer takes place (Fig. 7.16 (b)). Fig. 7.17 shows the band diagram at forward bias for the same device which was obtained from TAURUS simulation. The result is similar to that derived from PLED theory.

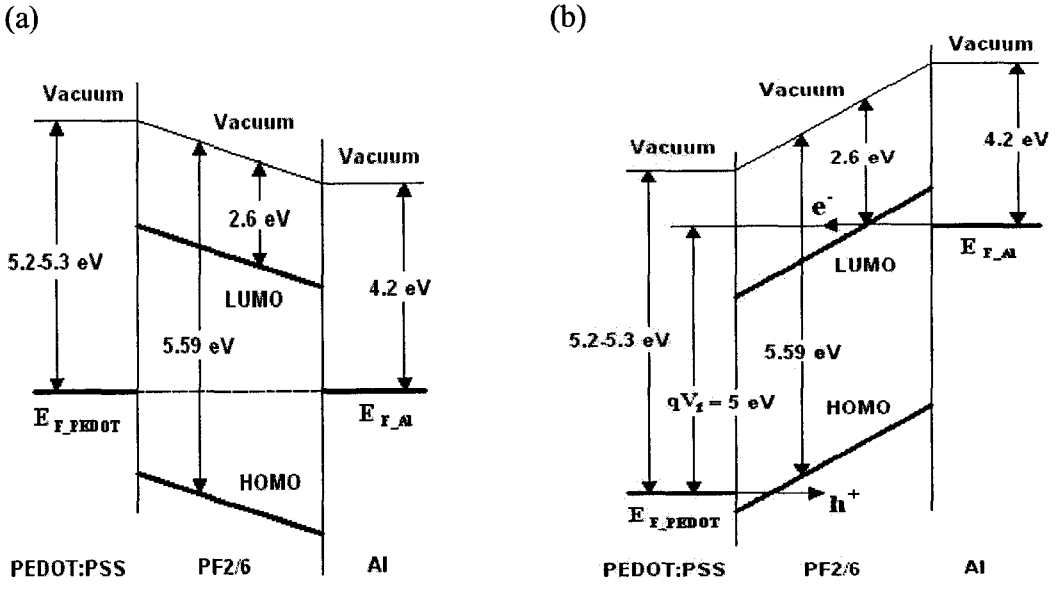

Fig. 7.16 Band diagrams for PF2/6-based LED derived from PLED theory: (a) zero bias, (b) forward bias.

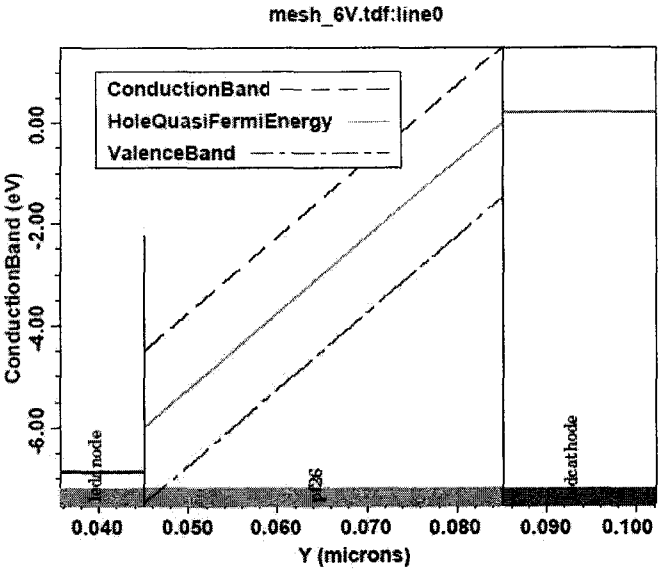

Fig. 7.17 Band diagram at forward bias for PF2/6-based LED derived from TAURUS simulation.

Fig. 7.18 presents the band diagrams for F8BT-based device that were obtained from PLED theory. The band diagram at forward bias for the same device, which was derived from TAURUS simulation, is shown in Fig. 7.19. The analyses of band bending in these diagrams are the same as those for the case of the PF2/6-based device.

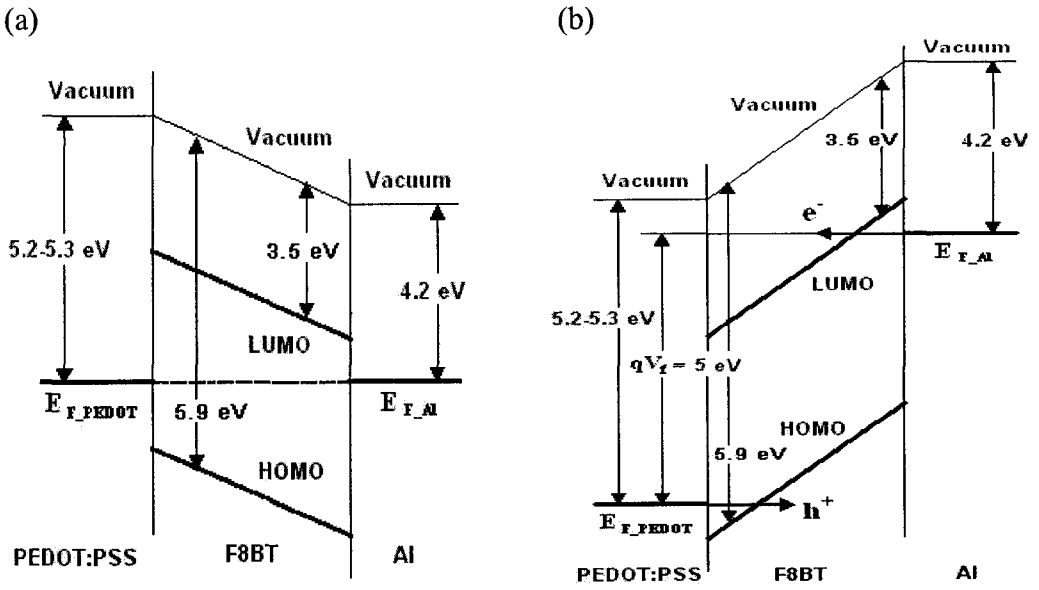

Fig. 7.18 Band diagrams for F8BT-based LED derived from PLED theory: (a) zero bias, (b) forward bias.

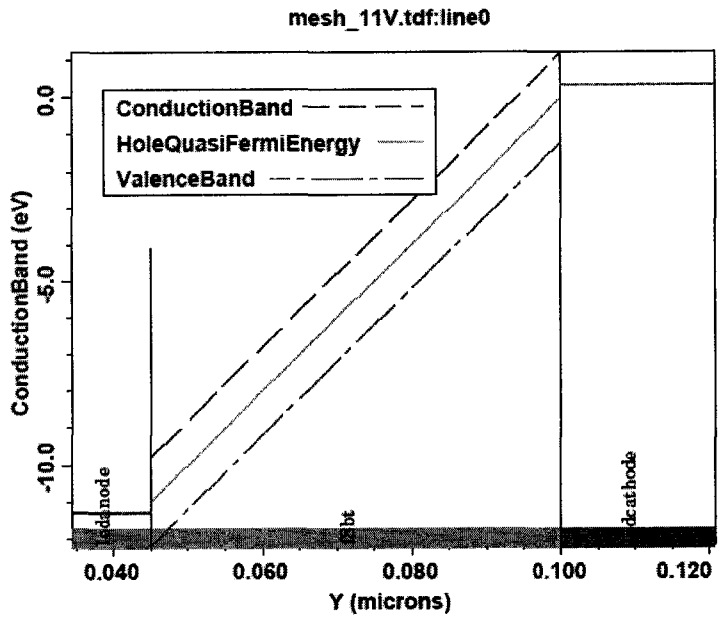

Fig. 7.19 Band diagram at forward bias for F8BT-based LED derived from TAURUS simulation.

7.4 Summary

We have used space charge limited current theory for the single-carrier case to model PF2/6-based LED, taking into account field-dependent hole mobility. At 300 K, we find a zero-field mobility $\mu_0 = 2.7646 \times 10^{-9} \text{cm}^2/\text{Vs}$, and an electric-field coefficient for the hole mobility $\gamma = 3.512 \times 10^{-3} (\text{cm}/\text{V})^{1/2}$. With these parameters, the theoretical calculation agrees very well with the *J-V* measurement for bias voltages above 2.6 V.

We have also employed the commercial software TAURUS to carry out the numerical simulation of the *J-V* characteristics for PF2/6-based LED and F8BT-based LED. For the PF2/6-based device, although the calculations can be fitted to the experimental data very well for bias voltages above ~1.4 V, the values for the important parameters used in the simulation are very unreasonable. For the F8BT-based device, the calculated *J-V* characteristics are in good agreement with the measurements from ~3 V through ~13.5 V. The values found for the important parameters are close to the values for polymers that were reported in the literature. The calculated carrier mobilities are consistent with those in F8BT reported in the literature. Thus, the theories involved in the TAURUS simulation can explain the electrical characteristics of F8BT-based devices to a certain degree.

CHAPTER 8

CONCLUSIONS AND FUTURE WORK

As a promising light-emitting polymer, PF has received considerable attention in PLED applications. Four strategies (synthesis of new PFs, refinement of device structure, modification of substrate or electrode, and blending) were carried out to enhance device performance or obtain the desired EL characteristics. Long-wavelength emission is the primary drawback of blue PFs, which can be depressed by macromolecular engineering, modification of device structure, or blending. Recent investigations on PF-based LEDs are directed toward PF molecular modification, suppression of the low-energy emission band, realization of white light emission, introduction of nano materials, as well as utilization of a SAM-modified ITO anode.

We fabricated and characterized PLEDs based on selected PFs, which are PF2/6, end-capped PF2/6, and F8BT. The results demonstrated that blending and end-capping can effectively improve EL properties and/or depress long-wavelength emission. Compared to pure PFs, the enhanced device performance was observed from PF2/6 blended with PFB, F8BT doped with PPB, and end-capped PF2/6 blended with F8BT (EQE of 0.16%). The low-energy emission band was suppressed to a certain extent by blending PF2/6 with PFB, and nearly completely suppressed via end-capping PF2/6 with

DMP or TPA. Additionally, end-capped PF2/6 displayed clearly increased EL properties (EQE of 0.16%) in comparison with PF2/6.

We used SCLC theory for the single-carrier case to model the fabricated PF2/6-based LED, taking into account field-dependent hole mobility. With the found parameters, a zero-field mobility and an electric-field coefficient for the hole mobility, the theoretical calculation agreed very well with the *J-V* measurement for bias voltages above 2.6 V. However it was also shown that the model is not applicable to the low electric field region. We also employed software package TCAD to conduct numerical simulation of the electrical characteristics of the pristine F8BT-based device and the above pristine PF2/6-based device. The calculation results demonstrated that the theories involved in the TAURUS simulation can explain the electrical characteristics of F8BT-based device to a great extent.

In the future, the following issues in the development of PF-based LEDs should be investigated:

1) Incorporation of electron transport/hole blocking layer into the device;

2) Usage of composite cathode such as Ca/Al;

3) Introduction of nano materials into the emitting layer;

4) Exploration of a device with optical grating;

5) Improvement of device stability via encapsulation;

6) Simulation of *J-V* characteristics of PF2/6-based LED in the lower electric field region ($<6.5\times10^5$ V/cm);

7) Further investigations on phase separation observed in PF2/6:PFB blends via using the Schroeder – van Laar Equation and Differential Scanning Calorimenter.

APPENDIX A

THE NUMERICAL SIMULATION INPUT FILE

AND OUTPUT DATA DEVELOPED

WITH SAS PROC REG

A.1 Transformation

PF2/6

VA(V)	IA(A)	J (A/m^2)	E (V/m)	SQRT(E) $(V/m)^{1/2}$	J/E^2 (A/V^2)	$lg(J/E^2)$
2.6	9.92E-05	1.10E+01	65000000	8062.258	2.61E-15	-14.5835
2.8	0.000122	1.36E+01	70000000	8366.6	2.78E-15	-14.5567
3	0.000152	1.69E+01	75000000	8660.254	3.00E-15	-14.523
3.2	0.000187	2.07E+01	80000000	8944.272	3.24E-15	-14.4896
3.4	0.000228	2.54E+01	85000000	9219.544	3.51E-15	-14.4546
3.6	0.00029	3.22E+01	90000000	9486.833	3.97E-15	-14.4009
3.8	0.000348	3.86E+01	95000000	9746.794	4.28E-15	-14.3686
4	0.00042	4.67E+01	1E+08	10000	4.67E-15	-14.3306
4.2	0.000507	5.63E+01	1.05E+08	10246.95	5.10E-15	-14.292
4.4	0.00064	7.11E+01	1.1E+08	10488.09	5.88E-15	-14.2307
4.6	0.000698	7.76E+01	1.15E+08	10723.81	5.87E-15	-14.2317
4.8	0.000822	9.13E+01	1.2E+08	10954.45	6.34E-15	-14.1978
5	0.000962	1.07E+02	1.25E+08	11180.34	6.84E-15	-14.1647
5.2	0.001123	1.25E+02	1.3E+08	11401.75	7.38E-15	-14.1319
5.4	0.0013	1.44E+02	1.35E+08	11618.95	7.93E-15	-14.101
5.6	0.001497	1.66E+02	1.4E+08	11832.16	8.48E-15	-14.0714
5.8	0.001716	1.91E+02	1.45E+08	12041.59	9.07E-15	-14.0424
6	0.001956	2.17E+02	1.5E+08	12247.45	9.66E-15	-14.0151
6.2	0.002228	2.48E+02	1.55E+08	12449.9	1.03E-14	-13.987
6.4	0.002526	2.81E+02	1.6E+08	12649.11	1.10E-14	-13.96
6.6	0.00286	3.18E+02	1.65E+08	12845.23	1.17E-14	-13.9329
6.8	0.003225	3.58E+02	1.7E+08	13038.4	1.24E-14	-13.9066
7	0.003622	4.02E+02	1.75E+08	13228.76	1.31E-14	-13.8813
7.2	0.004069	4.52E+02	1.8E+08	13416.41	1.40E-14	-13.8553
7.4	0.004559	5.07E+02	1.85E+08	13601.47	1.48E-14	-13.8297
7.6	0.00509	5.66E+02	1.9E+08	13784.05	1.57E-14	-13.8051
7.8	0.00565	6.28E+02	1.95E+08	13964.24	1.65E-14	-13.7822
8	0.006274	6.97E+02	2E+08	14142.14	1.74E-14	-13.7588
8.2	0.006919	7.69E+02	2.05E+08	14317.82	1.83E-14	-13.7377
8.4	0.007616	8.46E+02	2.1E+08	14491.38	1.92E-14	-13.717
8.6	0.008333	9.26E+02	2.15E+08	14662.88	2.00E-14	-13.6983
8.8	0.009082	1.01E+03	2.2E+08	14832.4	2.08E-14	-13.6809
9	0.009934	1.10E+03	2.25E+08	15000	2.18E-14	-13.6615
9.2	0.010665	1.19E+03	2.3E+08	15165.75	2.24E-14	-13.6497
9.4	0.012007	1.33E+03	2.35E+08	15329.71	2.42E-14	-13.6169
9.6	0.013439	1.49E+03	2.4E+08	15491.93	2.59E-14	-13.5863
9.8	0.014788	1.64E+03	2.45E+08	15652.48	2.74E-14	-13.5627
10	0.015962	1.77E+03	2.5E+08	15811.39	2.84E-14	-13.547

A.2 Input

```
data one;
input y x;
cards;
-14.58351377    8062.257748
-14.55669265    8366.600265
-14.52297884    8660.254038
-14.48955739    8944.271910
-14.45459347    9219.544457
-14.40092897    9486.832981
-14.36863494    9746.794345
-14.33063146    10000.00000
-14.29200736    10246.95077
-14.23070543    10488.08848
-14.23171433    10723.80529
-14.19783358    10954.45115
-14.16470692    11180.33989
-14.13190418    11401.75425
-14.10096669    11618.95004
-14.07136382    11832.15957
-14.04238531    12041.59458
-14.015145      12247.44871
-13.98699072    12449.89960
-13.95999755    12649.11064
-13.93288992    12845.23258
-13.90659717    13038.40481
-13.8813222     13228.75656
-13.8553105     13416.40786
-13.82970685    13601.47051
-13.80506606    13784.04875
-13.78224023    13964.24004
-13.75878568    14142.13562
-13.73771318    14317.82106
-13.71696557    14491.37675
-13.69831805    14662.87830
-13.68090637    14832.39697
-13.66148339    15000.00000
-13.64973732    15165.75089
-13.61694372    15329.70972
-13.58629804    15491.93338
-13.56266524    15652.47584
-13.54703522    15811.38830
;
proc print;
proc reg;
model y=x/all;
output out=new p=pr lcl=lci ucl=uci lclm=lcm uclm=ucm;
proc plot;
plot pr*x='*' lci*x='-' uci*x='+'/overlay;
plot pr*x='*' lcm*x='-' ucm*x='+'/overlay;
run;
```

A.3 Output

The SAS System 23:54 Wednesday, December 14, 2006 11

The REG Procedure
Model: MODEL1

Model Crossproducts X'X X'Y Y'Y

Variable	Intercept	x	y
Intercept	38	469097.53665	-532.3432371
x	469097.53665	5984999999.7	-6545246.084
y	-532.3432371	-6545246.084	7461.1959307

The REG Procedure
Model: MODEL1
Dependent Variable: y

X'X Inverse, Parameter Estimates, and SSE

Variable	Intercept	x	y
Intercept	0.8112503034	-0.000063585	-15.68491249
x	-0.000063585	5.1507956E-9	0.0001357573
y	-15.68491249	0.0001357573	0.004092615

Analysis of Variance

Source	DF	Sum of Squares	Mean Square	F Value	Pr > F
Model	1	3.57810	3.57810	31474.1	<.0001
Error	36	0.00409	0.00011368		
Corrected Total	37	3.58219			

Root MSE	0.01066	R-Square	0.9989
Dependent Mean	-14.00903	Adj R-Sq	0.9988
Coeff Var	-0.07611		

Parameter Estimates

Variable	DF	Parameter Estimate	Standard Error	t Value	Pr > |t|	Type I SS	Type II SS
Intercept	1	-15.68491	0.00960	-1633.3	<.0001	7457.61374	303.25595
x	1	0.00013576	7.652201E-7	177.41	<.0001	3.57810	3.57810

Parameter Estimates

Squared	Squared	Squared	Squared

Variable	DF	Standardized Estimate	Semi-partial Corr Type I	Partial Corr Type I	Semi-partial Corr Type II	Partial Corr Type II	Tolerance
Intercept	1	0	.	.	.	.	.
x	1	0.99943	0.99886	0.99886	0.99886	0.99886	1.00000

Parameter Estimates

Variable	DF	Variance Inflation	95% Confidence Limits	
Intercept	1	0	-15.70439	-15.66544
x	1	1.00000	0.00013421	0.00013731

The SAS System 23:54 Wednesday, December 14, 2006 13

The REG Procedure
Model: MODEL1
Dependent Variable: y

Covariance of Estimates

Variable	Intercept	x
Intercept	0.000092226	-7.228568E-9
x	-7.228568E-9	5.855618E-13

Correlation of Estimates

Variable	Intercept	x
Intercept	1.0000	-0.9836
x	-0.9836	1.0000

Sequential Parameter Estimates

Intercept	x
-14.009033	0
-15.684912	0.000136

APPENDIX B

TAURUS SIMULATION INPUT FILE

FOR PF2/6-BASED LED

```
####################
# PF26LED_struc.pdm #
####################

# Device Structure Generation
Taurus {device}

DefineDevice (
  name=PF26LED
  minX=0.0 maxX=3.000
  minY=0.0 maxY=0.285
  Region (material=silicon name=PF26)
  Region (material=electrode name=ledanode)
  Region (material=aluminum name=ledcathode)
  x=0 dx=0.100
  y=0 dy=0.020
  y=0.045 dy=0.005
  y=0.085 dy=0.05
  y=0.285
)

# Define PF26 region
DefineBoundary (
  region="PF26",
  polygon2d (
    Point (x=0.0 y=0.045) Point (x=3.000  y=0.045)
    Point (x=3.000 y=0.085) Point (x=0 y=0.085)
  )
)

# Define PEDOT:PSS region
DefineBoundary (
  region="ledanode",
  polygon2d (
    Point (x=0.0 y=0.0) Point (x=3.000  y=0.0)
    Point (x=3.000 y=0.045) Point (x=0 y=0.045)
  )
)

# Define aluminum region
DefineBoundary (
  region="ledcathode",
  polygon2d(
    Point (x=0.0 y=0.085) Point (x=3.000  y=0.085)
    Point (x=3.000 y=0.285) Point (x=0 y=0.285)
  )
)

# Refine the mesh structure
Regrid (
  GridProgram="NonLevelSet",
  minDelta=0.05um, maxDelta=0.05um)

# Define contacts
DefineContact (
  name=anode
  X (min=0.0  max=3um)    Y (min=0.0   max=0.045um )
```

```
)
DefineContact (
  name=cathode
  X (min= 0um max=3um)     Y (min=0.085  max=0.285um ))

# Save mesh structure
save (meshFile=mesh.tdf)


######################
# PF26LED_physics.pdm #
######################

# Set contact type and work function of PEDOT:PSS contact
setAttributes {Contact (name=anode,
                  type=ohmic,
                  transparent=true
                  workfunction=5.25,
                  barrierlowering=true,
                  alpha=0){PF26LED(region=ledanode)}}


# Set contact type and work function of Aluminum contact
setAttributes {Contact (name=cathode,
                  workfunction=4.05
                  ){PF26LED(region=ledcathode)}}

# Define the fixed charge in the interfaces
setAttributes{interface(
                  #qf=5e10
                  sn=1e7 #The surface electron recombination velocity
                  sp=1e7 #The surface hole recombination velocity
                  material(m0=silicon m1=electrode)
                  addup
                  ){PF26LED}}

# Define optical properties of Aluminium
Physics (Aluminum (
            OpticsModels(
                  RefractiveIndex   (
                        useIndexTable=false
                        nrReal=0.13
                        nrImag=6.08 )
                  Absorption(useconstabsorption=true,
constabsorption=2093))
            Global(Permittivity=36)
)){PF26LED(region=ledcathode)}

# Define optical and physical properties of PF2/6
Physics (Silicon (
             Global (
                        SurfaceDisorder=5e-4 #default value
                  Permittivity=3.0
                        electronAffinity=2.6) # [eV]

      # Define the density of states
            Poissons (
```

```
                        ValenceDensityofStates
                        ( AtRoomTemperature=2.5e34)
                  ConductionDensityofStates
                        ( AtRoomTemperature=2.5e34)
                        Bandgap (Eg300=2.99)
                  #ElectronEffectiveMass(me=0.067)    #default 0.067
                  holeEffectiveMass(me=0.4868) #  default 0.4868
                  )
            Electroncontinuity (
                              Recombination (
                             SRHActive=True
                        AugerActive=True
                        srhRecombination (
                                    ElectronLifeTime
                              (taun0=1e-5)
                                    HoleLifeTime
                              (taup0=1e-6))))
))

#AugerRecombination(AugN=0E0, AugP=0e0))

# Activate my mobility model for low and high electric field
Physics(Silicon(
        HoleContinuity(
                  Mobility(
                  lowFieldMobility (PMEImodel=myholemobility)
                  highFieldMobility (PMEIModel=myholemobilityhigh)
      ))))

#Physics(Silicon(
         #ElectronContinuity(
                  #Mobility(
                  #LowFieldMobility(PMEIModel=myelectronmobility)
                  #highFieldMobility (PMEIModel=myelectronmobilityhigh)
                  #))))

Physics(Silicon(mymobility( Mup0=0.15
                        #Mun0=1.5e-8
                        myholemobility(  Ep0=7.46e-4)
                        myholemobilityhigh(Ep1=7.46e-4)
                        #myelectronmobility(  En0=3.16e-4)
                        #myelectronmobilityhigh(  En1=3.16e-4)
            )))


################
# Mobility.pdm #
################

# It was found that carrier mobility is described by a Poole-Frenkel-
like field-dependent form.

# Include the data base for pre-defined variables
EquationDatabase{poissons.db,holecontinuity.db,electroncontinuity.db}

# Define equation for mobility model
DefineEquation
```

```
(      Name=mymobility,
 Material=Silicon,
 IsDeviceEquation,
 VariableName=Dummy,
 Parameter(Name=Mup0, Default=2.8e-9)
      Parameter(Name=Mun0, Default=2.8e-9)

Model (name=normfield
         expression{"sqrt(electricfield*electricfield)"})

      # Define hole mobility model at low field, the formulation is the
same as the following. But it is flexible to define the field-
dependence factor at different electric field.
Model
(Name=myholemobility,
parameter(name=Ep0, default=3.1e-3)
expression{"Mup0*exp(Ep0*sqrt(normfield))"}
)
       Model
(Name=myholemobilityhigh,
parameter(name=Ep1, default=3.1e-3)
expression{"Mup0*exp(Ep1*sqrt(normfield))"})

Model
(Name=myelectronmobility,
parameter(name=En0, default=3.1e-3)
expression{"Mun0*exp(En0*sqrt(normfield))"})

Model
(Name=myelectronmobilityhigh,
parameter(name=En1, default=3.1e-3)
expression{"Mun0*exp(En1*sqrt(normfield))"})

Expression{"dummy"}
)



####################
# PF26LED_simul.pdm #
####################

Taurus {device}

# Define area factor to match real device area
define (width=3000000)

# Call mesh file saved in PF26LED_struc.pdm
DefineDevice (name=PF26LED meshFile="mesh.tdf" areafactor=$width)

# Call  physics_definition saved in PF26LED_physics.pdm
include (physics_2.pdm)

Symbolic (carriers=0)
Solve {init}
Symbolic (carriers=1 Newton
          holes)
```

```
# Set contact bias to be zero

setBias (value=0.0) {Contact(name=anode  type=contactVoltage)}
setBias (value=0.0) {Contact(name=cathode  type=contactVoltage)}

Solve {}

#Ramp anode
Ramp (logfile=sr.data,
      Voltage (electrode=anode, startValue=0,vStep=0.2,nSteps=50))
```

APPENDIX C

TAURUS SIMULATION INPUT FILE

FOR F8BT-BASED LED

```
#####################
# F8BTLED_struc.pdm #
#####################

# Device Structure Generation

Taurus {device}

DefineDevice (

name=F8BTLED
minX=0.0 maxX=3.000
minY=0.0 maxY=0.3
Region (material=silicon name=F8BT)
Region (material=electrode name=ledanode)
Region (material=aluminum name=ledcathode)
x=0 dx=0.100
y=0 dy=0.02
y=0.045 dy=0.005
y=0.1 dy=0.05
y=0.3
)

# Define F8BT region
DefineBoundary
(
    region="F8BT",
    polygon2d(
Point (x=0.0 y=0.045) Point (x=3.000  y=0.045)
Point (x=3.000 y=0.1) Point (x=0 y=0.1)

  )
)

# Define PEDOT:PSS region
DefineBoundary

(
    region="ledanode",
    polygon2d(
Point (x=0.0 y=0.0) Point (x=3.000  y=0.0)
Point (x=3.000 y=0.045) Point (x=0 y=0.045)

  )
)

# Define aluminum region
DefineBoundary
(
    region="ledcathode",
    polygon2d(
Point (x=0.0 y=0.1) Point (x=3.000  y=0.1)
Point (x=3.000 y=0.3) Point (x=0 y=0.3)

  )
)
```

```
# Refine the mesh structure
Regrid (
  GridProgram="NonLevelSet",
  minDelta=0.05um, maxDelta=0.05um

)

# Define contacts
DefineContact (name=anode  X (min=0.0  max=3um)    Y (min=0.0
max=0.045um ))
DefineContact (name=cathode   X (min= 0um max=3um)    Y (min=0.1
max=0.3um ))

# Save mesh structure
save (meshFile=mesh.tdf)

########################
# F8BTLED_physics.pdm #
########################

# Set contact type and work function of PEDOT:PSS contact
setAttributes {Contact (name=anode,
                  type=ohmic,
                  transparent=true
                  workfunction=5.25,
                  barrierlowering=true,
                  alpha=0){F8BTLED(region=ledanode)}}


# Set contact type and work function of Aluminum contact
setAttributes {Contact (name=cathode,
                  workfunction=4.2
                  ){F8BTLED(region=ledcathode)}}


# Define physical properties of F8BT
Physics (Silicon (
             Global (
                  Permittivity=4.0
                        electronAffinity=3.5) # [eV]

      # Define the density of states
            Poissons (
                        ValenceDensityofStates
                        ( AtRoomTemperature=3.6e26)
                  ConductionDensityofStates
                        ( AtRoomTemperature=3.6e26)
                        Bandgap (Eg300=2.4)
                  ElectronEffectiveMass(me=0.067)    #default 0.067
                  holeEffectiveMass(me=0.4868) #  default 0.4868
                  )
            Electroncontinuity (
                              Recombination (
                             SRHActive=True
                  AugerActive=True
                           directActive=True
                  srhRecombination (
```

```
                                    ElectronLifeTime
                                (taun0=1e-9)
                                    HoleLifeTime
                                (taup0=2e-8))))
))


# Activate my mobility model for low and high electric field
Physics(Silicon(
        HoleContinuity(
                Mobility(
                lowFieldMobility (PMEImodel=myholemobility)
                highFieldMobility (PMEIModel=myholemobilityhigh)
      ))))

Physics(Silicon(
         ElectronContinuity(
                Mobility(
                LowFieldMobility(PMEIModel=myelectronmobility)
                highFieldMobility (PMEIModel=myelectronmobilityhigh)
                ))))

Physics(Silicon(mymobility( Mup0=3.18e-4
                    Mun0=3.18e-4
                    myholemobility(  Ep0=1.44e-3)
                    myholemobilityhigh(Ep1=1.44e-3)
                    myelectronmobility(  En0=1.440e-3)
                    myelectronmobilityhigh(  En1=1.44e-3)
           )))


#################
# Mobility.pdm #
#################

# It was found that carrier mobility is described by a Poole-Frenkel-
like field-dependent form.

# Include the data base for pre-defined variables
EquationDatabase{poissons.db,holecontinuity.db,electroncontinuity.db}

# Define equation for mobility model
DefineEquation
(      Name=mymobility,
 Material=Silicon,
 IsDeviceEquation,
 VariableName=Dummy,
 Parameter(Name=Mup0, Default=2.8e-9)
      Parameter(Name=Mun0, Default=2.8e-9)

Model (name=normfield
         expression{"sqrt(electricfield*electricfield)"})

      # Define hole mobility model. It is flexible to define the field-
dependence factor at different electric field.
Model
(Name=myholemobility,
```

```
parameter(name=Ep0, default=3.1e-3)
expression{"Mup0*exp(Ep0*sqrt(normfield))"}
)
Model
(Name=myholemobilityhigh,
parameter(name=Ep1, default=3.1e-3)
expression{"Mup0*exp(Ep1*sqrt(normfield))"})

Model
(Name=myelectronmobility,
parameter(name=En0, default=3.1e-3)
expression{"Mun0*exp(En0*sqrt(normfield))"})

Model
(Name=myelectronmobilityhigh,
parameter(name=En1, default=3.1e-3)
expression{"Mun0*exp(En1*sqrt(normfield))"})

Expression{"dummy"}
)

######################
# F8BTLED_simul.pdm #
######################

Taurus {device}

# Define area factor to match real device area
define (width=3000000)

# Call mesh file resulting from running F8BTLED_struc.pdm
DefineDevice (name=F8BTLED meshFile="mesh.tdf" areafactor=$width)

# Call physical properties defined by F8BTLED_physics.pdm
include (F8BTLED_physics.pdm)

Symbolic (carriers=0)
Solve {}
Symbolic (carriers=2 Newton)

# Set contact bias to be zero

setBias (value=0.0) {Contact(name=anode  type=contactVoltage)}
setBias (value=0.0) {Contact(name=cathode  type=contactVoltage)}

Solve {}

#Ramp anode
Ramp (logfile=sr.data,
      Voltage (electrode=anode, startValue=0,vStep=0.5,nSteps=26))
```

BIBLIOGRAPHY

[1] J. H. Burroughes, D. D. C. Bradley, A. R. Brown, R. N. Marks, K. Mackey, R. H. Friend, P. L. Burn, and A. B. Holmes, "Light-emitting diodes based on conjugated polymers," *Nature*, vol. 347, pp. 539-541, 1990.

[2] H. N. Cho, J. K. Kim, D. Y. Kim, C. Y. Kim, N. W. Song, and D. Kim, "Statistical Copolymers for Blue-Light-Emitting Diodes," *Macromolecules*, vol. 32, pp. 1476-1481, 1999.

[3] J. Shinar, *Organic Light-Emitting Devices*. New York, USA: Springer-Verlag, 2004, pp. 22-53.

[4] L. Bozano, S. A. Carter, J. C. Scott, G. G. Malliaras, and P. J. Brock, "Temperature- and Field-dependent electron and hole mobilities in polymer light-emitting diodes," *Applied Physics Letters*, vol. 74, pp. 1132-1134, 1999.

[5] P. W. M. Blom, M. J. M. de Jong, and J. J. M. Vleggaar, "Electron and hole transport in poly(*p*-phenylene vinylene) devices," *Applied Physics Letters*, vol. 68, pp. 3308-3310, 1996.

[6] B. V. Zeghbroeck. (2004, Jan. 10). *Principles of Semiconductor Devices*. [Online]. Available: http://ece-www.colorado.edu/~bart/book/book/title.html

[7] R. H. Friend, R. W. Gymer, A. B. Holmes, J. H. Burroughes, R. N. Marks, C. Taliani, D. D. C. Bradley, D. A. Dos Santos, J. L. Bredas, M. Logdlund, and W. R. Salaneck, "Electroluminescence in conjugated polymers," *Nature*, vol. 397, pp. 121-128, 1999.

[8] Yoshihiro Ohno, "NIST measurement services: photometric calibrations," in *Nist Special Publication 250-37*, Gaithersburg, MD: National Institute of Standards and Technonolgy, 1997, pp. 1-5.

[9] A. Ryer. (1997). *The Light Measurement Handbook*. International Light, Inc.. Newburyport, MA, U. S. A.. [Online]. Available: http://files.intl-light.com/handbook.pdf

[10] N. C. Greenham, R. H. Friend, and D. D. C. Bradley, "Angular dependence of the emission from a conjugated polymer light-emitting diode: implication for efficiency calculations," *Advanced Materials*, vol. 6, pp. 491-494, 1994.

[11] Y. Ohmori, M. Uchida, K. Muro, and K. Yoshino, "Blue electroluminescent diodes utilizing poly(alkylfluorene)," *Japanese Journal of Applied Physics*, vol. 30, pp. L1941-L1943, 1991.

[12] C.-F. Shu, R. Dodda, F.-I. Wu, M. S. Liu and A. K.-Y. Jen, "Highly efficient blue-light-emitting diodes from polyfluorene containing bipolar pendant groups macromolecules," *Macromolecules*, vol. 36, pp. 6698-6703, 2003.

[13] W. Wu, M. Inbasekaran, M. Hudack, D. Welsh, W. Yu, Y. Cheng, C. Wang, S. Kram, M. Tacey, M. Bernius, R. Fletcher, K. Kiszka, S. Munger, and J. O'Brien, "Recent development of polyfluorene-based RGB materials for light emitting diodes," *Microelectronics Journal*, vol. 35, pp. 343-348, 2004.

[14] C. Ego, A. C. Grimsdale, F. Uckert, G. Yu, G. Srdanov, and K. Mullen, "Triphenylamine-substituted polyfluorene-A stable blue-emitter with improved charge injection for light-emitting diodes," *Advanced Materials*, vol. 14, pp. 809-811, 2002.

[15] T. Miteva, A. Meisel, W. Knoll, H. G. Nothofer, U. Scherf, D. C. Muller, K. Meerholz, A. Yasuda, and D. Neher, "Improving the performance of polyfluorene-based organic light-emitting diodes via end-capping ," *Advanced Materials*, vol. 13, pp. 565-570, 2001.

[16] H.-J. Su, F.-I. Wu, Y.-L. Tung, Y. Chi, G.-H. Lee, "Polyfluorene containing diphenylquinoline pendants and their applications in organic light emitting diodes," *Journal of Polymer Science, Part A: Polymer Chemistry*, vol. 43, pp. 859-869, 2005.

[17] M. S. Liu, X. Jiang, P. Herguth, S. Liu, A. K.-Y. Jen, "Development of efficient electron-transporting polymers for light-emitting diodes," *Proceedings of SPIE - The International Society for Optical Engineering*, vol. 4800, pp. 130-137, 2002.

[18] F. Li, Z. Chen, B. Qu, W. Wei, Q. Gong, "Electroluminescence property of a novel dendritic polyfluorene derivative containing a triphenylamine group," *Journal of Physics D: Applied Physics*, vol. 38, pp. 847-851, 2005.

[19] N. C. Yang, S. M. Lee, Y. M. Yoo, J. K. Kim, D. H. Suh, "New Blue Electroluminescent n-Type Polyfluorene Copolymers with a 1,3,4-Oxadiazole Unit in the Main Chain," *Journal of Polymer Science, Part A: Polymer Chemistry*, vol. 42, pp. 1058-1068, 2004.

[20] G. Kwag, E. Park, and S. N. Lee, "Thermally stable and amorphous polyfluorene," *Journal of Applied Polymer Science*, vol. 96, pp. 1335-1340, 2005.

[21] S. Tokito, K.-H. Weinfurtner, H. Fujikawa, T. Tsutsui, Y. Taga, "Acene containing polyfluorenes for red, green and blue emission in organic light-emitting diodes," *Proceedings of SPIE - The International Society for Optical Engineering*, vol. 4105, pp. 69-74, 2001.

[22] J. H. Park, H. C. Ko, J. H. Kim, H. Lee, "Light emitting polyfluorene derivatives with three different structural configurations," *Synthetic Metals*, vol. 144, pp. 193-199, 2004.

[23] P. Qiang, M. Xie,V. Huang, Z. Lu, D. Xiao, "New series of highly phenyl-substituted polyfluorene derivatives for polymer light-emitting diodes," *Journal of Polymer Science, Part A: Polymer Chemistry*, vol. 42, pp. 2985-2993, 2004.

[24] H.-J. Su, F.-I. Wu, and C.-F. Shu, "Tuning Wavelength: Synthesis and Characterization of Spiro-DPVF-Containing Polyfluorenes and Applications in Organic Light-Emitting Diodes," *Macromolecules*, vol. 37, pp. 7197-7202, 2004.

[25] W.-L. Yu, J. Pei, W. Huang,A. J. Heeger, "Spiro-functionalized polyfluorene derivatives as blue light-emitting materials," *Advanced Materials*, vol. 12, pp. 828-831, 2000.

[26] G. Klarner, M. H. Davey, W.-D. Chen, J. C. Scott, R. D. Miller, "Colorfast blue-light-emitting random copolymers derived from di-n-hexylfluorene and anthracene," *Advanced Materials*, vol. 10, pp. 993-997, 1998.

[27] X.-M. Liu, C. He, X.-T. Hao, L.-W. Tan, Y. Li, K. S. Ong, "Hyperbranched blue-light-emitting alternating copolymers of tetrabromoarylmethane/silane and 9,9-dihexylfluorene-2,7-diboronic acid," *Macromolecules*, vol. 37, pp. 5965-5970, 2004.

[28] J. Lee, H.-J. Cho, B.-J. Jung, N. S. Cho, H.-K. Shim, "Stabilized blue luminescent polyfluorenes: Introducing polyhedral oligomeric silsesquioxane," *Macromolecules*, vol. 37, pp. 8523-8529, 2004.

[29] W.-J. Lin, W.-C. Chen, W.-C. Wu, Y.-H. Niu, A. K.-Y. Jen, "Synthesis and Optoelectronic Properties of Starlike Polyfluorenes with a Silsesquioxane Core," *Macromolecules*, vol. 37, pp. 2335-2341, 2004.

[30] C.-H. Chou, S.-L. Hsu, K. Dinakaran,M.-Y. Chiu, K.-H. Wei, "Synthesis and characterization of luminescent polyfluorenes incorporating side-chain-tethered polyhedral oligomeric silsesquioxane units," *Macromolecules*, vol. 38, pp. 745-751, 2005.

[31] J. Li, Y. Hirayama, T. Sano, T. Tomita, H. Fujii, and K. Wakisaka, "Reduction of chain interactions in a class of blue fluorene copolymers with adamantane units," *Thin Solid Films*, vol. 515, pp. 2686-2691, 2006.

[32] S. H. Jung, J. B. Kim, D. H. Suh, H. N. Cho, "Highly phenyl-substituted polyfluorenes for light-emitting diodes," *Synthetic Metals*, vol. 137, pp. 1049-1050, 2003.

[33] J. Liu, G. Tu, Q. Zhou, Y. Cheng, Y. Geng, L. Wang, D. Ma, X. Jing, and F. Wang, "Highly efficient green light emitting polyfluorene incorporated with 4-diphenylamino-1,8-naphthalimide as green dopant," *Journal of Materials Chemistry*, vol. 16, pp. 1431-1438, 2006.

[34] N. S. Cho, D.-H. Hwang, B.-J. Jung, E. Lim, J. Lee, and H.-K. Shim, "Synthesis, characterization, and electroluminescence of new conjugated polyfluorene derivatives containing various dyes as comonomers," *Macromolecules*, vol. 37, pp. 5265-5273, 2004.

[35] E. Lim, B.-J. Jung, H.-K.-Shim, "Synthesis and characterization of a new light-emitting fluorene-thieno[3,2-b]thiophene-based conjugated copolymer," *Macromolecules*, vol. 36, pp. 4288-4293, 2003.

[36] A. P. Kulkarni,Y. Zhu, S. A. Jenekhe, "Quinoxaline-containing polyfluorenes: Synthesis, photophysics, and stable blue electroluminescence," *Macromolecules*, vol. 38, pp. 1553-1563, 2005.

[37] G. Tu, Q. Zhou, Y. Cheng, L. Wang, D. Ma, X. Jing, and F. Wang, "White electroluminescence from polyfluorene chemically doped with 1,8-napthalimide moieties," *Applied Physics Letters*, vol. 85, pp. 2172-2174, 2004.

[38] Y. He, S. Gong, R. Hattori, and J. Kanicki, "High performance organic polymer light-emitting heterostructure devices," *Applied Physics Letters*, vol. 74, pp. 2265-2267, 1999.

[39] J. P. Chen, G. Klaerner, J-I Lee, D. Markiewicz, V. Y. Lee, R. D. Miller, and J. C. Scott, "Efficient, blue light-emitting diodes using cross-linked layers of polymeric arylamine and fluorine," *Synthetic Metals*, vol. 107, pp. 129-135, 1999.

[40] J. Morgado, R. H. Friend, and F. Cacialli, "Improved efficiency of light-emitting diodes based on polyfluorene blends upon insertion of a poly(p-phenylene vinylene) electron confinement layer," *Applied Physics Letters*, vol. 80, pp. 2436-2438, 2002.

[41] A. K-Y. Jen, Y. Liu, Q.-S. Hu, and L. Pu, "Efficient light-emitting diodes based on a binaphthalene-containing polymer," *Applied Physics Letters*, vol. 75, pp. 3745-3747, 1999.

[42] X. Jiang, S. Liu, H. Ma, and A. K.-Y. Jen, "High-performance blue light-emitting diode based on a binaphthyl-containing polyfluorene," *Applied Physics Letters*, vol. 76, pp. 1813-1815, 2000.

[43] J. Lu, Y. Tao, M. D'iorio, Y. Li, J. Ding, and M. Day, "Pure deep blue light-emitting diodes from alternating fluorene/carbazole copolymers by using suitable hole-blocking materials," *Macromolecules*, vol. 37, pp. 2442-2449, 2004.

[44] X. Gong, P. K. Iyer, D. Moses, G. C. Bazan, A. J. Heeger, and S. S. Xiao, "Stabilized blue emission from polyfluorene-based light-emitting diodes: elimination of fluorenone defects," *Advanced Functional Materials*, vol. 13, pp. 325-330, 2003.

[45] T. Kawase, P. K. H. Ho, R. H. Friend, and T. Shimoda, "Low voltage operation of polymer light-emitting device with conducting polymer distributed Bragg reflector," *Electrical, optical, and magnetic properties of organic solid-state materials V (Materials Research Society Symposium – Proceedings)*, vol. 598, pp. BB11.49.1-BB11.49.6, 2000.

[46] K. Pichler, D. D. C. Bradley, P. L. Burn, R. H. Friend, D. A. Halliday, and A. B. Holmes, "Optical spectroscopy of highly ordered poly(p-phenylene vinylene)," *Journal of Physics: Condensed Matter*, vol. 5, pp. 7155-7172, 1993.

[47] J. Cornil, D. Beljonne, Z. Shuai, T. Hagler, D. D. C. Bradley, I. Campbell, J.-L. Bre´das, C. W. Spangler, and K. Mu¨llen, "Vibronic structure in the optical absorption spectra of phenylene vinylene oligomers: a joint experimental and theoretical study," *Chemical Physics Letters*, vol. 247, pp. 425-432, 1995.

[48] T. Virgili, D. G. Lidzey, and D. D. C. Bradley, "Efficient Energy Transfer from Blue to Red in Tetraphenylporphyrin-Doped Poly(9,9-dioctylfluorene) Light-Emitting Diodes," *Advanced Materials*, vol. 12, pp. 58-62, 1999.

[49] M. A. Baldo, D. F. O'Brien, Y. You, A. Shoustikov, S. Sibley, M. E. Thompson, and S. R. Forrest, "Highly efficient phosphorescent emission from organic electroluminescent devices," *Nature* (London), vol. 395, pp. 151-154, 1998.

[50] R. B. Fletcher, D. G. Lidzey, D. D. C. Bradley, M. Bernius, and S. Walker, "Spectral properties of resonant-cavity, polyfluorene light-emitting diodes," *Applied Physics Letters*, vol. 77, pp. 1262-1264, 2000.

[51] Y. He, and J. Kanicki, "Polyfluorene light emitting devices on flexible plastic substrates," *Proceedings of SPIE - The International Society for Optical Engineering (Organic Light-Emitting Materials and Devices IV)*, vol. 4105, pp. 143-151, 2001.

[52] M. P. de Jong, L. J. van Ijzendoorn, and M. J. A. de Voigt, "Stability of the interface between indium-tin-oxide and poly(3,4-ethylenedioxythiophene) /poly(styrenesulfonate) in polymer light-emitting diodes," *Applied Physics Letters*, vol. 77, pp. 2255-2257, 2000.

[53] K. W. Wong, H. L. Yip, Y. Luo, K. Y. Wong, W. M. Lau, K. H. Low, H. F. Chow, Z. Q. Gao, W. L. Yeung, and C. C. Chang, "Blocking reactions between indium-tin oxide and poly (3,4-ethylene dioxythiophene):poly(styrene sulphonate) with a self-assembly monolayer," *Applied Physics Letters*, vol. 80, pp. 2788-2790, 2002.

[54] H. Yan, Q. Huang, J. Cui, J. G. C. Veinot, M. M. Kern, and T. J. Marks, "High-brightness blue light-emitting polymer diodes via anode modification using self-assembled monolayer," *Advanced Materials*, vol. 15, pp. 835-838, 2003.

[55] J. Morgado, N. Barbagallo, A. Charas, M. Matos, L. Alcacer, and F. Cacialli, "Self-assembly surface modified indium-tin oxide anodes for single-layer light-emitting diodes," *Journal of Physics D: Applied Physics*, vol. 36, pp. 434-438, 2003.

[56] J. Morgado, A. Charas, N. Barbagallo, L. Alcacer, M. Matos, and F. Cacialli, "Effect of a dipolar self-assembly monolayer formation on indium-tin oxide on the performance of single-layer polymer-based light-emitting diodes," *Macromolecular Symposia*, vol. 212, pp. 381-386, 2004.

[57] J. S. Kim, R. H. Friend, and F. Cacialli, "Improved operational stability of polyfluorene-based organic light-emitting diodes with plasma-treated indium–tin–oxide anodes," *Applied Physics Letters*, vol. 74, pp. 3084-3086, 1999.

[58] J. S. Kim, R. H. Friend, and F. Cacialli, "Improved electroluminescence lifetime and efficiency of polymer light-emitting diodes with plasma-treated indium tin oxide anodes," *Materials Research Society Symposium Proceedings*, vol. 558, pp. 439-444, 2000.

[59] T. M. Brown, R. H. Friend, I. S. Millard, D. J. Lacey, J. H. Burroughes, and F. Cacialli, "Efficient electron injection in blue-emitting polymer light-emitting diodes with LiF/Ca/Al cathodes," *Applied Physics Letters*, vol. 79, pp. 174-176, 2001.

[60] C. J. Lawrence, "The mechanics of spin coating of polymer films," *Physics of Fluids*, vol. 31, pp. 2786-2795, 1988.

[61] D. Meyerhofer, "Characteristics of resist films produced by spinning," *Journal of Applied Physics*, vol. 49, pp. 3993-3997, 1978.

[62] S. Walheim, M. Boltau, J. Mlynek, G. Krausch, and U. Steiner, "Structure Formation via Polymer Demixing in Spin-Cast Films," *Macromolecules*, vol. 30, pp. 4995-5003, 1997.

[63] A. P. Kulkarni, and S. A. Jenekhe, "Blue light-emitting diodes with good spectral stability based on blends of poly(9,9-dioctylfluorene): interplay between morphology, photophysics, and device performance," *Macromolecules*, vol. 36, pp. 5285-5296, 2003.

[64] M. Bernius, M. Inbasekaran, E. Woo, W. Wu, and L. Wujkowski, "Light-emitting diodes based on fluorene polymers," *Thin Solid Films,* vol. 363, pp. 55-57, 2000.

[65] E. Moons, "Conjugated polymer blends: linking film morphology to performance of light emitting diodes and photodiodes," *Journal of Physics: Condensed Matter*, vol. 14, pp. 12235-12260, 2002.

[66] A. Cirpan, L. Ding, and F. E. Karasz, "Efficient light emitting diodes from polyfluorene copolymer blends," *Synthetic Metals*, vol. 150, pp. 195-198, 2005.

[67] L. C. Palilis, D. G. Lidzey, M. Redecker, D. D. C. Bradley, M. Inbasekaran, E. P. Woo, and W. W. Wu, "High performance blue light-emitting diodes based on conjugated polymer blends," *Synthetic Metals*, vol. 121, pp. 1729-1730, 2001.

[68] V. Casasanta, T. Londergan, and R. Dinu, "Polymer blend LEDs using polyfluorene copolymers and thermally cross-linked fluoropolymers," *Proceedings of SPIE - The International Society for Optical Engineering (Organic Photonic Materials and Devices VI)*, vol. 5351, pp. 217-225 , 2004.

[69] A. Cirpan, L. Ding, and F. E. Karasz, "Optical and electroluminescent properties of polyfluorene copolymers and their blends," *Polymer*, vol. 46, pp. 811-817, 2005.

[70] A. Charas, J. Morgado, L. Alcacer, J. M. G. Martinho, and F. Cacialli, "Luminescence properties of polyfluorenes blends," *Synthetic Metals*, vol. 137, pp. 1039-1040, 2003.

[71] S. Cina, N. Baynes, E. Moons, R. H. Friend, J. Burroughes, C. Towns, K. Heeks, R. O'Dell, S. O'Connor, and N. Athanassopoulou, "New, efficient light emitting polymer diode for flat panel display applications," *Proceedings of SPIE - The International Society for Optical Engineering (Organic Photonic Materials and Devices III)*, vol. 4279, pp. 221-228, 2001.

[72] L. C. Palilis, D. G. Lidzey, M. Redecker, D. D. C. Bradley, M. Inbasekaran, E. P. Woo, and W. W. Wu, "Bright and efficient blue and green light-emitting diodes based on conjugated polymer blends," *Synthetic Metals*, vol. 111-112, pp. 159-163, 2000.

[73] D. Sainova, T. Miteva, H. G. Nothofer, U. Scherf, I. Glowacki, J. Ulanski, H. Fujikawa, and D. Neher, "Control of color and efficiency of light-emitting diodes based on polyfluorenes blended with hole-transporting molecules," *Applied Physics Letters*, vol. 76, pp. 1810-1812, 2000.

[74] A. R. Buckley, M. D. Rahn, J. Hill, J. Cabanillas-Gonzalez, A. M. Fox, and D. D. C. Bradley, "Energy transfer dynamics in polyfluorene-based polymer blends," *Chemical Physics Letters*, vol. 339, pp. 331-336, 2001.

[75] D. F. O'Brien, C. Giebeler, R. B. Fletcher, A. J. Cadby, L. C. Palilis, D. G. Lidzey, P. A. Lane, D. D. C. Bradley, and W. Blau, "Electrophosphoresence from a doped polymer light emitting diode," *Synthetic Metals*, vol. 116, pp. 379-383, 2001.

[76] X. Gong, J. C. Ostrowski, G. C. Bazan, D. Moses, A. J. Heeger, M. S. Liu, and A. K.-Y. Jen, "Electrophosphorescence from a Conjugated Copolymer Doped with an Iridium Complex: High Brightness and Improved Operational Stability," *Advanced Materials*, vol. 15, pp. 45-49, 2003.

[77] J. H. Kim, M. S. Liu, A. K.-Y. Jen, B. Carlson, L. R. Dalton, C.-F. Shu, and R. Dodda, "Bright red-emitting electrophosphorescent device using osmium complex as a triplet emitter," *Applied Physics Letters*, vol. 83, pp. 776-778, 2003.

[78] G.-K. Ho, H.-F. Meng, S.-C. Lin, S.-F. Horng, C.-S. Hsu, L.-C. Chen, and S.-M. Chang, "Efficient white light emission in conjugated polymer homojunctions," *Applied Physics Letters*, vol. 85, pp. 4576-4578, 2004.

[79] F.-I. Wu, P.-I. Shih, Y.-H. Tseng, C.-F. Shu, Y.-L. Tung, and Y. Chi, "Highly efficient white-electrophosphorescent devices based on polyfluorene copolymers containing charge-transporting pendent units," *Journal of Materials Chemistry*, vol. 17, pp. 167-173, 2007.

[80] A. J. Campbell, D. D. C. Bradley, T. Virgili, D. G. Lidzey, and H. Antoniadis, "Improving efficiency by balancing carrier transport in poly(9,9-dioctylfluorene) light-emitting diodes using tetraphenylporphyrin as a hole-trapping, emissive dopant," *Applied Physics Letters*, vol. 79, pp. 3872-3874, 2001.

[81] M. Grell, D. D. C. Bradley, G. Ungar, J. Hill, and K. S. Whitehead, "Interplay of Physical Structure and Photophysics for a Liquid Crystalline Polyfluorene," *Macromolecules*, vol. 32, pp. 5810 – 5817, 1999.

[82] K.-H. Weinfurtner, H. Fujikawa, S. Tokito, and Y. Taga, "Highly efficient pure blue electroluminescence from polyfluorene: Influence of the molecular weight distribution on the aggregation tendency," *Applied Physics Letters*, vol. 76, pp. 2502-2504, 2000.

[83] G. Klarner, J.-I. Lee, M. H. Davey, and R. D. Miller, "Exciton Migration and Trapping in Copolymers Based on Dialkylfluorenes," *Advanced Materials*, vol. 11, pp. 115-119, 1999.

[84] J.-I. Lee, G. Klaerner, and R. D. Miller, "Oxidative Stability and Its Effect on the Photoluminescence of Poly(Fluorene) Derivatives: End Group Effects," *Chemistry of Materials*, vol. 11, pp 1083-1088, 1999.

[85] C. Xia, and R. C. Advincula, "Decreased Aggregation Phenomena in Polyfluorenes by Introducing Carbazole Copolymer Units," *Macromolecules*, vol. 34, pp. 5854-5859, 2001.

[86] S. Setayesh, A. C. Grimsdale, T. Weil, V. Enkelmann, K. Mullen, F. Meghdadi, E. J. W. List, and G. Leising, "Polyfluorenes with Polyphenylene Dendron Side Chains: Toward Non-Aggregating, Light-Emitting Polymers," *Journal of the American Chemical Society*, vol. 123, pp. 946-953, 2001.

[87] V. N. Bliznyuk, S. A. Carter, J. C. Scott, G. Klarner, R. D. Miller, and D. C. Miller, "Electrical and Photoinduced Degradation of Polyfluorene Based Films and Light-Emitting Devices," *Macromolecules*, vol. 32, pp. 361-369, 1999.

[88] U. Scherf, and E. J. W. List, "Semiconducting Polyfluorenes - Towards Reliable Structure-Property Relationships," *Advanced Materials*, vol. 14, pp. 477-487, 2002.

[89] E. J. W. List, R. Guentner, P. S. de Freitas, and U. Scherf, "The Effect of Keto Defect Sites on the Emission Properties of Polyfluorene-Type Materials," *Advanced Materials*, vol. 14, pp. 374-378, 2002.

[90] J. M. Lupton, M. R. Craig, and E. W. Meijer, "On-chain defect emission in electroluminescent polyfluorenes," *Applied Physics Letters*, vol. 80, pp. 4489-4491, 2002.

[91] M. Gaal, E. J. W. List, and U. Scherf, "Excimers or Emissive On-Chain Defects?," *Macromolecules*, vol. 36, pp. 4236 – 4237, 2003.

[92] E. J. W. List, R. Guentner, P. S. De Freitas, U. Scherf, and M.Gaal, "The role of keto defect sites for the emission properties of polyfluorene-type materials," *Synthetic Metals*, vol. 139, pp. 759-763, 2003.

[93] X. H. Yang, F. Jaiser, D. Neher, P. V. Lawson, J.-L. Bredas, E. Zojer, R. Guntner, P. S. De Freitas, M. Forster, and U. Scherf, "Suppression of the keto-emission in polyfluorene light-emitting diodes: Experiments and models," *Advanced Functional Materials*, vol. 14, pp. 1097-1104, 2004.

[94] S. Gamerith, H.-G. Nothofer, U. Scherf, and E. J. W. List, "Identification of emissive interface-related defects in polyfluorene-based light emitting devices," *Japanese Journal of Applied Physics, Part 2: Letters*, vol. 43, pp. L891-L893, 2004.

[95] S. Gamerith, C. Gadermaier, H.-G. Nothofer, U. Scherf, and E. J. W. List, "Degradation of polyfluorene type polymers - Interface and bulk related defects," *Proceedings of SPIE - The International Society for Optical Engineering (Organic Optoelectronics and Photonics)*, vol. 5464, pp. 104-113 , 2004.

[96] X. Gong, D. Moses, A. J. Heeger, and S. Xiao, "White light electrophosphorescence from polyfluorene-based light-emitting diodes: Utilization of fluorenone defects," *Journal of Physical Chemistry B*, vol. 108, pp. 8601-8605, 2004.

[97] J. H. Kim, P. Herguth, M.-S. Kang, A. K.-Y. Jen, Y.-H. Tseng, and C.-F. Shu, "Bright white light electroluminescent devices based on a dye-dispersed polyfluorene derivative," *Applied Physics Letters*, vol. 85, pp. 1116-1118, 2004.

[98] Q. Xu, H. M. Duong, F. Wudl, and Y. Yang, "Efficient single-layer "twistacene"-doped polymer white light-emitting diodes," *Applied Physics Letters*, vol. 85, pp. 3357-3359, 2004.

[99] J. Liu, Q. Zhou, Y. Cheng, Y. Geng, L. Wang, D. Ma, X. Jing, and F. Wang, "White electroluminescence from a single-polymer system with simultaneous two-color emission: Polyfluorene as the blue host and a 2,1,3-benzothiadiazole derivative as the orange dopant on the main chain," *Advanced Functional Materials*, vol. 16, pp. 957-965, 2006.

[100] P.-I. Shih, Y.-H. Tseng, F.-I. Wu, A. K. Dixit, and C.-F. Shu, "Stable and efficient white electroluminescent devices based on a single emitting layer of polymer blends," *Advanced Functional Materials*, vol. 16, pp. 1582-1589, 2006.

[101] P.-I. Lee, S. L.-C. Hsu, and R.-F. Lee, "White-light-emitting diodes from single polymer systems based on polyfluorene copolymers end-capped with a dye," *Polymer*, vol. 48, pp. 110-115, 2007.

[102] J. H. Park, Y. T. Lim, O O. Park, J. K. Kim, J.-W. Yu, and Y. C. Kim, "Stabilized blue emission from polymer-dielectric nanolayer nanocomposites," *Advanced Functional Materials*, vol. 14, pp. 377-382, 2004.

[103] J. Morgado, E. Moons, R.H. Friend, and F. Cacialli, "Optical and morphological investigations of non-homogeneity in polyfluorene blends," *Synthetic Metals*, vol. 124, pp.63-66, 2001.

[104] J. Chappell, D. Lidzey, P. Jukes, A. Higgins, R. Thompson, S. O'Connor, I. Grizzi, R. Fletcher, J. O'Brien, M. Geoghegan, and R. Jones, "Correlating structure with fluorescence emission in phase-separated conjugated-polymer blends," *Nature Materials,* vol. 2, pp.616–621, 2003.

[105] J. Kim, P. K. H. Ho, C. E. Murphy, and R. H. Friend, "Phase separation in polyfluorene-based conjugated polymer blends: Lateral and vertical analysis of blend spin-cast thin films," *Macromolecules*, vol. 37, pp. 2861-2871, 2004.

[106] A. M. Higgins, S. J. Martin, R. L. Thompson, J. Chappell, M. Voigt, D. G. Lidzey, R. A. L. Jones, and M. Geoghegan, "Surface segregation and self-stratification in blends of spin-cast polyfluorene derivatives," *Journal of Physics: Condensed Matter*, vol. 17, pp. 1319–1328, 2005.

[107] G. Yu, H. Nishino, A. J. Heeger, T.-A. Chen, and R. D. Rieke, "Enhanced electroluminescence from semiconducting polymer blends," *Synthetic Metals*, vol. 72, pp. 249-252, 1995.

[108] A. Dogariu, R. Gupta, A. J. Heeger, and H. Wang, "Time-resolved Förster energy transfer in polymer blends," *Synthetic Metals*, vol. 100, pp. 95-100, 1999.

[109] L. Ding, F. E. Karasz, Z. Lin, M. Zheng, L. Liao, and Y. Pang, "Effect of Fo¨rster energy transfer and hole transport layer on performance of polymer light-emitting diodes," *Macromolecules*, vol. 34, pp. 9183-9188, 2001.

[110] X. Zhang, D. M. Kale, and S. A. Jenekhe, "Electroluminescence of multicomponent conjugated polymers.2.Photophysics and enhancement of electroluminescence from blends of polyquinolines," *Macromolecules*, vol. 35, pp. 382-393, 2002.

[111] A. J. Campbell, H. Antoniadis, T. Virgili, D. G. Lidzey, X. Wang, and D. D. Bradley, "Balancing electron and hole currents in single layer poly(9,9-dioctylfluorene) light-emitting diodes," *Proceedings of SPIE - The International Society for Optical Engineering (Organic Light-Emitting Materials and Devices V)*, vol. 4464, pp. 211-222, 2002.

[112] T. M. Brown, J. S. Kim, R. H. Friend, F. Cacialli, R. Daik, and W. J. Feast, "Effect of Poly(3,4-ethylene dioxythiophene) on the Built-in Field in Polymer Light-Emitting Diodes Probed by Electroabsorption Spectroscopy," *Synthetic Metals*, vol. 111-112, pp. 285-287, 2000.

[113] Y. C. Tseng, M. Tzolov, E. H. Sargent, P. W. Cyr, and M. A. Hines, "Control over Exciton Confinement versus Separation in Composite Films of Polyfluorene and CdSe Nanocrystals," *Applied Physics Letters*, vol. 81, pp. 3446-3448, 2002.

[114] Y. Huang, Z. Lu, Q. Peng, Q. Jiang, R. Xie, S. Han, L. Dong, J. Peng, Y. Cao, and M. Xie, "Luminescent properties of coumarin-doped MEH-PPV and novel coumarin-terminated MEH-PPV," *Materials Chemistry and Physics*, vol. 93, pp. 95-99, 2005.

[115] J. Cao, Q. Zhou, Y. Cheng, Y. Geng, L. Wang, D. Ma, X. Jing, F. Wang, L. A. P. Kane-Maguire, and D. L. Officer, "Polyfluorenes containing 1,8-naphthalimide dye as endcapping groups," *Synthetic Metals*, , vol. 152, pp. 237-240, 2005.

[116] M. Jikei, R. Mori, S. Kawauchi, M.-A. Kakimoto, and Y. Taniguchi, "Synthesis and properties of hyperbranched poly(triphenylamine)s prepared by palladium catalyzed C-N coupling reaction," *Polymer Journal*, vol. 34, pp. 550-557, 2002.

[117] Y. K. Nakazawa, S. A. Carter, H.-G. Nothofer, U. Scherf, V. Y. Lee, R. D. Miller, and J. C. Scott, "Effects of polymer sidebranching in double- and single-layer polyfluorene light-emitting diodes," *Appiled Physics Letters*, vol. 80, pp. 3832-3834, 2002.

[118] Jeong-Ik Lee, Victor Y. Lee, and Robert D. Miller, "Excimer and Aggregate Formations in Poly(fluorene)s," *ETRI Journal*, vol. 24, pp. 409-414, 2002.

[119] D. Neher, "Polyfluorene Homopolymers: Conjugated Liquid-Crystalline Polymers for Bright Blue Emission and Polarized Electroluminescence," *Macromolecular Rapid Communications*, vol. 22, pp. 1365-1385, 2001.

[120] A. Kadashchuk, R. Schmechel, H. von Seggern, U. Scherf , and A. Vakhnin, "Charge-carrier trapping in polyfluorene-type conjugated polymers," *Journal of Applied Physics*, vol. 98, pp. 024101.1-024101.8, 2005.

[121] J. I. Lee, D. H. Hwang, H. Park, L. M. Do, H, Y. Chu, T. Zyung, and R. D. Miller, "Light-emitting electrochemical cells based on poly(9,9-bis(3,6-dioxaheptyl)-fluorene-2,7-diyl)," *Synthetic Metals,* vol. 111-112, pp. 195-197, 2000.

[122] G. Klärner, J. I. Lee, V. Y. Lee, E. Chan, J. P. Chen, A. Nelson, D. Markiewicz, R. Siemens, J. C. Scott, and R. D. Miller, "Cross-linkable Polymers Based on Dialkylfluorenes," *Chemistry of Materials*, vol. 11, pp. 1800-1805, 1999.

[123] J.-I. Lee, G. Klärner, J. P. Chen, J. C. Scott, and R. D. Miller, "Novel polymers based on poly(fluorene)s for LED applications," *Proceedings of SPIE - The International Society for Optical Engineering*, vol. 3623, pp. 2-12, 1999.

[124] L. Fenenko, Y. Nakanishi, S. Tokito, and A. Konno, "Electronic characterization of new bright-blue-light-emitting poly(9,9-dioctylfluorenyl-2,7-diyl)-end capped with polyhedral oligomeric silsesquioxanes," *Japanese Journal of Applied Physics, Part 1: Regular Papers and Short Notes and Review Papers*, vol. 45, pp. 550-554, 2006.

[125] N. Tessler, N. T. Harrison, D. S. Thomas, and R. H. Friend, "Current heating in polymer light emitting diodes," *Applied Physics Letters*, vol. 73, pp. 732-734, 1998.

[126] J. F. Ding, M. Day, G. Robertson, and J. Roovers, "Synthesis and Characterization of Alternating Copolymers of Fluorene and Oxadiazole," *Macromolecules*, vol. 35, pp. 3474-3483, 2002.

[127] X. Gong , W. Ma , J. C. Ostrowski , K. Bechgaard , G. C. Bazan , A. J. Heeger, S. Xiao, and D. Moses, "End-Capping as a Method for Improving Carrier Injection in Electrophosphorescent Light-Emitting Diodes," *Advanced Functional Materials*, vol. 14, pp. 393–397, 2004.

[128] J. Morgado, E. Moons, R. H. Friend, and F. Cacialli, "De-mixing of polyfluorene-based blends by contact with acetone: electro- and photo-luminescence probes," *Advanced Materials*, vol. 13, pp. 810-814, 2001.

[129] R. Stevenson, R. Riehn, R. G. Milner, D. Richards, E. Moons, D.-J. Kang, M. Blamire, J. Morgado, and F. Cacialli, "Ultraviolet–visible near-field microscopy of phase-separated blends of polyfluorene-based conjugated semiconductors," *Applied Physics Letters*, vol. 79, pp. 833-835, 2001.

[130] M. Redecker, D. D. C. Bradley, M. Inbasekaran, and E. P. Woo, "Nondispersive hole transport in an electroluminescent polyfluorene," *Applied Physics Letters*, vol. 73, pp. 1565-1567, 1998.

[131] G. G. Malliaras, and J. C. Scott, "Numerical simulations of the electrical characteristics and the efficiencies of single-layer organic light emitting diodes," *Journal of Applied Physics*, vol. 85, pp. 7426-7432, 1999.

[132] P. W. M. Blom, H. F. M. Schoo, and M. Matters, "Electrical characterization of electroluminescent polymer/nanoparticle composite devices," *Appiled Physics Letters*, vol. 73, pp. 3914-3916, 1998.

[133] Y. Kawabe, M. M. Morrell, G. E. Jabbour, S. E. Shaheen, B. Kippelen, and N. Peyghambarian, "A numerical study of operational characteristics of organic light-emitting diodes," *Journal of Applied Physics*, vol. 84, pp. 5306-5313, 1998.

[134] P. W. M. Blom, M. J. M. de Jong, and S. Breedijk, "Temperature dependent electron-hole recombination in polymer light-emitting diodes," *Applied Physics Letters*, vol. 71, pp.930-932, 1997.

[135] A. J. Campbell, and D. D. C. Bradley, "Quantifying the efficiency of electrodes for positive carrier injection into poly(9,9-dioctylfluorene) and representative copolymers," *Journal of Applied Physics*, vol. 89, pp. 3343-3351, 2001.

[136] A. J. Campbell, M. S. Weaver, D. G. Lidzey, and D. D. C. Bradley, "Bulk limited conduction in electroluminescent polymer devices," *Journal of Applied Physics*, vol. 84, pp. 6737-6746, 1998.

[137] R. Coehoorn, S. Vulto, S. L. M. van Mensfoort, J. Billen, M. Bartyzel, H. Greiner, and R. Assent, "Measurement and modeling of carrier transport and exciton formation in blue polymer light emitting diodes," *Proceedings of SPIE - The International Society for Optical Engineering*, vol. 6192, pp. 61920O, 2006.

[138] I. H. Campbell, D. L. Smith, C. J. Neef, and J. P. Ferraris, "Consistent time-of-flight mobility measurements and polymer light-emitting diode current–voltage characteristics," *Applied Physics Letters*, vol. 74, pp. 2809-2811, 1999.

[139] B. K. Crone, P. S. Davids, I. H. Campbell, and D. L. Smith, "Device model investigation of single layer organic light emitting diodes," *Journal of Applied Physics*, vol. 84, pp. 833-842, 1998.

[140] K. Murata, S. Cina, and N. C. Greenham, "Barriers to electron extraction in polymer light-emitting diodes," *Appiled Physics Letters*, vol. 79, pp. 1193-1195, 2001.

[141] P. S. Davids, I. H. Campbell, and D. L. Smith, "Device model for single carrier organic diodes," *Journal of Applied Physics*, vol. 82, pp. 6319-6325, 1997.

[142] A. J. Campbell, D. D. C. Bradley, and D. G. Lidzey, "Space-charge limited conduction with traps in poly(phenylene vinylene) light emitting diodes," *Journal of Applied Physics*, vol. 82, pp. 6326-6342, 1997.

[143] A. J. Campbell, D. D. C. Bradley, H. Antoniadis, M. Inbasekaran, W. W. Wu, and E. P. Woo, "Transient and steady-state space-charge-limited current in polyfluorene copolymer diode structures with ohmic hole injecting contacts," *Appiled Physics Letters*, vol. 76, pp. 1734-1736, 2000.

[144] S. A. Carter, M. Angelopoulos, S. Karg, P. J. Brock, and J. C. Scott, "Polymeric anodes for improved polymer light-emitting diode performance," *Applied Physics Letters*, vol. 70, pp. 2067-2069, 1997.

[145] M. Abkowitz, J. S. Facci, and J. Rehm, "Direct evaluation of contact injection efficiency into small molecule based transport layers: Influence of extrinsic factors," *Journal of Applied Physics*, vol. 83, pp. 2670-2676, 1998.

[146] P. W. M. Blom, M. J. M. de Jong, and M. G. van Munster, "Electric-field and temperature dependence of the hole mobility in poly(p-phenylene vinylene)," *Physical Review B*, vol. 55, pp. R656-R659, 1997.

[147] E. M. Conwell and M. W. Wu, "Contact injection into polymer light-emitting diodes," *Applied Physics Letters*, vol. 70, pp. 1867-1869, 1997.

[148] Mark R. Pinto, Conor S. Rafferty, and Robert W. Dutton, "PISCES II: Poisson and Continuity Equation Solver", Copyright 1984 The Board of Trustees of the Leland Stanford Junior University and "PISCES-IIB Supplementary Report", by Mark R. Pinto, Conor S. Rafferty, Hal R. Yeager, and Robert W. Dutton, Copyright 1985 The Board of Trustees of the Leland Stanford Junior University.

[149] J. Frenkel, "On pre-breakdown phenomena in insulators and electric semiconductors," *Physical Review*, vol. 54, pp. 647-648, 1938.

[150] H. Bassler, "Charge transport in disordered organic photoconductors," *Physica Status Solidi (B)*, vol. 175, pp. 15-56, 1993.

[151] Z. G. Yu, D. L. Smith, A. Saxena, R. L. Martin, and A. B. Bishop, "Molecular Geometry Fluctuation Model for the Mobility of Conjugated Polymer," *Physical Review Letters*, vol.84, pp. 721-724, 2000.

[152] S. J. Martin, A. B. Walker, A. J. Campbell, and D. D. C. Bradley. (2003, Oct.). Electrical Transport Characteristics of Single Layer Organic Devices from Theory and Experiment. Imperial College, London, United Kindom. [online]. Available: http://www.bath.ac.uk/~pysabw/research/organics/tpdpaper.pdf

[153] P. W. M. Blom, H. C. F. Martens, and J. N. Huiberts, "Charge transport in polymer light-emitting diodes," *Synthetic Metals*, vol. 121, pp. 1621-1624, 2001.

[154] A. J. Campbell, D. D. C. Bradley, and H. Antoniadis, "Dispersive electron transport in an electroluminescent polyfluorene copolymer measured by the current integration time-of-flight method," *Applied Physics Letters*, vol. 79, pp. 2133-2135, 2001.

[155] M. Redecker, D. D. C. Bradley, M. Inbasekaran, W. W. Wu, and E. P. Woo, "High Mobility Hole Transport Fluorene-Triarylamine Copolymers," *Advanced Materials*, vol. 11, pp. 241-246, 1999.

[156] W. R. Salaneck, S. Stafstrom, and J.-L. Bredas, *Conjugated Polymer Surfaces and Interfaces*. Cambridge, UK: Cambridge University Press, 1996, pp. 68-69.